IMPROVEMENT OF DOWN-AISLE STABILITY AND DUCTILITY FOR UNBRACED ADJUSTABLE PALLET RACKS

Article-based Doctoral Thesis

Oriol Bové Tous

Supervisors:

Francesc López Almansa
Miquel Ferrer i Ballester

Departament de Resistència de Materials i Estructures a l'Enginyeria
PhD in Structural Analysis

Universitat Politècnica de Catalunya

December 2021

Acta de qualificació

To my family

CONTENTS

Acknowledgements

The elaboration of this Thesis has been the most challenging milestone of my life. It surely would not have been possible without the help of the persons I cite in the following lines.

First, I want to sincerely thank the help, guidance, and thorough work of my supervisors (and friends) Prof. Francesc López Almansa, and Prof. Miquel Ferrer Ballester during these years. Our hard work has led to the three publications that compose this Thesis. Moreover, with their help, I have learned a lot about seismic engineering, continuum mechanics, and technical writing; this knowledge is kindly appreciated and will be of great use for my academic and professional future. In addition, I also want to express my gratitude to Prof. Miquel Casafont Ribera, who has always helped, supported, and encouraged me. Indeed, Prof. Casafont is the second author of one of the presented papers and the person who heartened its elaboration.

Also, I want to thank Mecalux for the provided specimens and years of learning in the professional field. Thanks to the staff of LERMA laboratory and its coordinator, Francesc Roure, for making the experimental campaign possible. Thanks to Maria Rosa Somalo, whose wide experience in the laboratory and thorough dedication (and patience) has been indispensable. I also want to thank my colleague Milad Soltanalipour for his kind and good-quality help in linguistic and software-related issues.

Last but foremost, the author wholeheartedly wishes to thank his family and friends for their years of help, support, and patience.

Abstract

Pallet racking systems are structures intended to store products. Their proper structural design is of paramount importance as its collapse can lead to significant economic losses and even human. This type of structures is prone to instabilities and also presents low ductility; consequently, the integrity of these structures is compromised, especially when exposed to extreme actions such as seismic events. Therefore, selective racks' stability and ductility improvement is a relevant issue. Nevertheless, the costs must be as low as possible due to tough industrial competitiveness. The objective of this Thesis is to provide numerical tools and technological solutions aiming to enhance, in an inexpensive way, the stability and ductility of racks.

In the first step of this Thesis –presented in the paper: *Systemized Structural Predesign Method for Selective Racks*– a systemized predesign method of non-regular racks is developed based on a single-column model made with 2-D beam elements. This model considers the down-aisle global behavior of unbraced pallet racks under both gravitational and lateral actions. The aim is to obtain optimal structures in terms of cost while satisfying certain used-defined stability requirements. The results highlight the crucial role of the beams (and the beam-to-upright connections) in the inexpensive improvement of global stability. Since the solutions are non-regular and not obvious, no simplified design rules are given; some computationally efficient numerical tools are provided instead.

The second step of this research is focused on one specific beam-to-upright connection. The objective is to improve its ductility, energy dissipation capacity, and stiffness under seismic excitation as inexpensively as possible. This objective is achieved by modifying the welding layout in order to distribute the stresses more efficiently and, as a consequence, move the failure point away from the welds; the new failure mode is more ductile. The effectiveness of this technique is demonstrated through FEM numerical analyses of monotonic tests, shown in the publication: *Numerical investigation on a seismic testing campaign on adjustable pallet rack speed-lock connections*. The models are first calibrated with experiments, and then the stress distributions in both the elastic and plastic range are deeply analyzed. Finally, continuing with the research on this specific joint, a wide experimental campaign is performed, including monotonic and cyclic tests; these tests are presented in the publication: *Ductility improvement of*

adjustable pallet rack speed-lock connections: Experimental study. This paper successfully demonstrates the aforementioned enhanced properties of the novel welding layout. Additionally, two different cyclic testing protocols are compared and proven to influence the failure mode and, thus, the obtained ductility and energy dissipation capacity.

Resum

Les prestatgeries de paletització industrial són estructures destinades a emmagatzemar productes. El seu correcte disseny estructural és de gran importància, ja que el seu col·lapse pot derivar en importants pèrdues econòmiques i fins i tot humanes. Aquest tipus d'estructures és força inestable i poc dúctil; com a conseqüència, la seva integritat està compromesa, especialment quan s'exposen a accions severes com ho poden ser les sísmiques. Per aquesta raó, existeix un interès creixent a millorar l'estabilitat i la ductilitat de les prestatgeries. Tanmateix, la dura competitivitat industrial obliga a minimitzar els costos. L'objectiu d'aquesta tesi és aportar eines numèriques i solucions tecnològiques per millorar l'estabilitat i la ductilitat d'aquest tipus d'estructures sense que això impacti dramàticament als costos.

En un primer pas d'aquesta tesi, presentat a l'article: "*Systemized Structural Predesign Method for Selective Racks*", s'avalua un nou mètode per al pre-disseny sistematitzat de prestatgeries no regulars mitjançant un model mono-columna elaborat amb barres 2-D; aquest model té en compte el comportament lateral longitudinal (en la direcció del passadís) de prestatgeries no travades sotmeses tant a accions gravitatòries com laterals. L'objectiu (del mètode de pre-disseny) és obtenir prestatgeries òptimes en termes de cost, que alhora satisfacin determinats requisits d'estabilitat definits per l'usuari. Els resultats posen de manifest el paper fonamental dels travessers i les unions puntal-travesser en l'estabilitat global de l'estructura i en la seva optimització econòmica. Atès que les solucions no són intuïtives ni òbvies, no es poden proporcionar regles de disseny simplificades; en lloc d'això, doncs, es proporcionen altres eines numèriques computacionalment eficients.

El segon pas d'aquesta investigació se centra en una unió puntal-travesser en concret amb l'objectiu de millorar la seva ductilitat i capacitat de dissipació d'energia sota excitació sísmica. L'objectiu s'aconsegueix modificant el traçat de la soldadura; amb la intenció de distribuir les tensions de manera més eficient i, com a conseqüència, desplaçar el punt de fallada lluny de la soldadura; en fer això, el nou mode de fallada és més dúctil. L'article presentat a la publicació "*Numerical investigation on a seismic testing campaign on adjustable pallet rack speed-lock connections*", inclosa en aquesta tesi, demostra l'eficàcia d'aquesta tècnica mitjançant la simulació amb elements finits

d'experiments incrementals. Els models numèrics es calibren amb experiments i després s'hi analitzen les distribucions de tensions en profunditat. Finalment, i seguint amb la investigació sobre aquesta unió en concret, es realitza una àmplia campanya experimental, que inclou assaigs incrementals i cíclics, presentada a la publicació: "*Ductility improvement of adjustable pallet rack speed-lock connections: Experimental study*". En aquest article, es demostren amb èxit les propietats millorades del nou disseny de la soldadura. A més, es contrasten dos protocols d'assaigs cíclics diferents i es demostra que influeixen en el mode de fallada i, per tant, en la ductilitat i capacitat de dissipació d'energia.

1 INTRODUCTION

1.1 Background and motivation

Adjustable pallet racks are heavy-duty steel-shelved structures intended to store goods. Their proper structural design is important as its collapse can lead to significant human and economic losses [1]. Moreover, these structures are prone to instabilities and commonly present low ductility; consequently, their structural integrity is compromised, especially when exposed to severe actions such as seismic events. In fact, studying the seismic behavior of racks has been the main objective of the recent European projects SEISRACKS I and II [2,3]. Moreover, due to tough industrial competitiveness, the costs of these structures must be as inexpensive as possible. The objective of this Thesis is to provide numerical tools and technological solutions aiming to enhance, in an inexpensive way, the stability and ductility of racks.

To fulfil the objectives described above, understanding how each element influences the global behavior of the structure is crucial. Pallet racks are mainly composed of vertical (uprights), horizontal (beams), and sloping (braces) bar-like elements (***Figure 1***.a); all these are commonly thin-gauge cold-formed steel members. Speed-lock beam-to-upright joints are used to ease the rack erection; the connection consists in inserting hooks of the beam-end-connector into the upright perforations (as displayed in ***Figure 1***.*b*). The cross-aisle direction is always braced (***Figure 1***.a), while the down-aisle only occasionally.

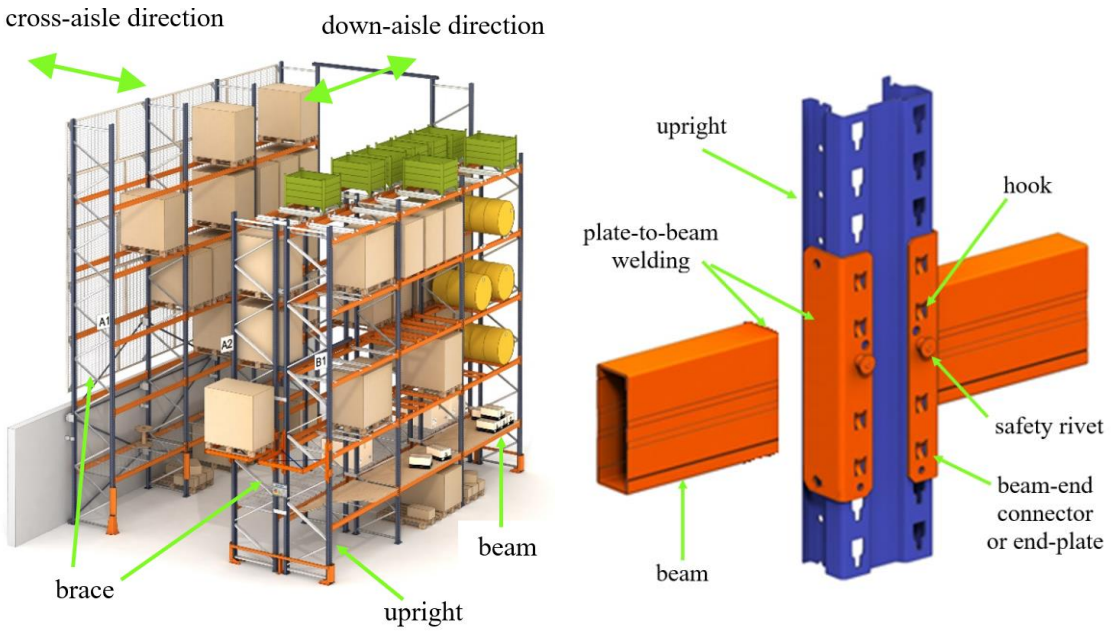

(a) Adjustable pallet-rack

(b) Beam-to-upright connection

***Figure 1**. Analyzed racking systems*

Global stability of pallet racks strongly depends on their uprights; therefore, many recent works have studied their behavior, both numerically and experimentally [4-6]. These works remark the unstable character of these elements, mainly contributed by their aforementioned cold-formed nature, but also for using open-section profiles and being regularly perforated [7]. On the other hand, the connections (beam-to-upright and base) are not totally rigid, and, consequently, the global lateral stability of racks is influenced by their flexibility. In fact, as already mentioned, pallet racks are sometimes braced in the down-aisle direction in order to improve its intrinsically poor lateral stiffness [8,9]. This bracing is placed in the rear position, as the stored products are handled from the front (aisle); this represents a drawback as its eccentricity induces global torsion to the structure in the presence of severe lateral actions, such as seismic. The alternative of using bracing is to use stronger columns and/or beams, leading to sharp over costs if only uniform designs are contemplated. On the other hand, the conventional design of non-uniform structures is time-consuming and, thus, needs computationally efficient design tools [10]. Moreover, also due to the unstable character of the members, the ductility of unbraced racks relies exclusively on their connections. These issues point out that beam-to-upright connections (***Figure 1***.b) are crucial for the lateral stability and ductility of unbraced pallet racking systems. Thus, improving the stiffness, ductility, and energy dissipation capacity of these joints is of interest.

1.2 Objectives

The exposed motivations and scopes exposed in ***Section 1.1*** highlight the necessity of achieving the following main objectives:

- Providing tools to facilitate the design of unbraced non-uniform pallet racks that can be economically competitive if compared with braced solutions.
- Inexpensively improve the stiffness, ductility, and energy dissipation capacity of beam-to-upright connections.

During the Thesis, the following side-objectives are also expected to be achieved:

- Gain understanding of the parameters that most contribute to the global stability of racks.
- Gain understanding of the parameters that most contribute to the stiffness, ductility, and energy dissipation capacity of beam-to-upright connections.
- Compare different cyclic protocols, aiming to find out its possible influence on the failure mode.

1.3 Global discussion on the State-of-the-art

For the reasons exposed in ***Section 1.1***, there is a need to unify design criteria for pallet racks. In this way, the codes intended for buildings [11-15] are not fully adequate, as pallet racks present particularities. These can be summarized in two: (i) neither their member profiles nor connections are standardly considered in general construction and (ii) oppositely to buildings, their self-weigh represents only a small fraction of the live loads ([1]). As a consequence, pallet racks producers from Europe (F.E.M.) and also from U.S.A. (R.M.I.) have heartened the elaboration of specific codes for adjustable pallet racks [9,16-18] that complement the standards of general use. These specific codes establish how to perform experiments for individual elements; this issue is important since the behavior of the members and the connections is rather complex and, thus, cannot

be studied only numerically. Moreover, the verification of racks is also particularly complex, and these standards provide methods and tools to assist engineers.

Regarding the verification of racks, Annex C and Annex G of code EN 15512 [9] provide a simplified methodology for static design; nonetheless, no simplified recommendations are provided for the design (or predesign) of non-regular structures. This issue motivates the elaboration of a systemized predesign method for non-regular unbraced pallet racks. In general, formal optimization methods [19] can be efficient in finding safe and inexpensive non-regular solutions. However, these approaches are time-consuming and not fully adequate for pallet racks design because of the following reasons:

- The cost function of pallet racks is not easily represented as a closed form; indeed, the costs are related to the members' weight but also to the process of production.
- The problem is discrete, and the number of (Boolean) variables involved is very high; this is due to the mutual dependence between the different design parameters (for example, the stiffness of the beam-to-upright connection depends on both the upright and the beam).

Similarly, and regarding the design of cold-formed structures, Liu [20] states that intuitive and practice-oriented optimization methodologies are commonly preferred; in this paper, a Fully Drifted Design methodology for steel moment frames is presented. This algorithm is an evolution of the Fully Stressed Design [21]. Similarly, Manickarajah et al. [22] present a simple optimization algorithm for the design of columns and frames based on enhancing their buckling elastic resistance. The algorithm uses an iterative procedure for gradually shifting the material from the strongest part of the structure to the weakest part while keeping the structural weight constant. Moreover, other works [23,24] consider the sensitivity of the buckling elastic factor with respect to the design parameters for improving the stability of slender structures. Finally, **Appendix A** of this Thesis presents a conference paper that proposes a predesign methodology for structures also based on improving their stability.

Going to previous studies on full racks, works [25,26] present 2-D and 3-D global numerical analyses aimed to find out which parameters most influence the stability. In particular, [25] proves numerically and experimentally that rigidizing the upright cross-

sections with a spacer bar increases considerably the load carrying capacity of frames. Moreover, work [26] studies and points out the considerable impact of small imperfections on global behavior. This issue highlights the relevance of second-order effects in this type of structure. In fact, code [9] states that the second-order effects must be considered and recommends using full 3-D global analyses; nevertheless, separate 2-D analyses in down and cross-aisle directions are also allowed. In this way, the use of simplified models that approximately (and rather accurately) consider the 2-D behavior [27-29] and the second-order effects are of interest in the pallet racking industry. Similarly, the study carried out in ***Section 2*** of the present Thesis presents a single-column model that characterizes the down aisle direction of non-regular racks and also takes the geometrical nonlinearity into account. The results of all these studies highlight the key role of beam-to-uptight connections on global stability. Moreover, these joints represent the main source of ductility and energy dissipation ([39]).

For the exposed reasons, the study of the stiffness and ductility of these connections is of interest; in this way, paper [40] deeply analyzes the topic and highlights the importance of these connections for the lateral behavior of racks. This issue motivates the elaboration of ***Section 3*** and the paper included in it as part of this Thesis. This paper presents simulations of pallet rack beam-to-upright experiments; the FEM software Ansys [41] is used for this purpose. This paper aims to demonstrate the benefits of modifying the welding layout between beam and end-plate (Figure 1.b) for the ductility of joints numerically; the simulated tests are monotonic. Similarly, other researchers have studied the behavior of pallet racks joints under tests numerically [55-60]. Nevertheless, unlike these studies, the simulations of the present Thesis aim to gain knowledge on how the stresses are distributed in the nearby of the welded joint.

Once the ductility improvement of this joint is proved for monotonic tests, the next logical step is to study its cyclic performance. Cyclic tests, contrarily to monotonic experiments, take fatigue into account. As a consequence, they are commonly used for calibrating efficient moment-rotation (cyclic or monotonic) models [52-54]. These models can be used for global seismic transient or pushover [55-59] numerical analyses aimed to characterize behavior factors of full racks (parameter q in Eurocodes, and R in AISI standards). Alternatively, shake table testing of full racks [76-78] can also be used with the same objective.

As a result of this necessity, ***Section 4*** presents a wide experimental campaign on pallet rack beam-to-upright connections, including cyclic testing. Other authors have also performed similar studies [1,45-49,63,69]; these serve as a starting point for the present work. Moreover, as a side objective of this study, two different cyclic protocols are compared: an ECCS recommendation [70] and a novel methodology proposed by Castiglioni [1]; the latter protocol, oppositely to the conventional ones, considers the gravitational loads. The results of this study highlight that the testing protocol influences the obtained stiffness, ductility, and energy dissipation capacity.

1.4 Organisation of this document

For the reasons discussed in ***Section 1.1***, only the following structural elements and connections are considered in this Thesis: uprights, beams, beam-to-upright connections, and base connections. ***Section 2*** focuses on studying the influence of all these elements on global lateral stability. A systemized pallet rack predesign method is developed and proven to provide non-regular rack configurations that are optimum in terms of cost while satisfying the desired stability requirements. This study highlights the crucial role of beam-to-upright connections to the global behavior of racks, and the next logical step is to enhance its behavior. In this line, ***Section 3*** and ***Section 4*** focus on redesigning one specific beam-to-upright connection. This particular joint fails at the welding border between the beam and the end-plate (***Figure 1***.b); this failure is brittle and, thus, represents a significant danger for the structure's integrity after severe seismic events. The redesign of this welding leads to a redistribution of stresses in the beam profile that turns the failure mode from brittle to ductile. ***Section 3*** deeply studies the stress distributions with FEM models; complementarily, ***Section 4*** presents a wide experimental campaign aimed to prove the enhanced properties of this new design. Finally, ***Section 5*** summarizes the most relevant results of this Thesis, highlighting its main achievements; additionally, the future lines of research are presented.

2 SISTEMIZED STRUCTURAL PREDESIGN METHOD FOR SELECTIVE RACKS

2.1.1 Article data

Title: Systemized Structural Predesign Method for Selective Racks
equation.

Authors: O. Bové, M. Casafont, M. Ferrer, F. López-Almansa, F. Roure

Journal: Journal of structural engineering (ASCE) (2020)

DOI: 10.1061/(ASCE)ST.1943-541X.0002849.

2.1.2 Transcription of the original paper

SYSTEMIZED STRUCTURAL PRE-DESIGN METHOD FOR SELECTIVE RACKS

Abstract: This paper presents a simplified stability-based method for practical structural pre-design of down-aisle unbraced frames of selective racks. Given the uniformity of actual racks, only a single upright and their adjoining half beams are modelled, being discretized with 2-D beam elements; the flexibility of the upright-beam and upright-floor connections is represented with linear springs. Such model is used for linear buckling and second order analyses. The proposed method consists in resizing iteratively the structural members according to cost and stability criteria (linear buckling analysis) until the SLS and ULS are satisfied (second order analysis). Specific procedures have been developed to speed up the computations. Two practical examples are analyzed to assess the performance of the proposed method. When compared to conventional design approaches for racks, the method shows to be faster, and results in less expensive structures. The simplification involved in the single-column consideration is sufficiently accurate. Finally, some ideas about efficient methods of improving the stability of racks are presented.

Keywords: Adjustable Pallet Racking, Design of Racks, Stability, Buckling Analysis.

Introduction

Pallet rack design is not a routine task, as it depends on highly variable issues, such as size and weight of the stored goods, rack location (indoor or outdoor), rack usage (public or private), and site seismicity, and so on. On the other hand, the pallet rack market is very competitive, requiring that the costs are minimized. Therefore, rack design is a crucial issue; conversely, commonly it is not highly systematized, and experience-based procedures are combined with trial-and-error approaches. Such design strategies do not always provide the cheapest and most efficient solution; furthermore, these types of design process are too slow. Thus, computer systemized approaches might be considered instead; beyond their obvious advantages, such methodologies might be also useful to

find innovative solutions and to determine the cost sensitivity with respect to the design parameters (Farkas and Jarmai 2013).

Given these circumstances, this paper presents a computer systemized procedure for preliminary design of down-aisle unbraced frames of selective racks. The proposed method is practice-oriented and intuitive; see (Liu 2015) for the advantages of such practical optimization approaches. Formal optimization methods (Nocedal and Wright 2006) are not considered in this study as, although can certainly provide highly accurate results, the important number of involved parameters is a drawback for the interests of industrial companies needing to obtain solutions in a few seconds. It is noted that this high number of parameters is mainly contributed by the dependence of the connections stiffness with the upright and beam sections (third order table of Boolean parameters must be considered to take into account the location, beam and upright). Also, some peculiarities of the cost function hinder the use of formal optimization methods. An evolution of the classical Fully Stressed Design method (see, for instance Mueller, Liu, and Burns S. 2002) is adopted. That approach is called Fully Drifted Design, being proposed by Liu (2015); an initial design is iteratively improved until both strength and stiffness criteria are satisfied and the weight is sufficiently reduced. In the proposed method, such criteria are also contemplated, but the members are resized in a different way; members that generate low cost increment and high stability gain are changed at each iteration. The offered procedure begins with the cheapest structure that can be produced with the available steel profiles, and ends when both the strength and drift criteria are satisfied. The presented strategy is similar to the stability-based design by Manickarajah et al. (2000), although those authors used 2D solid finite elements while this study considers beam elements. Regarding the sensitivity of stability with respect to the design parameters, the works by Perelmuter and Slivker V. (2001) and Szalai (2010) have been used.

The proposed strategy does not consider the full down-aisle rack structure, but only a single column and its neighboring half-beams. Such reduced model is significantly less time-consuming, and allows easier understanding of the effects of the resizing operations; the conducted research shows that the results are sufficiently accurate for pre-design stage; as a matter of fact, the European design code (EN-15512 2009) permits performing separate 2D analyses in down and cross-aisle directions, even for final design.

More complex analyses (full 3-D if needed) are to be performed by the designer for validation. Similar simplified models have been used in drive-in racks design (see Godley 2002, Hua and Rasmussen 2006, Cheng and Wu 2015).

Apart from the reduction described in the previous paragraph, the proposed model involves other simplifications; they are described and discussed next. Load and connection eccentricities, and the effect of sectional instabilities and perforations in the global analysis are not taken into account (Tilburgs 2013). However, there are standardized simple approaches that can be easily implemented in the model to include some of the non-considered issues. For example, the effect of local and distortional buckling sectional deformations on member stiffness can be considered by simply reducing the cross-section properties of the beam element (the effective cross-section properties can be used in the global analysis, as proposed in (EN1993-1-3 draft, EN1991-1-5 2004)). In a similar way, the detrimental effect of perforations on member stiffness can be accounted for by means of equivalent reduced cross-section properties, as proposed in the latest version of the EN15512 (prEN15512 draft 2016). Another issue is that the structure is discretized with 2D finite elements and, therefore, warping is not accounted for; their relevance for rack structures is examined in (Bernuzzi et al. 2014, 2015, 2016). In this sense, the proposed model is simpler than other formulations (Trouncer and Rasmussen 2016, and Sena and Rasmussen 2016) as it is intended for practical pre-design. In any case, warping can be indirectly considered through the so-called "warping" factors defined in (Bernuzzi et al. 2014, 2015). Actually, the proposed method of global analysis can be considered similar to methods accepted in current standards of cold-formed steel design: Method 2a and 2b of (prEN15512 draft 2016); the M3 method recently incorporated to the EN1993-1-1 and EN1993-1-3 (EN1993-1-1 draft; EN1993-1-3 draft); and the Direct Analysis Method of the AISI Specification (mixed approach combined with B1 factor, see (AISI 2016)). As it will be seen bellow, P-Δ and sway imperfections will be included in the global analysis, while the effects of torsional buckling phenomena are considered in the verification stage.

No systemized structural design approaches for rack systems have been reported so far, thus, this is one of the main contributions of this paper. Other relevant contributions are: the efficient modelling of selective racks using only single-column models (even for non-totally uniform frames, as shown in Example 2), the use of analytical expressions of

the critical load factor (equation [11]) in terms of the design parameters, and the assessment of the sensitivity of such factor to those parameters. Noticeably, this study is computationally efficient, thus being intended for professional day use. In this sense, the risk of mistaking the location of different similar structural elements can be avoided by distinctive color painting or other similar easy-to-implement measures.

Future research will include first considering the warping degree-of-freedom, and later using finite elements derived from the Generalized Beam Theory (GBT). This last will allow considering local and distortional buckling (see Bonada et al. 2018) and accounting for the influence of the perforations (see Casafont et al. 2017). The single-column model in combination with GBT is expected to be computationally effective to compared shell elements.

Pallet rack design

This Section discusses some basic concepts of pallet rack design that are used in this paper.

Design specifications

When a given pallet rack aisle is designed, the stored product dimensions and the maximum product weights are set by the client. Consequently, all the global rack dimensions, such as level heights, bay widths and frame depths are part of the initial design specifications. However, these dimensions may vary slightly when the actual size of the structural profiles is considered in more advanced stages of design. The weights of the stored goods are also known at the beginning of the design process; the only load that depends on the selected profiles is their self-weight, but it represents only a small fraction of the gravity loads. Consequently, this variation is not taken into account in a first design stage (Crosbie 1998). Additionally, all possible horizontal actions, such as seismic, forklift impact, or wind (for outdoor racks), are also quantified at the beginning. On the other hand, the global imperfection effects can be modelled both as horizontal forces or as initial sways; in this study, they are modelled as forces. Paragraph 5.3.2 of EN15512 (2009) states that the imperfection action depends on: i) a specified out of plumb; and ii) the looseness of the beam-upright connector. Since such looseness depends on the considered structural profiles, this imperfection action cannot be established at the initial

stages of design; nevertheless, it is shown in the application examples that the presented design procedure can be initiated without knowing the final looseness. Finally, it is pointed out that no member imperfections (initial curvature) are considered in the global analysis, as permitted in EN15512 (2009).

The effects of seismic actions can be dealt with by representing them with equivalent static lateral forces (Lateral Force Method of Analysis (EN 16681 2016)). This rather conservative simplified approach is largely sufficient for the pre-design phase.

Design parameters

For unbraced pallet rack down aisle structures, the main members are basically uprights (omega-shaped) and beams (box-shaped); all such elements are cold-formed. Thus, in the simplified model used for design presented below, the in-plane upright and beam moments of inertia of each member, I_u and I_b, respectively, are the design parameters, i.e., the unknowns to be determined in the design process. Since, pallet rack producers usually make their structures using a limited range of perforated steel profiles, the design problem has a finite number of design solutions.

Commonly, gross-section properties are used in global analysis, as stated in paragraph 9.2.1 of EN15512 (2009). If more accuracy is needed, simplified approaches can be applied to account for the effect of perforations and sectional buckling phenomena on the member stiffness, such as those presented in prEN15512 (2016) and (AISI Specification 2016). In the present study no such stiffness reduction is considered, although could be easily included if required.

The beam-to-upright connections have speed-lock character, thus permitting to easily positioning any beam at any height of a regularly perforated upright. Such connections are modelled as semi-rigid, and their stiffness (K_{b-u}) are characterized using normative tests according A.2.4 of (EN15512 2009). These stiffness are also design parameters (see example at the end of the article), but they are related to the beam and upright moments of inertia (I_u, I_b); thus, the stiffness of the joints are not independent unknowns of the design process. The stiffness of the joints are considered constant. Consequently, it will not be possible to reproduce any nonlinear behavior of the joints in the analysis, such as yielding. The reason is, although it is feasible to implement such

elastic-plastic behavior of the joints (or even the multilinear behavior) in the model, it will never be capable of reproducing in a realistic way the progressive yielding of the different joints of the structure. This is due to the fact that, as will be seen below, a simplified single-column model will be used, which is a rather limiting factor if progressive yielding of the structure is to be modelled. On the other hand, nowadays nonlinear analyses are not highly popular in the professional practice, given that clause 9.5.4 (Design shear force and bending moment for beam end connectors) of (EN15512 2009) makes extremely difficult reaching the yielding moment.

The situation is similar for the floor connections. It should be noted, however, that in this case, their stiffness, determined according to A.2.7 of EN15512 (2009), is not only a function of the upright moment of inertia, but also of the axial force ($K_{\mathrm{f}}(N)$, where N is the axial force, tension positive).

All the parameters involved in the analysis are described in Fig. 1.

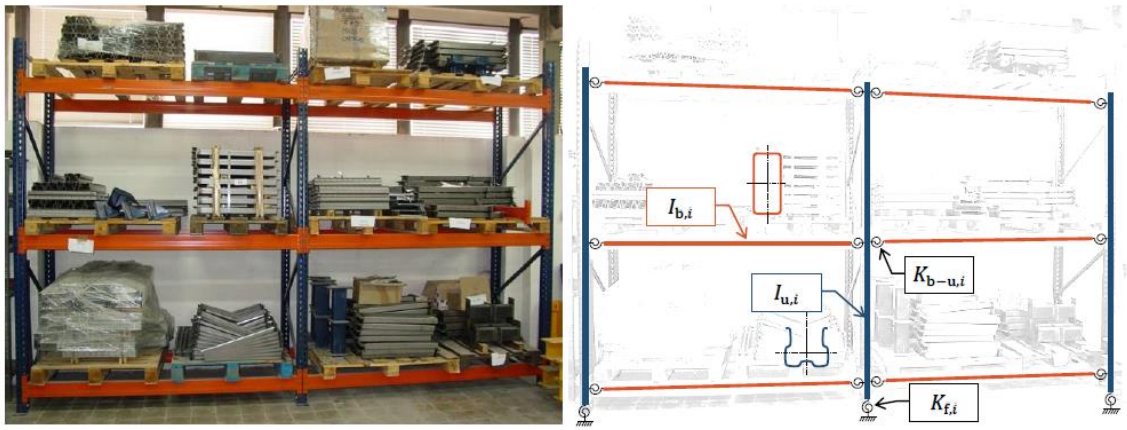

Fig. 1. Design parameters considered in the study.

Design verification

When designing a given pallet rack system, the Ultimate Limit State (ULS) and Serviceability Limit State (SLS) verifications are carried out in a similar way as for any ordinary structure. The ULS verifications are performed according to the conventional general approach (EN1990 2002):

$$E_{\mathrm{d}} \leq R_{\mathrm{d}} \qquad [1]$$

where E_{d} is the design value of the internal forces, and R_{d} is the resistance design value. In the design method presented in this article, E_{d} is obtained from a simplified analysis model and R_{d} is determined from experimental tests carried out according to EN15512 (2009). The considered tests are: i) stub column (to obtain the effective sectional properties accounting for the perforations), ii) distortional buckling (to obtain the distortional buckling effective area), iii) frame compression tests (to account for the global buckling), iv) upright bending (to determine the effective sectional flexural parameters and the lateral torsional buckling strength), v) beam bending (similar purpose), vi) beam-upright connections (to get their stiffness, moment and shear capacity), vii) floor connection (to find the bending stiffness and resistances for different levels of axial compression).

Noteworthy, although a verification scheme based on experimental tests is adopted in this study, the proposed design procedure can be easily adapted to R_{d} values derived from analytical calculations.

Concerning the SLS verification, the following condition should be fulfilled (EN1990 2002):

$$E_{\mathrm{d}} \leq C_{\mathrm{d}} \qquad [2]$$

where E_{d} are the horizontal displacements at each level of the rack, and C_{d} are limiting values defined in EN 15512 (2009).

Pallet racks considered in this study

A given pallet rack aisle can have a very high variety of beams and uprights and can be very irregular in beam level heights and bay widths. This is because the stored products can be very diverse in dimensions and weight, hence, each part of the rack must be designed accordingly. Nonetheless, this situation is not the most common, especially in long aisles, as usually the goods are stored following certain sorting criteria; thus, some regularity is normally assumed. Thus, this paper focusses on structures fulfilling the following conditions:

- In the down aisle direction, the rack dimensions, loads and structural members are uniform (Fig. 2). However, certain irregularities are considered, as shown in the second example below.
- The relative heights between levels are not necessarily equal.
- The loads in the different levels are not uniform.

- No braces are used in the down aisle direction.

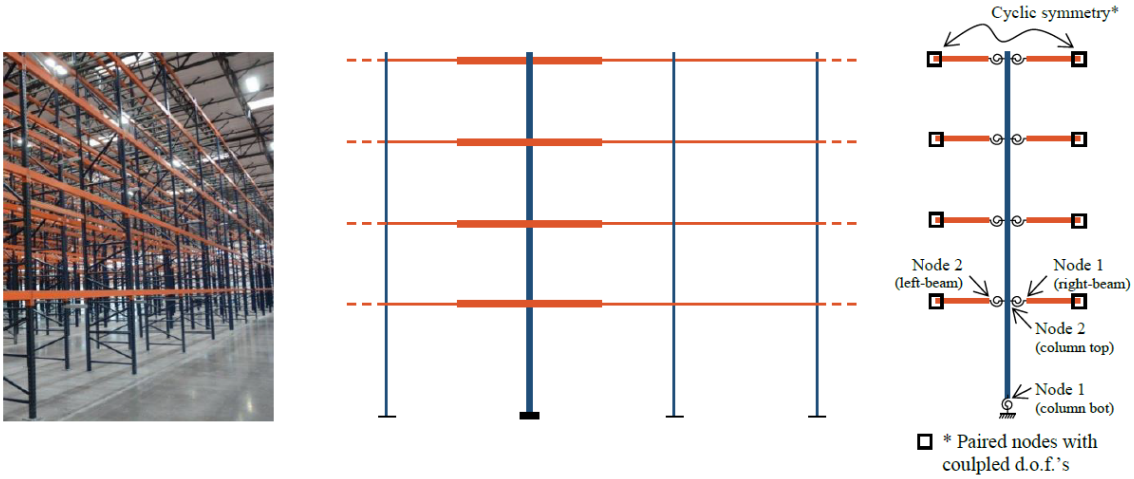

Fig. 2. Pallet rack structure and single column model.

One of the justifications of this vertical non-regularity is that, sometimes, the lowest levels shall be more accessible to people, as are reserved for picking; hence, are shorter than the higher ones (being employed for heavier unit loads, such as pallets). Furthermore, in racks with forklifts, the top beam levels are higher than the bottom ones (EN15620 2008); the aim is to leave more maneuverability space. Conversely to these vertical irregularities, there is uniformity in the down aisle direction, as the stored products are the same.

Annex C of EN15512 (2009) contains structural design criteria for regular racks; nonetheless, these criteria are intended for racks that use the same beam profile in all their levels. Conversely, the structures studied in this paper can have different beam profiles at different levels, even undergoing the same load. This irregularity is due to the relevant contribution of the beams to the lateral stability of the rack. In this sense, it is interesting to highlight that in any moment-resisting frame, lateral resistance (and, thus, stability) is strongly necessary to withstand seismic, wind, forklift impact and global imperfection effects. Such resistance is best provided by bracing; however, in some occasions bracing is not possible, mainly due to space restrains. In pallet racks, braces can be easily installed in the cross aisle direction but not in the down aisle one. The reason is that the front space must be kept clear to allow easy units placing; then, installing braces only in the rear space would lead to highly prejudicial torsion effects. Hence, ordinarily, pallet racks are only braced in the cross aisle direction; as a consequence, the stability in the down aisle

direction becomes a major design issue. Given these considerations, structures without down aisle bracings are considered in this study, being oriented to avoid bracing while limiting the need of stiffening the structural members and connections (Tilburgs 2013).

Down aisle single-column model

A 2D simplified finite element frame model of the rack is developed herein. Due to the horizontal uniformity of the structure, a single upright and its neighboring half-beams are included in the model (see Fig. 2); the members are discretized with 2-node beam elements. A linear spring at the bottom of the upright is introduced to represent the semi-rigid floor connection, and linear springs are also incorporated in the beam-upright connections. To impose the periodic condition in the finite element model, all the degrees of freedom (displacements and rotations) at the end of the modeled half-beams of each level are coupled (see Fig. 2). Given the high axial stiffness of the members, the vertical displacements of the upright nodes are suppressed; noticeably, they are not needed to determine approximately the uprights axial compression, since (neglecting influence of the beams bending moments) it can be calculated by summing up the vertical loads. With respect to the beams, all the degrees of freedom are considered (except the vertical displacement that is shared with the upright).

The linear and geometric stiffness matrices are shown in Table 1 for clarification. Noticeably, as the axial loads in the uprights are known, their geometric stiffness matrix can be directly set. A preliminary analysis is not carried out to determine the axial load distribution within the structure. Since there is no bracing, the axial forces in the beams are neglected.

Table 1. Stiffness Matrices

Elastic Matrices	Geometric and Rotational Matrices
$\mathbf{K^e} = \begin{bmatrix} \frac{12EI_u}{L^3} & \frac{6EI_u}{L^2} & -\frac{12EI_u}{L^3} & \frac{6EI_u}{L^2} \\ \frac{6EI_u}{L^2} & \frac{4EI_u}{L} & -\frac{6EI_u}{L^2} & \frac{2EI_u}{L} \\ -\frac{12EI_u}{L^3} & -\frac{6EI_u}{L^2} & \frac{12EI_u}{L^3} & -\frac{6EI_u}{L^2} \\ \frac{6EI_u}{L^2} & \frac{2EI_u}{L} & -\frac{6EI_u}{L^2} & \frac{4EI_u}{L} \end{bmatrix}$ (Upright)	$\mathbf{K_G^e} = \begin{bmatrix} \frac{6N}{5L} & \frac{N}{10} & -\frac{6N}{5L} & \frac{N}{10} \\ \frac{N}{10} & \frac{2LN}{15} & -\frac{N}{10} & -\frac{LN}{30} \\ -\frac{6N}{5L} & -\frac{N}{10} & \frac{6N}{5L} & -\frac{N}{10} \\ \frac{N}{10} & -\frac{LN}{30} & -\frac{N}{10} & \frac{2LN}{15} \end{bmatrix}$ (Upright Geometric)
$\mathbf{K^e} = \begin{bmatrix} \frac{A_bE}{L} & 0 & 0 & -\frac{A_bE}{L} & 0 & 0 \\ 0 & \frac{12EI_b}{L^3} & \frac{6EI_b}{L^2} & 0 & -\frac{12EI_b}{L^3} & \frac{6EI_b}{L^2} \\ 0 & \frac{6EI_b}{L^2} & \frac{4EI_b}{L} & 0 & -\frac{6EI_b}{L^2} & \frac{2EI_b}{L} \\ -\frac{A_bE}{L} & 0 & 0 & \frac{A_bE}{L} & 0 & 0 \\ 0 & -\frac{12EI_b}{L^3} & -\frac{6EI_b}{L^2} & 0 & \frac{12EI_b}{L^3} & -\frac{6EI_b}{L^2} \\ 0 & \frac{6EI_b}{L^2} & \frac{2EI_b}{L} & 0 & -\frac{6EI_b}{L^2} & \frac{4EI_b}{L} \end{bmatrix}$ (Beam)	$\mathbf{K^e} = \begin{bmatrix} k_r & -k_r \\ -k_r & k_r \end{bmatrix}$ (Rotational Spring)

This simplified model can be used to obtain the buckling loads of the rack by the following eigenvalue problem

$$(\mathbf{K} + \alpha_b \, \mathbf{K_G}) \, \boldsymbol{\phi_b} = 0 \quad [3]$$

where $\mathbf{K}$ is the initial (linear) stiffness matrix, $\mathbf{K_G}$ is the geometric stiffness matrix, α_b are the global dimensionless buckling factors (stability factors), and $\boldsymbol{\phi_b}$ are the buckling modes. In a similar way, second order analyses can be performed as

$$(\mathbf{K} + \mathbf{K_G}) \, \boldsymbol{\phi} = \mathbf{F} \quad [4]$$

where $\boldsymbol{\phi}$ and $\mathbf{F}$ are the displacement and external force vectors, respectively.

Given the aforementioned simplifications, the model results are not exact, but can be used as an approximation; its accuracy compared to 2D finite element models of the whole structure is assessed at the end of this paper.

Design strategy

The lateral stability of racks is a nonlinear problem, with material and geometric nonlinearities; nevertheless, the critical (lowest) sway stability factor, α_{cr}, is widely used in early design stages. This is because any increment of α_{cr} yields higher nonlinear ultimate loads. Thus, the sensitivity of α_{cr} to the design parameters can report on how to improve the ultimate load. Commonly, actual pallet racks are designed for low values of α_{cr}; in many cases they are lower than 2. For such low values, the second order moments and lateral displacements become high compared to the first order ones; however, can be significantly decreased with a small increase of α_{cr}. This study aims to improve the pallet racks behavior by increasing α_{cr}.

When α_{cr} is greater than 10, the EN1993-1-1 (2005) permits using linear analysis, because the global second order effects are not relevant. Thus, in this study it is considered that the improvement of the linear stability makes sense only when α_{cr} is less than 10. For high values of the stability factor, a design procedure based on the individual member strength and stiffness, such as the Fully Drifted Design (Liu 2015), would be more suitable. On the other hand, when α_{cr} is less or equal than 1 the structure becomes unstable; thus, it is recommended to begin by any $\alpha_{cr}^{min} > 1$. It should be pointed out that α_{cr} of a given pallet rack never decreases when a single parameter of the linear stiffness matrix grows; as a result, the considered structures do not exhibit relative extrema (maximum or minimum) in terms of linear stability.

The gradient of α_{cr}, $\nabla\alpha_{cr}$, describes the variation of stability with respect to the design parameters $I_{u,i}$, $I_{b,i}$, $K_{b-u,i}$, and $K_{f,i}$, where subscript i indicates member (either upright or beam) or joint (either beam-upright or upright-base connections). Consequently, the gradient of α_{cr} helps to identify which members of the structure contribute the most to increase the stability. Thus, a stability-based design procedure may be set where a path of "gradient-oriented" solutions leads to the final one; however, a slightly different approach is finally considered, by incorporating also the cost of the structure.

Derivation of the stability factor gradient for the single column model

The element linear stiffness matrix used in the analysis (see Table 1) shows linear dependence on the design parameters $I_{u,i}$, $I_{b,i}$, $K_{b-u,i}$, and $K_{f,i}$. If, for simplicity, these

parameters are referred as $\boldsymbol{\psi} = (\psi_1, \dots, \psi_n)$, the global stiffness matrix of the single column model can be written in as:

$$\mathbf{K} = \mathbf{K^{(0)}} + \sum_{i=1,\cdots,n} \psi_i \, \mathbf{K}^{(i)} \quad [5]$$

where $\mathbf{K^{(0)}}$ includes the assembled terms of the linear stiffness matrix that do not depend on the design parameters, namely the cross-section area of the beams; and $\mathbf{K^{(i)}}$ can be easily derived for each finite element (upright, beam or rotational stiffness) from Table 1. On the other hand, as the internal forces of the structure are directly obtained from the external loads, the geometric stiffness matrix $\mathbf{K_G}$ can be assumed to be constant.

The gradient of the stability factor can be obtained from the derivative with respect the design parameters ψ_i of the following expression obtained from [3] (see Manickarajah, Xie and Steven G. 2000):

$$\boldsymbol{\phi}_{\mathbf{cr}}^{\mathbf{T}} \left(\mathbf{K} + \alpha_{cr}\mathbf{K}_G\right) \boldsymbol{\phi}_{\mathbf{cr}} = \boldsymbol{\phi}_{\mathbf{cr}}^{\mathbf{T}} \, \mathbf{0} = \mathbf{0} \quad [6]$$

Due to the linear nature of the relationship between the design parameters and the terms in equation [6], its derivation becomes straightforward and results in:

$$\nabla\alpha_{cr} = \left(\frac{\partial\alpha_{cr}}{\partial\psi_1} \cdots \frac{\partial\alpha_{cr}}{\partial\psi_n}\right)^{T} \quad [7]$$

where:

$$\frac{\partial\alpha_{cr}}{\partial\psi_i} = \frac{\boldsymbol{\phi}_{\mathbf{b}}^{\mathbf{T}} \mathbf{K}^{(i)} \boldsymbol{\phi}_{\mathbf{b}}}{\boldsymbol{\phi}_{\mathbf{b}}^{\mathbf{T}} \mathbf{K_G} \boldsymbol{\phi}_{\mathbf{b}}} \quad [8]$$

As discussed in the previous Section, these partial derivatives with respect to the different parameters can be used to determine which member is the best to replace to improve the critical load of the structure. The following parameter is defined to quantify the influence of changing a specific member (see also Szalai 2010):

$$SIm_i = 100 \frac{\frac{\partial\alpha_{cr}}{\partial I_i}}{\sum_j \frac{\partial\alpha_{cr}}{\partial I_j}} = 100 \frac{\boldsymbol{\phi}_{\mathbf{b}}^{\mathbf{T}} \mathbf{K}^{(i)} \boldsymbol{\phi}_{\mathbf{b}}}{\sum_j \boldsymbol{\phi}_{\mathbf{b}}^{\mathbf{T}} \mathbf{K}^{(j)} \boldsymbol{\phi}_{\mathbf{b}}} \quad [9]$$

where SIm_i is the Parameter Sensitivity Indicator corresponding to member *i* expressed in percentage (the summation in the denominator includes all the members, but not the joints). A similar parameter can be defined for the rotational springs:

$$SIr_i = 100 \frac{\frac{\partial\alpha_{cr}}{\partial Ks_i}}{\sum_j \frac{\partial\alpha_{cr}}{\partial Ks_j}} = 100 \frac{\boldsymbol{\phi}_{\mathbf{b}}^{\mathbf{T}} \mathbf{K}^{(i)} \boldsymbol{\phi}_{\mathbf{b}}}{\sum_j \boldsymbol{\phi}_{\mathbf{b}}^{\mathbf{T}} \mathbf{K}^{(j)} \boldsymbol{\phi}_{\mathbf{b}}} \quad [10]$$

where SIr_i is the Parameter Influence Indicator corresponding to rotational stiffness *i* (the summation in the denominator includes all the joints, but no the members). The members and joints are treated separately because the moments of inertia ($I_{u,i}$ and $I_{b,i}$) and the rotational springs ($K_{b-u,i}$, and $K_{f,i}$) have different dimensional units. In the design

examples included bellow, it will be shown that the SIm_{i} and SIr_{i} parameters can be very useful to the designer to understand the global behavior of a rack structure and the evolution of its design towards the best solution. It is noted that, as discussed at the beginning of the article, the rotational stiffness are not actually independent design parameters of the structure due to its dependence on the members that are connected to the joint. The rotational stiffness are determined experimentally for each particular upright-beam set or upright base connection. Conversely, there is not any mathematical relationship between the member design parameters, $I_{\mathrm{u,i}}$ and $I_{\mathrm{b,i}}$, and the rotational stiffness of the corresponding associated joint. Consequently, the derivatives of α_{cr} with respect to $K_{\mathrm{b-u,i}}$ (or $K_{\mathrm{f,i}}$), as well as SIr_{i}, have to be calculated independently of the member design parameters.

Critical load factor approximation using FEM

The second-order Taylor approximation of $\alpha_{\mathrm{cr}}(\boldsymbol{\psi})$ is used to determine the critical load factor:

$$\alpha_{\mathrm{cr}} \approx Q_{\alpha} = \alpha_{\mathrm{cr}}(\boldsymbol{\psi}_0) + \nabla\alpha_{\mathrm{cr}}(\boldsymbol{\psi} - \boldsymbol{\psi}_0) + \frac{1}{2}(\boldsymbol{\psi} - \boldsymbol{\psi_0})^{\mathbf{T}}\,\mathbf{H}\,(\boldsymbol{\psi} - \boldsymbol{\psi_0}) \qquad [11]$$

where:

$\boldsymbol{\psi}_0$ is the vector of design parameters corresponding to a solution with a known stability factor; $\boldsymbol{\psi}$ is the vector of design parameters corresponding to another solution;

H is the Hessian matrix, its components being:

$$H_{\mathrm{ij}} = \frac{\partial^2\alpha_{\mathrm{cr}}}{\partial\psi_{\mathrm{i}}\,\partial\psi_{\mathrm{j}}} = 2\,\frac{\boldsymbol{\phi}_{\mathbf{b}}^{\mathbf{T}}\left(\mathbf{K}^{(\mathbf{i})} + \frac{\partial\alpha}{\partial\psi_{\mathrm{i}}}\mathbf{K_G}\right)\frac{\partial\boldsymbol{\phi}_{\mathbf{b}}}{\partial\psi_{\mathrm{j}}}}{\boldsymbol{\phi}_{\mathbf{b}}^{\mathbf{T}}\,\mathbf{K_G}\,\boldsymbol{\phi}_{\mathbf{b}}} \qquad [12]$$

$$\frac{\partial\boldsymbol{\phi}_{\mathbf{b}}}{\partial\psi_{\mathrm{j}}} = (\mathbf{K} - \alpha_{\mathrm{cr}}\mathbf{K_G})^{-1}\left(-\mathbf{K}^{(\mathbf{j})} - \frac{\partial\alpha_{\mathrm{cr}}}{\partial\psi_{\mathrm{j}}}\mathbf{K_G}\right)\boldsymbol{\phi}_{\mathbf{b}} \qquad [13]$$

From the computation point of view, the calculation of the stability factor trough equation [11] for all the possible solutions (or for a given group of possible solutions) is much less time consuming than solving [3]. It is noted that this prediction of the critical load factor for any structure is possible without creating and assembling the stiffness matrix at each iteration, since the value of $Q_{\alpha}(\boldsymbol{\psi})$ is calculated with a simple formula. This is the reason why [11] is applied in the design algorithm presented in the next Section. A Taylor linear approximation was tried instead of [11], but it did not work properly.

Design algorithm

A design algorithm is proposed; its objective is to obtain a structure that verifies the code ULS and SLS criteria at the minimum economic cost. The critical load factor prediction presented above is used to make decisions in the final solution search.

The design algorithm (Fig. 3) starts by setting an initial solution, S_0. This solution may be the cheapest one that can be produced with the available profiles, or the cheapest solution derived from some preliminary verifications. For instance, the beam profiles can be selected by carrying out simplified calculations where bending moments are estimated and verified. This will remove part of the possible solutions, usually nonsense, and make the process more efficient.

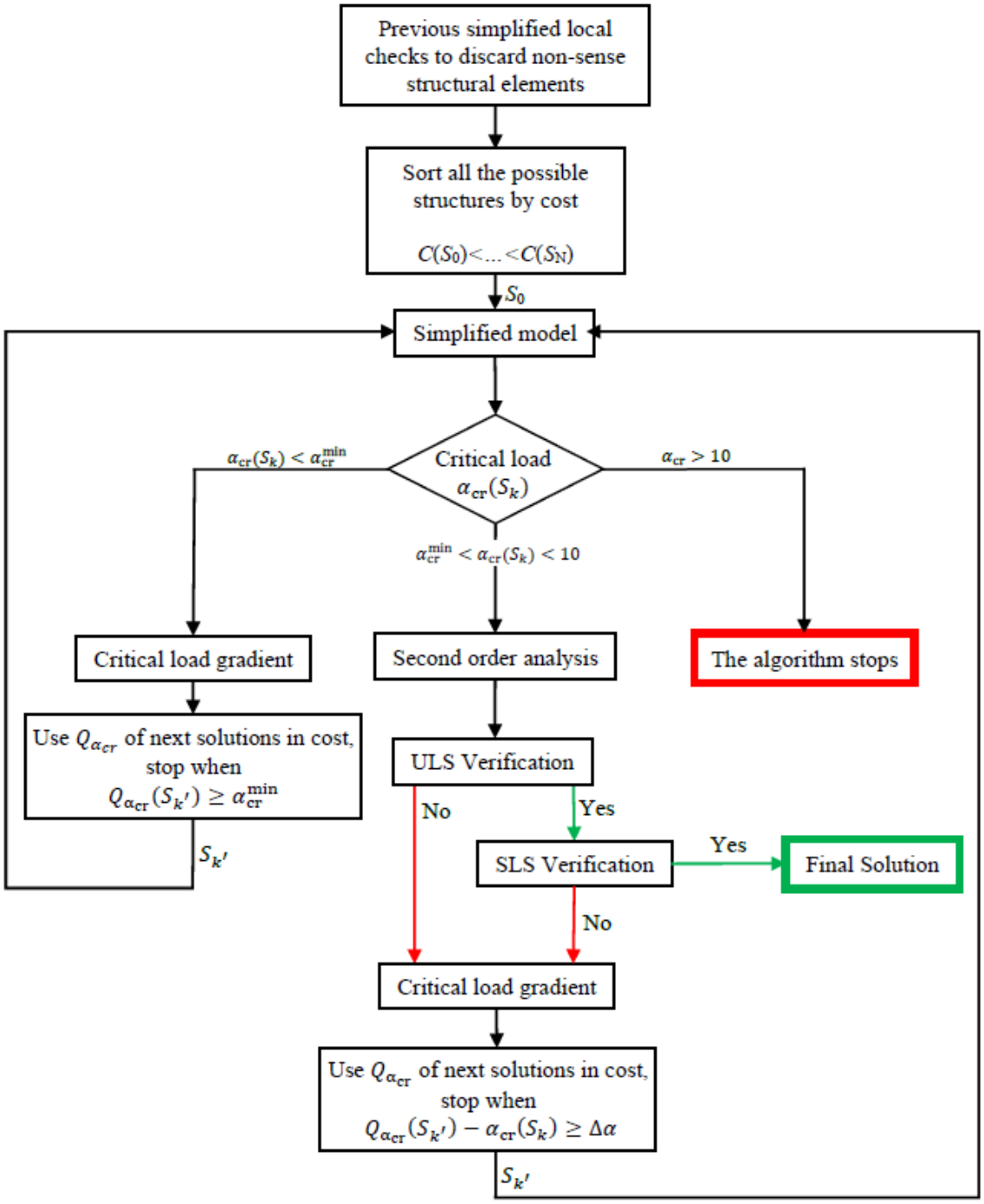

Fig. 3. Design algorithm flow-chart.

Next, the remaining possible solutions S_i are arranged by cost ($C(S_i)$), from lowest to highest: $C(S_0) <\ldots< C(S_n)$. Afterwards, the critical load factor α_{cr} corresponding to S_0 is determined by solving the eigenvalue problem [3] of the single column model. Then, depending on the value of the factor, a decision is made.

If the critical load factor is smaller than α_{cr}^{min}, no ULS or SLS analysis is performed. Instead, the linear critical load prediction [11] is used to find the cheapest solution S_k that fits the condition

$$Q_{\alpha_{cr}}(S_k) \geq \alpha_{cr}^{min} \quad [14]$$

Once a solution fulfilling [14] has been found, it is verified that the actual value of the critical load factor, determined from [3], is higher than α_{cr}^{min}. If it does not verify this condition, another solution $S_{k'}$ fitting [14] is checked. This time, the linear approximation departs from the structure $S_{k'}$. This process is repeated until finding the structure that complies $\alpha_{cr} \geq \alpha_{cr}^{min}$.

When in the structure S_k the critical load factor is greater than α_{cr}^{min} and smaller than 10, the corresponding second order analysis [4] of the single column model is solved. The resulting internal forces are used to perform the ULS and SLS checks pointed out at the beginning of this paper. If S_k verifies the ultimate limit criteria, the algorithm stops. The best solution has been found. Conversely, if S_k fails, the next solution of the cost list, $S_{k'}$, whose $Q_{\alpha_{cr}}(S_{k'})$ complies with [14] is studied, i.e., $S_{k'}$ goes through the whole verification loop from the beginning, as indicated in Fig. 3.

Aiming to speed up the process, the next solution $S_{k'}$ of the cost list is not actually analysed; the idea is to choose a new solution for which a significant structural improvement is achieved. Such new solution, $S_{k'}$, should comply $Q_{\alpha_{cr}}(S_{k'}) - \alpha_{cr}(S_k) \geq \Delta\alpha$; where $\Delta\alpha$ can be calibrated to ensure a significant improvement and a good prediction of $Q_{\alpha_{cr}}(S_{k'})$.

Finally, if $\alpha_{cr} > 10$, it is considered that the global stability does not play any relevant role, and, consequently, it does not make any sense to carry out a design process based of the stability factor, as discussed above. Thus, the algorithm stops.

Along this process, often several structures that have to be evaluated have the same cost; the most stable one is chosen.

Application example

In this Section, the design methodology is applied to the rack structures presented in Figs. 4 and 5. These examples are carried out in two steps. Firstly, the accuracy of the single column model is assessed by comparing the results of a 2nd order analysis (according to

[4]) with those produced by means of a full 2D beam finite element model. Secondly, the proposed design procedure is applied and the resulting solutions are discussed.

In all the examples, the following profiles are considered: i) uprights U_1 to U_5; and ii) beams B_1 to B_4; the properties of these profiles are included in Tables 2 and 3, respectively. Such properties are similar to those of real profiles that can be found in the market. It should be noted that the cost (including manufacturing and erection) is also listed.

Table 2. Beam Properties

Beam	I_{eff} (mm^4)	W_{eff} (mm^3)	f_y (N/mm^2)	Cost (€/m)
B1	407500	12000	355	16.67
B2	600000	15000	355	26.33
B3	800000	20000	355	25.56
B4	100000	25000	355	28.88

Table 3. Upright Properties

Up.	I_{eff} (mm^4)	W_{eff} (mm^3)	A_{eff} (mm^2)	f_y (N/mm^2)	Cost (€/m)
U1	400000	10000	360	355	55.87
U2	700000	20000	500	355	67.00
U3	1200000	30000	560	355	80.45
U4	1650000	35000	600	355	89.39
U5	1750000	40000	720	355	111.73

The stiffness of each upright-to-beam connection is included in Table 4. For simplification, only one upright base stiffness is considered, being $K_f = 84$ kNm/rad.

Table 4. Beam-to-Upright Stiffness K_{u-b} (kNm/rad)

	Beam			
Up.	B1	B2	B3	B4
U1	40	70	80	100
U2	60	80	90	120
U3	100	120	150	190
U4	150	160	175	220
U5	170	190	210	250

Example 1. Single-column model verification

Linear buckling and 2nd order analyses are carried out on the structure of Example 1 by considering the cheapest configuration: U_1 for uprights, and B_1 for beams. All the beams are loaded with a gravity force of $Q = 14$ kN, being uniformly distributed along

their length; no horizontal loading is considered other than the one corresponding to the sway imperfection. This load is calculated from: i) the out-of-plumb $\phi_{imp} = 0.002$ rad; and ii) the following looseness for each beam profile: B_1, $\phi_{l1} = 0.001$ rad; B_2, $\phi_{l2} = 0.00075$ rad; B_3, $\phi_{l3} = 0.0006$ rad; and B_4, $\phi_{l4} = 0.0006$ rad. It is worth mentioning that since only the upright U_1 is finally used in the example, only the looseness corresponding to the U_1-B_i connection is included herein. Both imperfections are finally combined according to EN15512 (2009) to set the horizontal forces to be applied to the model.

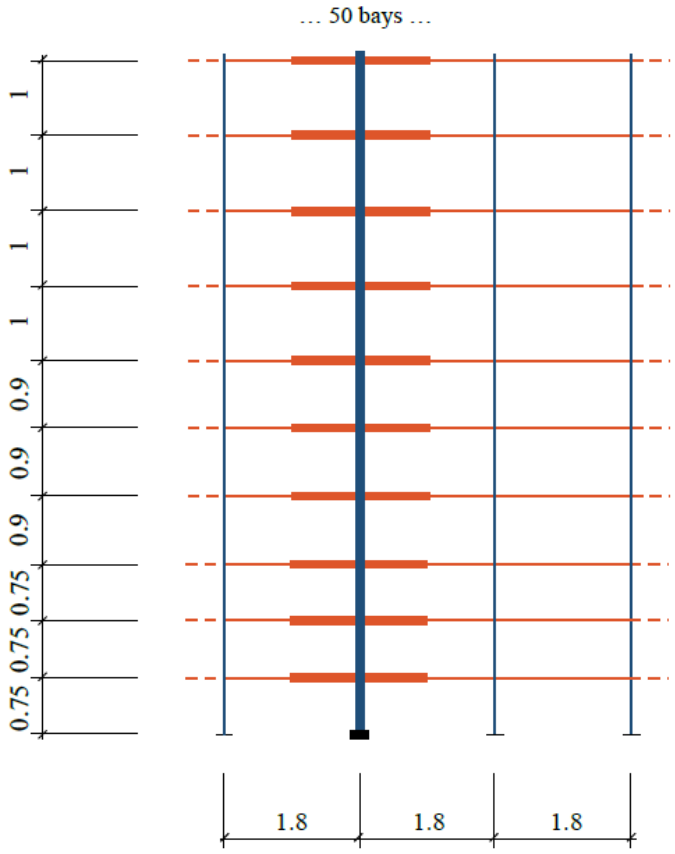

Fig. 4. Structure of Example 1 (dimensions in m.).

The critical stability factors obtained in the analyses are $\alpha_{cr} = 1.230$ and $\alpha_{cr} = 1.235$ for the single-column and full 2D models, respectively; these values can be considered identical. The corresponding buckling modes are also very similar:

-Single column model:

$$\boldsymbol{\phi}_{\mathbf{cr}}^{\mathbf{T}} = \{0, 0.49, 1.11, 1.75, 2.46, 3.03, 3.42, 3.69, 3.85, 3.92, 3.97\}\ 10^{-2}$$

(Displacements)

$$\boldsymbol{\phi}_{\mathbf{cr}}^{\mathbf{T}} = -\{4.96, 7.28, 8.12, 7.94, 6.76, 4.97, 3.30, 1.93, 1.01, 0.51, 0.29\}\, 10^{-6}$$

(Rotations)

-Full 2D model:

$$\boldsymbol{\phi}_{\mathbf{cr}}^{\mathbf{T}} = \{0, 0.49, 1.10, 1.74, 2.45, 3.01, 3.41, 3.69, 3.84, 3.92, 3.97\}\, 10^{-2}$$

(Displacements)

$$\boldsymbol{\phi}_{\mathbf{cr}}^{\mathbf{T}} = -\{4.89, 7.21, 8.07, 7.91, 6.77, 4.99, 3.34, 1.96, 1.04, 0.52, 0.30\}\, 10^{-6}$$

(Rotations)

The results of the 2nd order analysis of the single-column and the full models are compared in Tables 5 to 7 for an intermediate bay. Again, minor errors are observed concerning horizontal displacements, and beam and upright end moments. It should be noted that slightly high differences can be found in some uprights showing low bending moments, but they are not relevant from the design point of view.

Table 5. Example 1: Regular example. Displacements (%)

Level	Full model	Single column	Difference (%)
1	0.765	0.765	0.045
2	0.858	0.859	0.126
3	0.903	0.905	0.221
4	0.917	0.920	0.309
5	0.890	0.894	0.283
6	0.840	0.843	0.297
7	0.772	0.775	0.231
8	0.702	0.705	0.208
9	0.635	0.638	0.154
10	0.576	0.578	0.096

Table 6. Example 1: Column moments (% of the resistance moment)

Level	NODE 1			NODE 2		
	Full	Single column	Difference (%)	Full	Single column	Difference (%)
1	-18.22	-18.19	0.17	-2.51	-2.36	5.89
2	-14.12	-14.29	-1.19	-8.32	-8.29	0.34
3	-10.23	-10.34	-1.10	-10.47	-10.50	-0.25
4	-8.00	-8.08	-1.09	-12.97	-13.08	-0.84
5	-3.52	-3.51	0.11	-12.10	-12.20	-0.82
6	-0.99	-0.95	3.63	-9.61	-9.66	-0.57
7	-0.09	-0.08	12.92	-7.31	-7.34	-0.42
8	0.74	0.77	-3.73	-4.98	-4.99	-0.11
9	0.87	0.89	-1.96	-3.05	-3.05	-0.05
10	0.62	0.63	-2.36	-1.53	-1.51	1.30

Table 7. Example 1: Beam-End Bending Moments (% of the resistance moment)

	NODE 1			NODE 2		
Level	Full	Single column	Difference (%)	Full	Single column	Difference (%)
1	17.66	17.68	0.09	-3.80	-3.80	0.03
2	18.47	18.50	0.19	-3.01	-2.98	1.14
3	18.44	18.48	0.24	-3.05	-3.00	1.64
4	17.61	17.65	0.25	-3.87	-3.83	1.13
5	16.19	16.22	0.16	-5.28	-5.26	0.49
6	14.79	14.80	0.07	-6.69	-6.68	0.19
7	13.48	13.48	0.01	-8.00	-8.00	0.02
8	12.45	12.45	-0.03	-9.03	-9.03	-0.05
9	11.75	11.75	-0.03	-9.72	-9.73	-0.13
10	11.39	11.37	-0.21	-10.12	-10.11	0.06

If the number of bays decreases, the observed differences increase since the periodic nature of the structure is lost. However, the accuracy of results can still be considered reasonably good for pre-design purposes for two reasons: i) the safety of the final design is not compromised, as a further detailed verification is yet to be done, and ii) the most relevant elements for design purposes show the smallest differences in the comparison. As expected, the accuracy of this model is higher for racks with many bays; fortunately, in such structures the provided savings are more important. For instance, Tables 8-10 (corresponding to a structure similar to that of Example 1, but with 15 bays) show that the relevant differences do not exceed 5%.

Table 8. Example 1 with 15 bays: Displacements (%)

Level	Full model	Single column	Difference (%)
1	0.770	0.765	0.454
2	0.808	0.859	4.148
3	0.853	0.905	4.414
4	0.870	0.920	4.382
5	0.847	0.894	3.915
6	0.801	0.843	3.356
7	0.739	0.775	2.706
8	0.673	0.705	2.138
9	0.610	0.638	1.686
10	0.554	0.578	1.328

Table 9. Example 1 with 15 bays: Column moments (% of the resistance moment)

Level	NODE 1			NODE 2		
	Full	Single column	Difference (%)	Full	Single column	Difference (%)
1	-18.22	-18.19	0.17	-2.51	-2.36	5.89
2	-14.12	-14.29	-1.19	-8.32	-8.29	0.34
3	-10.23	-10.34	-1.10	-10.47	-10.50	-0.25
4	-8.00	-8.08	-1.09	-12.97	-13.08	-0.84
5	-3.52	-3.51	0.11	-12.10	-12.20	-0.82
6	-0.99	-0.95	3.63	-9.61	-9.66	-0.57
7	-0.09	-0.08	12.92	-7.31	-7.34	-0.42
8	0.74	0.77	-3.73	-4.98	-4.99	-0.11
9	0.87	0.89	-1.96	-3.05	-3.05	-0.05
10	0.62	0.63	-2.36	-1.53	-1.51	1.30

Table 10. Example 1 with 15 bays: Beam-End Bending Moments (% of the resistance moment)

Level	NODE 1			NODE 2		
	Full	Single column	Difference (%)	Full	Single column	Difference (%)
1	17.26	21.22	-2.46	-5.05	-4.56	9.60
2	18.08	22.21	-2.37	-4.09	-3.57	12.65
3	18.08	22.18	-2.25	-4.08	-3.60	11.88
4	17.33	21.18	-1.84	-4.97	-4.59	7.67
5	16.02	19.47	-1.26	-6.55	-6.31	3.68
6	14.69	17.76	-0.73	-8.15	-8.02	1.63
7	13.44	16.18	-0.33	-9.65	-9.60	0.53
8	12.44	14.94	-0.02	-10.85	-10.84	0.07
9	11.76	14.10	0.07	-11.65	-11.68	-0.24
10	11.41	13.64	0.32	-12.13	-12.13	-0.03

Example 1. Design algorithm

The design algorithm is applied to Example 1 considering the following loading combinations:

-ELU: $1.4\left(Q+Q_{\mathrm{imp}}\right)$

-ELS: $\left(Q+Q_{\mathrm{imp}}\right)$

The 1.4 factor is set according to the EN15519 (2009). The initial solution (S_0) is the cheapest one, which has already been presented in the previous Section. The chosen algorithm parameters are $\alpha_{\mathrm{cr}}^{\mathrm{min}}=1.5$ and $\Delta\alpha=0.0$, see Fig. 3. Noticeably, the chosen value of α_{cr}^{min} is rather low, and represents a rather potentially unstable situation; even it does not fulfill some code design recommendations (EN 16681 2016) for seismic situations. It has been chosen as being, to a certain extent, common in actual racks, and to analyze the performance of the proposed algorithm in such situations.

A valid solution is achieved after four iterations. Table 11 shows the resulting profiles and the cost of the structure. It is worth mentioning that it was decided to use the same upright profile in all the levels of the rack, as commonly occurs in practice. Consequently, Table 11 shows only one column for the upright solution. The results of the ELS and ULS verifications expressed in terms of utilization percentage are (maximum values within the structure):

Table 11. Example 1: Evolution of the design solution at iteration *i* of the algorithm.

S_i	Q_α	α_{cr}	Up.	Beam at level:										Cost
				1	2	3	4	5	6	7	8	9	10	(€)
1	-	1.23	U1	B1	B1	B1	B1	B1	B1	B1	B1	B1	B1	55500
2	1.50	1.49	U1	B1	B2	B2	B1	B1	B1	B1	B1	B1	B1	58300
3	1.53	1.53	U1	B1	B2	B3	B1	B1	B1	B1	B1	B1	B1	58700
4	1.56	1.57	U1	B1	B3	B3	B1	B1	B1	B1	B1	B1	B1	58900
5	1.60	1.60	U1	B1	B4	B1	B2	B1	B1	B1	B1	B1	B1	59100

-ELU: beams 98%; uprights 98%; joints 48%.

-ELS: sway displacement 56%; beam deflection 64%.

The ELU verifications have been carried out considering resistance values similar to real experimental values obtained from the tests mentioned in the second Section of this paper.

The *SI* values of the different solution (S_i) are determined and discussed. Tables 12 and 13 show the *SI* values corresponding to the beam-upright joint stiffness and the beams, respectively. It can be observed that for the beams the higher values correspond to the lower levels of the rack. This is consistent with the decisions taken by the design algorithm, which proposed to upsize those members of these levels showing the highest *SI* (see Table 11). It is noted that, for the fourth iteration, this consistency does not occur. This can be explained because, for solution S_4, the H term of the α approximation [11] is more relevant than the $\nabla\alpha$ term. The latter term is directly reflected in the SI's, conversely, the former is not. It is reasonable that such consistent results are obtained because: i) the solutions considered should show an increase in stability factor higher than the minimum $\Delta\alpha$. Consequently, the solutions with low *SI* values are eliminated (in this example, however, $\Delta\alpha$ was taken equal to 0 and has no influence); and ii) when there is more than one solution with the same cost, the algorithm always selects the solution with

the highest stability factor. For instance, in the second iteration (from S_2 to S_3) in Table 11, the cost of switching one B2 to B3 is the same for level two and three, but, in the end, B3 is introduced in the third level because the resulting stability factor is higher than for the other solution.

Table 12. Example 1: Parameter Sensitivity Indicator for Rotational Spring Stiffness, SI_r

Iteration	Level									
	1	2	3	4	5	6	7	8	9	10
1	19.76	24.55	23.49	17.05	9.19	4.06	1.38	0.38	0.10	0.03
2	19.42	14.98	14.85	20.59	15.95	9.00	3.66	1.14	0.31	0.10
3	17.25	12.00	12.45	21.22	18.65	11.39	4.90	1.57	0.43	0.15
4	20.45	14.67	13.24	19.87	16.38	9.62	4.02	1.27	0.35	0.12

Table 13. Example 1: Parameter Sensitivity Indicator for Beam Inertias, SI_m

Iteration	Level									
	1	2	3	4	5	6	7	8	9	10
1	19.76	24.55	23.49	17.05	9.19	4.06	1.38	0.38	0.10	0.03
2	17.29	18.84	18.67	18.33	14.20	8.02	3.26	1.01	0.27	0.09
3	19.19	19.45	12.90	18.64	15.37	9.03	3.78	1.20	0.33	0.11
4	17.09	12.34	12.80	21.03	18.47	11.28	4.85	1.56	0.43	0.15

To close this example, the structure is designed following a conventional manufacturer's approach, and the resulting solution is compared to the one obtained with the methodology proposed herein. If the design process is not systematized and automated in some way, the option of changing the beam of only one level is not considered. This is because the amount of possible solutions is very high, and the selection process would be very slow. For example, in the present example more than 5 million combinations are possible (of course, some of them do not make sense). Consequently, the same beam cross-section is used in all levels.

When the conventional approach is applied to Example 1, the solutions are firstly sorted by cost. Afterwards, as in the previous method, the initial solution is taken equal to the cheapest one, which does not satisfy the ELU and ELS design criteria. Then, the next solution in terms of cost is studied: U_1 for the uprights and B_2 for all beams. This solution is already good, showing $\alpha_{cr} = 1.83$, and the following utilization ratios:

-ELU: beams 78%; uprights 96%; joints 31%.

-ELS: sway displacement 45%; beam deflection 52%.

More conservative values are obtained, but the final cost is, obviously, higher: 67500 €. It should be noted that this structure is 8400 € more expensive per aisle (14% more expensive), see last row of Table 11.

As discussed previously, the value of $\alpha_{cr}^{min} = 1.5$ is rather low; therefore, this example has been also worked using $\alpha_{cr}^{min} = 3$. The results are shown in Table 14; it shows that, under this requirement, the algorithm reaches a value of α_{cr} that is very close to the required one in only two steps, and that many members are changed, mainly in the bottom levels.

Table 14. Example 1 ($\alpha_{cr}^{min} = 3$): Evolution of the design solution at iteration i of the algorithm

S_i	Q_α	α_{cr}	Up.	Beam at level:										Cost
				1	2	3	4	5	6	7	8	9	10	(€)
1	-	1.23	U1	B1	B1	B1	B1	B1	B1	B1	B1	B1	B1	55500
2	3.13	3.02	U2	B4	B4	B4	B4	B2	B2	B1	B1	B1	B1	71200

Example 2. Single-column model verification

A second example is included aiming to show that the proposed single-column model and design algorithm can work properly when applied to rack structures with some kind of singularity in the down aisle direction. In Fig. 5, It can be observed that the structure of Example 2 is the same as that of Example 1, except for the fact that the last four upper levels have been removed from the first half of the rack.

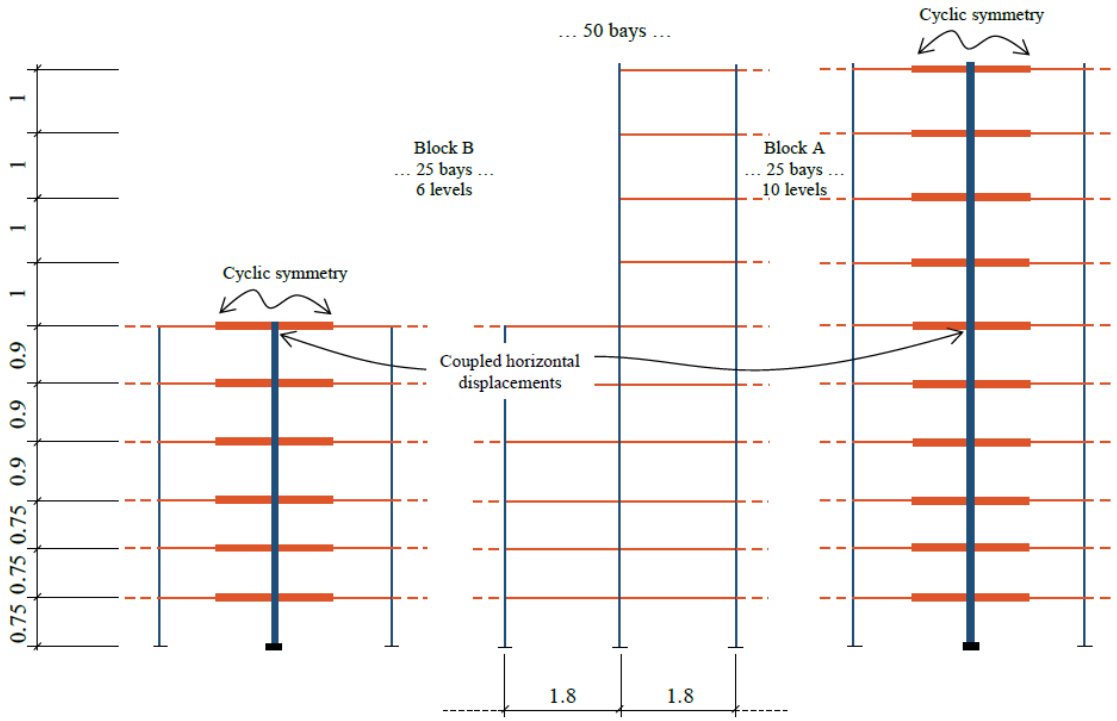

Fig. 5. Structure of Example 2 (dimensions in m.).

The single column model is applied to this structure, but this time two columns are considered, one for each block of the rack (Fig. 5). The degrees of freedom and couplings of each column model are the same as those used in Example 1. However, additional couplings have to be added to link both column models. It is imposed that the upright nodes at the same level of each model should have the same displacement (see Fig.5).

Linear buckling and 2nd order analyses are performed considering the same loading as in Example 1. The results of the analyses are compared with the results of a full 2D finite element model. The critical stability factors obtained are $\alpha_{cr} = 1.384$ and $\alpha_{cr} = 1.377$ for the single-column model and full model, respectively. There seems to be a good agreement. The corresponding buckling modes are also similar:

-Single column model:

$$\boldsymbol{\phi}_{\mathbf{cr}}^{\mathbf{T}} = \{0, 0.61, 1.17, 1.61, 2.00, 2.27, 2.43, 2.55, 2.62, 2.66, 2.68\}\ 10^{-2}$$

(Displacements)

$$\boldsymbol{\phi}_{\mathbf{cr}}^{\mathbf{T}} = -\{7.87, 7.53, 6.30, 4.90, 3.39, 2.16, 1.39, 0.85, 0.46, 0.23, 0.13\}\ 10^{-6}$$

(Rotations)

-Full model:

$$\boldsymbol{\phi}_{\mathbf{cr}}^{\mathbf{T}} = \{0, 0.61, 1.16, 1.60, 1.99, 2.26, 2.43, 2.55, 2.62, 2.65, 2.67\}\, 10^{-2}$$

(Displacements)

$$\boldsymbol{\phi}_{\mathbf{cr}}^{\mathbf{T}} = -\{7.83, 7.50, 6.28, 4.90, 3.39, 2.17, 1.40, 0.86, 0.47, 0.24, 0.14\}\, 10^{-6}$$

(Rotations)

Tables 15 to 17 also show a reasonably good agreement when comparing results of the 2nd order analysis (large differences correspond to members with low bending moments).

Table 15. Example 2: Displacements (%)

Block	Level	Full model	Single column	Difference (%)
A	1	0.63	0.64	1.57
	2	0.60	0.61	1.36
	3	0.57	0.58	1.15
	4	0.53	0.53	0.93
	5	0.48	0.49	0.75
	6	0.44	0.44	0.55
	7	0.40	0.40	0.44
	8	0.37	0.37	0.35
	9	0.34	0.34	0.28
	10	0.31	0.31	0.17
B	1	0.63	0.64	1.71
	2	0.60	0.61	1.41
	3	0.57	0.58	1.18
	4	0.53	0.53	0.97
	5	0.48	0.49	0.75
	6	0.44	0.44	0.65

Table 16. Example 2: Column Bending Moments (% of the resisting moment)

Block	Level	NODE 1			NODE 2		
		Full	Single column	Difference (%)	Full	Single column	Difference (%)
A	1	-6.73	-6.84	-1.63	-7.57	-7.77	-2.66
	2	-3.96	-3.91	1.22	-7.91	-8.12	-2.68
	3	-2.30	-2.21	4.01	-6.89	-7.06	-2.46
	4	-1.82	-1.71	6.32	-6.30	-6.41	-1.72
	5	-0.62	-0.57	9.02	-4.94	-5.17	-4.58
	6	-0.27	-0.06	77.56	-2.68	-2.58	3.55
	7	-1.59	-1.67	-4.91	-3.11	-3.18	-2.20
	8	-0.50	-0.43	14.67	-2.79	-2.79	-0.07
	9	0.17	0.17	-2.64	-1.96	-3.05	-2.57
	10	0.24	0.31	-26.75	-1.13	-1.51	2.96
B	1	-6.71	-6.82	-1.66	-7.47	-7.76	-3.75
	2	-4.04	-3.90	3.48	-8.01	-8.11	-1.24
	3	-2.22	-2.19	1.70	-6.97	-7.02	-0.72
	4	-1.74	-1.72	0.94	-6.36	-6.47	-1.71
	5	-0.57	-0.44	21.78	-4.94	-4.81	2.70
	6	-0.31	-0.43	-40.59	-3.90	-3.92	-0.53

Table 17. Example 2: Beam-End Bending Moments (% of the resisting moment)

Block	Level	NODE 1			NODE 2		
		Full	Single column	Difference (%)	Full	Single column	Difference (%)
A	1	15.56	15.60	-0.22	5.90	5.88	0.20
	2	15.00	15.03	-0.20	6.46	6.45	0.06
	3	14.36	14.38	-0.12	7.09	7.10	-0.07
	4	13.61	13.63	-0.09	7.85	7.85	-0.05
	5	12.92	12.89	0.18	8.53	8.59	-0.67
	6	12.49	12.49	-0.07	8.87	8.98	-1.29
	7	12.24	12.23	0.05	9.21	9.25	-0.37
	8	11.84	11.82	0.19	9.64	9.66	-0.17
	9	11.45	11.44	0.07	10.02	10.04	-0.19
	10	11.23	11.20	0.27	10.29	10.28	0.09
B	1	15.54	15.60	-0.35	5.91	5.88	0.37
	2	15.00	15.03	-0.20	6.45	6.45	0.01
	3	14.37	14.38	-0.11	7.09	7.10	-0.09
	4	13.62	13.62	0.01	7.84	7.86	-0.25
	5	12.94	12.92	0.11	8.53	8.56	-0.24
	6	12.31	12.37	-0.54	9.13	9.11	0.31

It is worth to point out that a more sophisticated column model was tested in the study, where three columns had been considered: one column for the lower block, one for the higher, and one for the transition from the lower to the higher. The results obtained with this three-column model were somewhat worse than those presented above for the two-column model. That is the reason why the former was dismissed.

These results show that the proposed method can be applied to irregular structures provided that a sufficient number of columns are added to the single column model, and appropriate boundary conditions are considered. As well, simple non-uniform loading patterns, such as those required in (EN15512 2009), can also be analyzed with this approach. However, if the structure or the load pattern are very irregular, the use of the single column approach is not suitable because this single-column model would need a number of columns similar to that of the rack.

Example 2. Design algorithm

Table 18 displays results for Example 2. The final solution is reached as:

1. In the first iteration (S_1 to S_2), the stability increase is provided by upsizing the beams of the two first levels of the higher block (A).

2. In the second iteration (S_2 to S_3), the SI_{m} of the uprights of the lower (B) and higher (A) blocks are 49 % and 51 %, respectively. This means that, from the stability point of view, it is slightly better to upsize the higher block uprights; however, that strategy is more expensive because the uprights are longer. Therefore, the lower block uprights are upsized instead.

3. In the third iteration (S_3 to S_4), reinforcing the beams of the first level of block B is more effective, because the stiffness of the U_2-B_i connections are higher than those of the U_1-B_i ones.

Table 18. Example2: Evolution of the design solution of the algorithm.

			Block A										Block B							Cost (€)
				Beam at level:										Beam at level:						
S_i	Q_α	α_{cr}	Up.	1	2	3	4	5	6	7	8	9	10	Up.	1	2	3	4	5	6	
1	-	1.08	U1	B1	B1	B1	B1	B1	B1	B1	B1	B1	B1	U1	B1	B1	B1	B1	B1	B1	43413
2	1.50	1.50	U1	B2	B1	B1	B1	B1	B1	B1	B1	B1	B1	U1	B2	B1	B1	B1	B1	B1	44613
3	1.53	1.53	U1	B1	B1	B1	B1	B1	B1	B1	B1	B1	B1	U2	B1	B1	B1	B1	B1	B1	45913
4	1.61	1.62	U1	B1	B1	B1	B1	B1	B1	B1	B1	B1	B1	U2	B2	B1	B1	B1	B1	B1	46513

The utilization ratios of the resulting structure are:

-ELU: beams 99%; uprights 96%; joints 51%.

-ELS: sway displacement 88%; beam deflection 76%.

Conclusions

A simplified stability-based method for practical pre-design of down-aisle unbraced selective racks is presented; only a single upright and their adjoining half beams are modelled, being discretized with 2-D bar elements. The proposed strategy is significantly faster than the conventional design approaches and yields less expensive structures; in this sense, this paper shows that a design procedure based on improving the stability can lead to cost reduction.

The use of this method has provided some meaningful remarks: the key role of beams in improving in an inexpensive way the global stability (even not upsizing all the beams), and the fact that the final solution might not be obvious.

Notation

The following symbols are used in this paper.
Main symbols
A: Area
C: Condition (for SLS), Cost
E: Demand (for ULS)
SIm, SIr: Parameter Sensitivity Indicator for member (m) and for rotational stiffness (r)
$\mathbf{F}$, f: External force vector, Resistance (stress)
$\mathbf{H}$, H: Hessian matrix, Coefficient of the Hessian matrix
I: Moment of inertia
$\mathbf{K}$, K: Stiffness matrix, Stiffness coefficient
m: Member
N: Axial force
Q: Variable (live) load, Quadratic approximation
R: Resistance (for ULS)
S: Design solution
W: Sectional modulus
α: Linear stability factor
Δ: Increment

$\boldsymbol{\phi}$; ϕ: Buckling mode, Displacement vector; Out of plumb angle, Looseness angle

ψ: Design parameter

Subscripts and superscripts

b: Beam, Buckling

cr: Critical

d: Design

e: Element

eff: Effective

f: Floor

G: Geometric

i, *k*: Numbers

imp: Imperfection

j: Joint, Number

l: Looseness

min: Minimum

n: Number of elements

r: Rotational spring

u: Upright

y: Yielding

0: Initial

Data Availability Statement

Some or all data, models, or code that support the findings of this study are available from the corresponding author upon reasonable request.

Some or all data, models, or code generated or used during the study are proprietary or confidential in nature and may only be provided with restrictions.

References

AISI (American Iron and Steel Institute). 2016. *North American Specification for the Design of Cold-Formed Steel Structural Members*. AISI S100-16, American Iron and Steel Institute, Washington, DC: AISI.

Bernuzzi C., Gobetti A.,Gabbianelli G.,Simoncelli M. 2014. "Warping influence on the resistance of uprights in steel storage pallet racks" J. Const. Steel Research 101, 224–241. https://doi.org/10.1016/j.jcsr.2014.05.014

Bernuzzi C., Gobetti A.,Gabbianelli G.,Simoncelli M. 2015. "Simplified Approaches to Design Medium-Rise Unbraced Steel Storage Pallet Racks. I: Elastic Buckling Analysis" J. Struct. Eng. 141(11). https://doi.org/10.1061/(ASCE)ST.1943-541X.0001271

Bernuzzi C., Gobetti A.,Gabbianelli G.,Rosti A. 2016. "Beam design for steel storage racks" J. Const. Steel Research 116, 156-172. https://doi.org/10.1016/j.jcsr.2015.09.007

Bonada J., Casafont M., Roure F., Pastor M.M. 2018. "Introduction of sectional constraints in a first-order GBT formulation for open-cross sections." Eight International Conference on Thin-Walled Structures, Lisboa, Portugal.

Casafont M., Bonada J., Pastor M.M., Roure F., Susin A. 2017. "Linear buckling analysis of perforated cold-formed steel storage rack columns by means of the Generalised Beam Theory." International Journal of Structural Stability and Dynamics, 18(1), 1-32. https://doi.org/10.1142/S0219455418500049

CEN (European Committee for Standardisation). 2002. *Basis of structural design.* EN1990. Brussels, Belgium: CEN.

CEN (European Committee for Standardisation). 2005. *Design of steel structures – Part 1-1: General rules and rules for buildings.* EN1993-1-1. Brussels, Belgium: CEN.

CEN (European Committee for Standardisation). 2016. *Steel static storage systems- Adjustable pallet racking systems – Principles for seismic design.* EN16681. Brussels, Belgium: CEN.

CEN (European Committee for Standardisation). 2009. *Steel static storage systems- Adjustable pallet racking systems – Principles for structural design.* EN15512. Brussels, Belgium: CEN.

CEN (European Committee for Standardisation). 2008. *Steel static storage systems- Adjustable pallet racking- Tolerances, deformations and clearances.* EN15620. Brussels, Belgium: CEN.

CEN (European Committee for Standardisation). 2016. *Steel static storage systems- Adjustable pallet racking systems – Principles for structural design* prEN15512. Brussels, Belgium: CEN.

Cheng B., Wu Z.Y. 2015. "Simplified Method for Calculating the Lateral Stiffness of Drive-In Storage Racks" Pract.. Per. on Struct. Design and Const. 21(1). https://doi.org/10.1061/(ASCE)SC.1943-5576.0000266

Crosbie M.W.J. 1998. "The design and analysis of static pallet racking systems." Master Thesis, Sheffield Hallam University, Sheffield, U.K.

Farkas J., Jarmai K. 2013. *Optimum Design of Steel Structures* Springer, Hungary.

Godley, M. H. R. 2002. *The Behaviour of Drive-in Storage Structures*. International Specialty Conference on Cold-Formed Steel Structures, Orlando, Florida, USA.

Hua V., Rasmussen K. 2006. "The behaviour of drive-in racks under horizontal impact load". Research report no R871. School of Civil Engineering Sydney, The University of Sydney, Sydney.

Liu M. 2015. "Fast Procedure for Practical Member Sizing Optimization of Steel Moment Frames". Pract.. Per. on Struct. Design and Const. 20(4). https://doi.org/10.1061/(ASCE)SC.1943-5576.0000240

Manickarajah D., Xie M., Steven G. 2000. "Optimisation of columns and frames against buckling" Computers and Structures 75, 45–54. https://doi.org/10.1016/S0045-7949(99)00082-6

Mueller M., Liu M., Burns S. 2002. "Fully Stressed Design of Frame Structures and Multiple Load Paths" J. Struct. Eng. 128(6). https://doi.org/10.1061/(ASCE)0733-9445(2002)128:6(806)

Nocedal J. Wright S. J. 2006. "Numerical Optimization", 2nd Ed., Springer New York.

Perelmuter A., Slivker V. 2001. "The Problem of Interpretations of the Stability Analysis Results" European Conf. on Comp. Mech., Cracow, Poland.

Sena F., Rasmussen K. 2016. "Finite element (FE) modelling of storage rack frames" J. Const. Steel Research 126, 1–14. https://doi.org/10.1016/j.jcsr.2016.06.015

Szalai J. 2010. "Use of eigenvalue analysis for different levels of stability design" SDSS'Rio 2010 Stability and Ductility of Steel Structures, Rio de Janeiro, Brazil.

Tilburgs K. 2013. “Those peculiar structures in cold-formed steel:“racking & shelving”” Steel Const. Design and Research 6 (2), 95-106. https://doi.org/10.1002/stco.201310016

Trouncer A, Rasmussen,K 2016. “Ultra-light gauge steel storage rack frames. Part 2 – Analysis and design considerations of second order effects” J. Const. Steel Research 124 37-46. https://doi.org/10.1016/j.jcsr.2016.05.015

3 NUMERICAL INVESTIGATION ON A SEISMIC TESTING CAMPAING ON ADJUSTABLE PALLET RACK SPEED-LOCK CONNECTIONS

3.1.1 Article data

Title: Numerical investigation on a seismic testing campaign on adjustable pallet rack speed-lock connections. Engineering Structures. Pending
Authors: O. Bové, M. Ferrer, F. López-Almansa, F. Roure

Journal: Engineering Structures

DOI: 10.1016/j.engstruct.2021.113653

3.1.2 Transcription of the original paper

Numerical investigation on a seismic testing campaign on adjustable pallet rack speed-lock connections

Oriol Bové[1], Miquel Ferrer[2], Francisco López-Almansa[3], Francesc Roure[4]

[1] Assistant Professor, Universitat Politècnica de Catalunya – Barcelona Tech, Dept. of Strength of Materials and Structural Engineering, Barcelona, oriol.bove@upc.edu
[2] Professor, Universitat Politècnica de Catalunya – Barcelona Tech, Dept. of Strength of Materials and Structural Engineering, Barcelona, Barcelona, miquel.ferrer@upc.edu
[3] Professor, , Universitat Politècnica de Catalunya – Barcelona Tech, Architecture Technology Department, Barcelona, francesc.lopez-almansa@upc.edu
[4] Professor, Universitat Politècnica de Catalunya – Barcelona Tech, Dept. of Strength of Materials and Structural Engineering, Barcelona, francesc.roure@upc.edu

ABSTRACT

This paper presents numerical simulations of a suite of cantilever seismic tests of speed-lock connections between beam and upright members of adjustable pallet rack systems. The tested specimens differ in the endplate-to-beam weld beads geometric configuration; the experimental results show that each weld configuration leads to different behavior, significantly affecting the connection capacity and ductility. As a result, the performed numerical simulations aim to better understand and deepen these observations. Special attention is paid to the initial (elastic) behavior of the tested assembly, albeit the stress redistribution after the first yielding has also been studied and found to be relevant. The numerical results are satisfactory compared with the experimental ones, and specific remarks are derived. This work is a part of a broader research effort aimed to improve the dissipative seismic behavior of racks; such research activity involves also upright-base plate connections testing, advanced numerical simulation, and proposal of rack ductility behavior factors.

Keywords: *Adjustable pallet racking, Numerical simulation, Beam-upright connection, Seismic Performance, Weld Path*

Introduction

Adjustable pallet-rack systems are heavy-duty steel-shelved structures intended to store goods; they consist mainly of bar-like elements that are vertical (uprights) and horizontal (beams). Commonly, that structural members are made of thin-gauge cold-formed steel profiles; also, in order to facilitate the rack erection, speed-lock (boltless) upright-beam connections are frequently employed, being based on inserting hooks into upright perforations (tabs). Figure 4.a depicts such a connection (under test). Figure 4.a shows that the beam is welded to a vertical L-shaped (folded angle) endplate; the aforementioned hooks belong to that plate.

The elements of the pallet racks and their connections are rather complex; therefore their structural parameters (stiffness, strength, ductility, energy dissipation capacity, among others) need to be obtained through testing. On the other hand, numerical simulation of such experiments is necessary to corroborate the results, to better understand the observed behavior, and to calibrate the utilized numerical model. Uprights are important elements, both for gravity and lateral actions; therefore, many experiments have been performed. Works [1 - 3] present numerical simulations of tests of uprights; these studies highlight the influence of instabilities in their strength and stiffness. Moving to connections between different members, upright-beam joints, apart from exhibiting a highly complex behavior, are the main source of ductility (together with floor connections). Given this situation, a relevant worldwide experimental research effort on the cyclic behavior of these connections has been undertaken [4 - 12].

As a part of the experimental activity mentioned in the previous paragraph, the authors performed a testing campaign on a number of upright-beam connections [13, 14]; the tested specimens mainly differ in the weld path between the endplate and the beam. The results of the experiments showed a relevant influence of the weld beads geometric configuration in the connection strength and ductility. Therefore, the objective of this paper is to simulate the conducted tests numerically in order to confirm and deepen the observed remarks, and to gain knowledge into the connection behavior, mainly regarding the influence of the aforementioned weld beads. Notice that, although both seismic monotonic and cyclic tests were performed, only the monotonic ones are simulated in this paper, as the performed numerical analyses are aimed to obtain accurate and reliable

results, and this objective is rather unrealistic in advanced stages of the connection degradation. In fact, the cyclic behavior of beam-to-upright connections can be generally described with simplified moment-rotation hysteretic models directly calibrated with experimental results: Saws [15], Pinching 4 [16], and the pinching model by [17]).

State-of-the-art of numerical analyses of beam-upright connections

Apart from the papers cited in section 0, the following recent research papers focus on numerical simulation of tests of beam-to-column connections:

- **[Aguirre 2004].** This paper [18] analyses monotonic and cyclic tests on boltless beam-to-upright connections. It is concluded that these connections cannot be considered as perfectly rigid. Additionally, a change in the behavior of the connection after the yielding of the hooks is highlighted; this phenomenon leads to a premature failure of the beam due to stresses redistributions. Finally, the author concludes that these connections do not provide the necessary lateral stability to withstand seismic actions.
- **[Bajoria et al. 2006]**. This paper [19] describes two types of experiments on beam-to-upright connections: the (conventional) single cantilever test and a newly proposed double cantilever test; the first type is intended for external uprights (i.e. just one beam is framed to them) while the second one is oriented to internal uprights (two beams are framed to them). Both types of experiments refer to gravity loads only. The performed tests are simulated numerically using ANSYS software; an adequate agreement is obtained.
- **[Shah et al. 2017]**. This study [20] deals with double cantilever tests under gravity loads. The numerical simulations are performed with ABAQUS by using 3D (solid) finite elements; numerical and experimental results are satisfactorily compared. The effect of the tab thickness (among other parameters) is deeply studied.
- **[Gusella et al. 2018].** In this study [21], monotonic and cyclic experiments on bolted and speed-lock connections of adjustable pallet racks are presented. The tested connections differ in the weld layout, the number of hooks, and the relative thickness of the upright and the beam-end connector. It is concluded that the weld layout plays a decisive role in the failure mode.
- **[Lyu et al. 2018]**. This work [22] refers to cyclic single cantilever tests. Such proofs are numerically simulated by using ABAQUS; the backbone response is successfully

reproduced. The influence of several geometrical parameters (mainly the beam-end connector thickness and clearance) in the connection stiffness and ductility is numerically investigated.

- **[Vujanac et al. 2020]**. This research [23] proposes a simple polynomial formula that describes the connection behavior; this expression is calibrated with monotonic cantilever tests. Numerical FEM simulations using NX Nastran and LS-Dyna software are performed; the fit between the numerical, analytical (linear) and experimental results is correct. The influence of the column and beam wall thickness and height on the behavior of the connection is investigated.

This study belongs to the context of these previous works; the main novelty lies in the simulation of a new suit of monotonic and cyclic experiments, and, mainly, in the particular objectives of the numerical simulation (section 0). Regarding this last issue, the numerical model is not intended to obtain global connection parameters (stiffness, strength and ductility), but to analyze deeply particular details; in this sense, it needs accuracy in the nearby of the weld. As a consequence, special attention is paid to the constructional detail of the beam profile, and to all the mechanical issues that can affect the stress flow in the studied zone. Conversely, the behavior near failure is out of the scope of the performed analyses; this is mainly because high accuracy would be required in order to provide reliable conclusions, and such accuracy is difficult to obtain in severely damaged elements.

Simulated experiments

As stated in section 0, the performed tests are described in [13, 14]; a brief summary is included next. Figure 4 shows that the specimens are T-shaped and full-scaled, and consist of a 600 mm long beam horizontal segment connected to the mid-section of a 500 mm high upright vertical segment; monotonic and cyclic vertical displacement laws are imposed to the end section of the cantilevered beam segment by a driving jack (Figure 4.b). The monotonic tests are just intended to define the bounds of the cyclic proofs, which are continued until failure; as depicted in Figure 4.b, tests can be either downward (hogging, F positive) or upward (sagging, F negative). As discussed in section 0, only the monotonic tests are analyzed in this paper; such tests are performed according to regulations [24, 25].

In all the experiments, the upright segment is slightly compressed by a jack (Figure 4.a) in order to avoid uplift when the beam is being pushed up; no more compression is exerted on the upright. Also, a constant 5 kN force (Figure 4.b) is applied to the beam (near the endplate) to prevent the hooks' pull-out for sagging and cyclic tests. The upright segment is pinned at its top and bottom ends; all DOF's are restrained in both sections. Regarding the beam segment, its right end is free to rotate with respect to *z* and *y* axes (bending) while the rotation with respect to *x* axis (torsion) is restrained. Finally, Figure 4.b shows that there is a gap between the endplate and the upright.

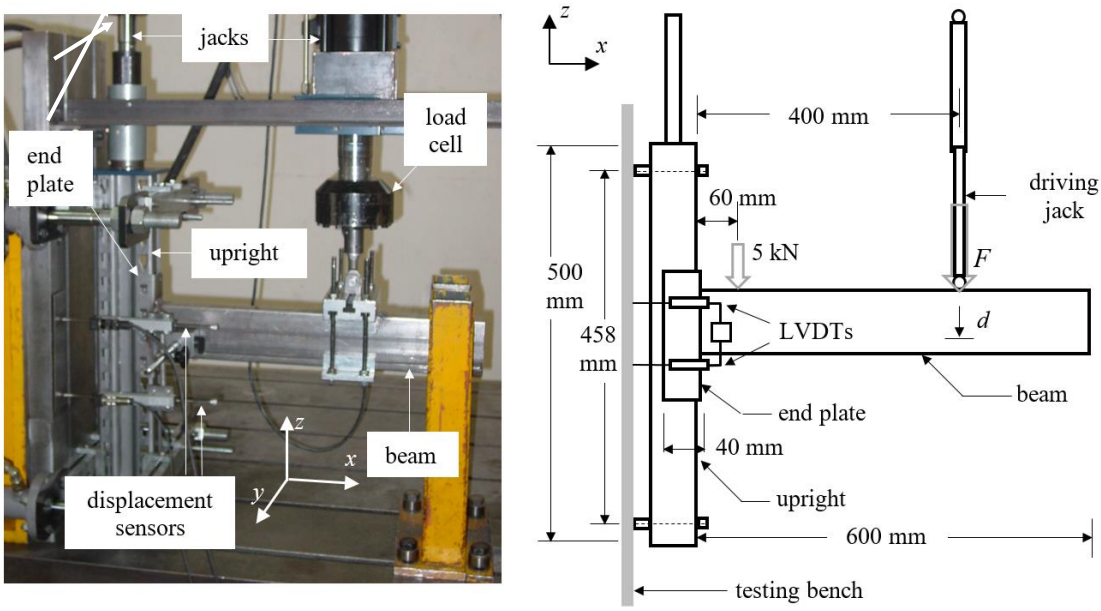

(a) General view (b) Lateral sketched view

Figure 2. Testing mock-up [13, 14]

Figure 4.a shows that sensing consists of two displacement transducers that measure the horizontal longitudinal (*x*) displacements at two (up and down) sections of the endplate, and a load cell that measures the jack driving force (*F*). From these measured magnitudes, the main outputs of the tests are the bending moment (*M*, Figure 4.b) and the rotation angle (θ, Figure 3 and Figure 7.a) in the connection.

For further clarity, Figure 3 presents the final situations of the tested connections; Figure 3.a depicts the meaning of the rotation angle θ.

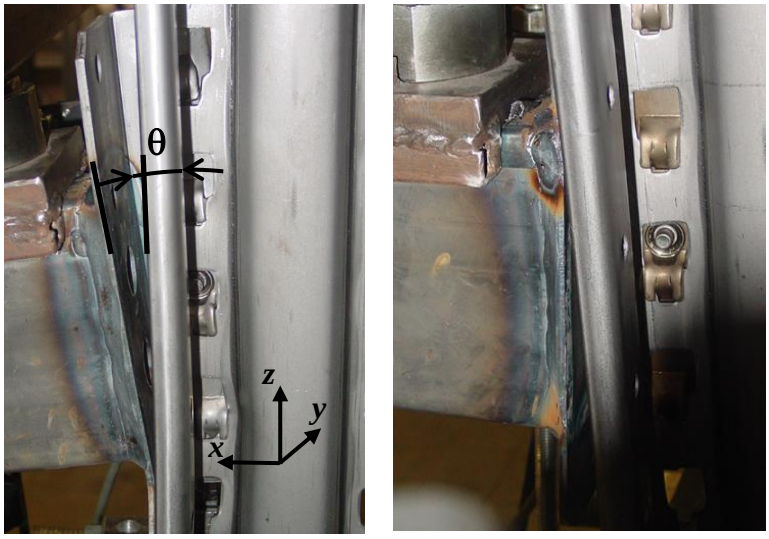

(a) Hogging test (b) Sagging test

Figure 3. Tested connections

To provide deeper information on the tested elements, Figure 4 shows the section geometry of the beam (Figure 4.a) and the upright (Figure 4.b).

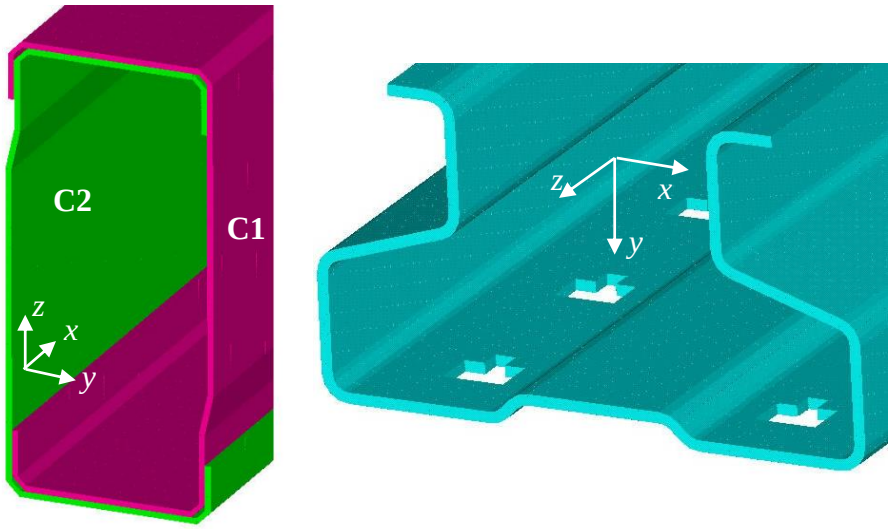

(a) Beam section (b) Upright section

Figure 4. Beam and upright sections

Figure 4.a shows that the beam section is made of two mutually nested C-lipped channel profiles; these profiles are called C1 and C2. In actual racks, they are spot-welded regularly; in the tests, they are directly welded to the endplate and spot-welded at the free

end. Finally, Figure 4.b reveals that the upright is a regularly perforated beam-like element with open Omega-shaped section.

As mentioned in sections 0 and 0, the tested specimens differ in the weld bead path between the endplate and the beam. Regarding this issue, three beads geometries have been utilized; in crescent order of weld bead length, they are: VS (Vertical Sides only), FP (Full Perimeter) and FPIF (Full Perimeter and Internal Flanges). Figure 3.a, Figure 3.b and Figure 3.c display, respectively, images of these connection options. To understand the FPIF option, it is necessary to keep in mind the beam section configuration (Figure 4.a); Figure 3.c contains a sketch depicting the trims ("bites") in the external flanges in order to allow the weld to connect both the inner and outer flanges (even their folded ends) to the endplate.

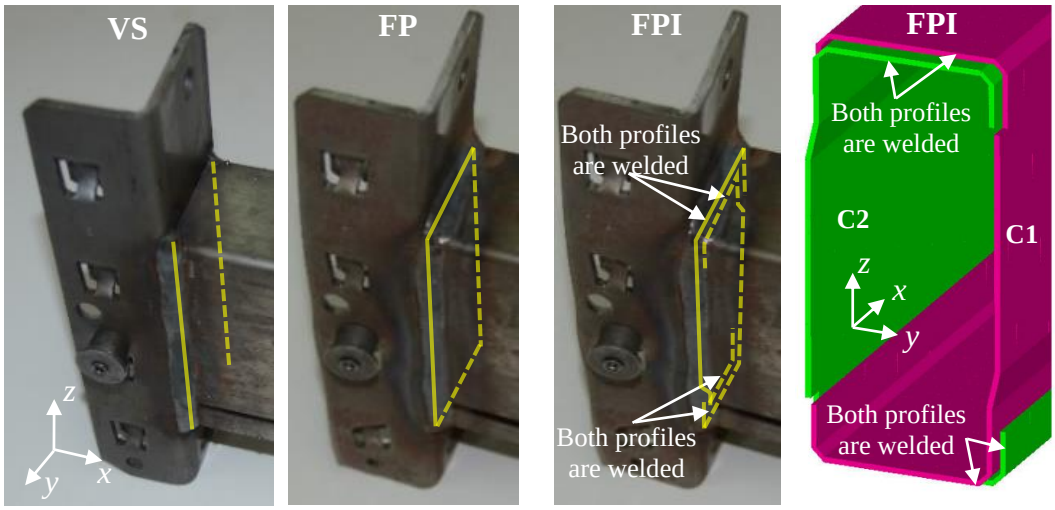

(a) Vertical sides (VS) (b) Full perimeter (FP) (c) Full perimeter and internal (hidden) flanges (FPIF)

Figure 5. Beam-to-endplate weld beads configurations [14]

The first welding option (Figure 3.a) refers to the unmodified commercially available product, while the other ones (Figure 3.b, Figure 3.c and Figure 3.d) incorporate alterations aiming to strengthen the plate-to-beam welding. Noticeably, all these variations maintain the speed-lock character of the connection.

As discussed in section 0, only monotonic tests are simulated.

Numerical simulation of the beam-upright connections structural behavior

As discussed in section 0, the main objectives of this simulation are to understand the linear elastic initial behavior of the beam-upright connection (particularly the welding between the beam and the endplate), and to compare with the corresponding monotonic tests results. Additionally, the initial after-yielding behavior is also studied in order to analyze the stress redistribution in the welds of the different tested specimens (Figure 3). Then, the employed model is designed to reach these goals. Noticeably, the reliable and accurate full numerical simulation of all the performed experiments (both monotonic and cyclic) is a much more complex and ambitious task, since it involves low-cycle fatigue, cold-forming residual stresses, gaps in the hooks (generating pinching in the cyclic tests), geometrical imperfections, uncertainty in the gap between each hook and its corresponding upright hole (and in other geometrical issues), and thermal effects due to welding, among other relevant topics. The work [26] discusses the influence of mechanical and geometric uncertainties on rack connections.

The nonlinear 3-D behavior of the tested specimens is described with ANSYS [27]. This software has been chosen for being well suited for simulation of the involved structural problems. The domain, discretization, boundary conditions, contact modeling, steel constitutive law, and analysis are described in the next six paragraphs, respectively.

- **Domain**. The analyzed volume encompasses the relevant parts of the tested specimen (Figure 4); i.e. the beam segment between the connection and the actuator (400 mm long), the beam-end connector and the whole upright segment (500 mm high). Figure 6.a displays a 3-D view of the resultant model and Figure 6.b presents a zoomed view of the connection itself. The hooks are not specifically discretized, but represented by node-to-node DOF coupling (points H1, H2, H3 and H4, Figure 6.b); this simplification has been introduced because of the aforementioned objectives of the simulations (section 0). Additionally, the weld beads are represented by an equivalent thickness increase (Figure 6.b). Noticeably, the edge fillets (in the beam, upright and endplate) have been modeled in order to avoid singularities and to better reproduce the stress flow.

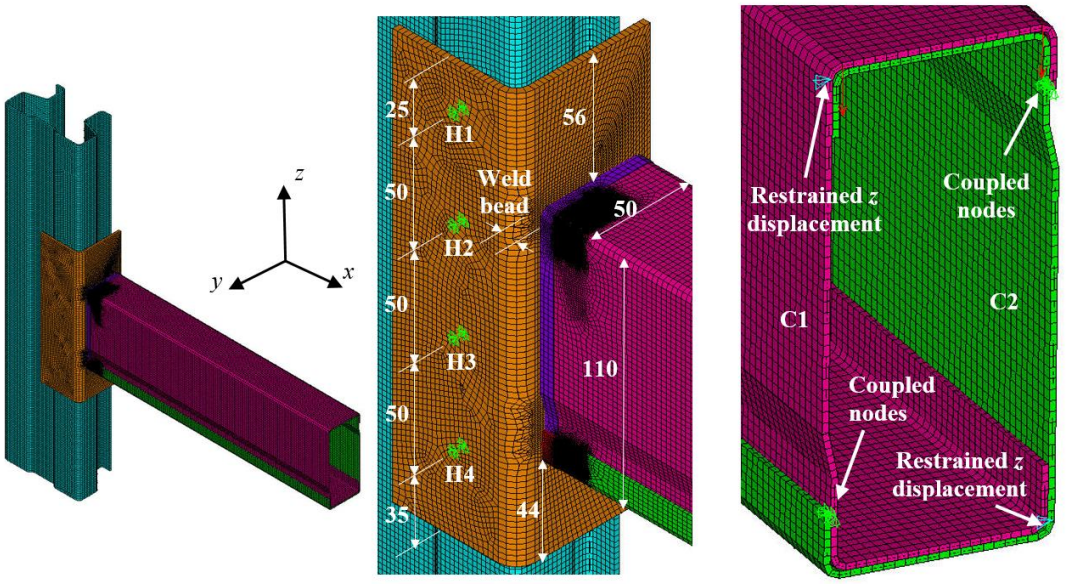

(a) Finite element mesh

(b) Beam-upright connection detail

(c) Boundary and link conditions at the free end

Figure 6. Structural model of the tested specimens

- **Discretization**. The specimen is discretized with higher-order 8-node 2-D quadrilateral thick shell elements (SHELL281) governed by the 1st order shear deformation theory (Reissner-Mindlin); six DOFs (three translations and three rotations) are considered per node. Both membrane and bending behavior are considered. Figure 6.a presents the discretization mesh and Figure 6.b displays a more detailed view of the hottest zone. Figure 6.a and Figure 6.b show that the mesh is refined in the beam segments that are near the endplate, as high stress gradients are expected.
- **Boundary, loading and link conditions**. The boundary conditions in the upright top and bottom ends (Figure 4.a) correspond to total restrain (fixed support); the beam end is free. The permanent 5 kN force is applied in a first load step at the beam top flange, as in the experiments (Figure 4.b). In a second load step, the-imposed vertical displacement is modeled by forces applied to the external beam flanges (to the top flange for hogging, and the bottom one for sagging). The beam lateral displacement (Figure 6.c) is prevented, in order to avoid torsion and lateral buckling. Noticeably, this boundary condition is not exactly reproducing the test, as the vertical controlled motion and the lateral displacement prevention are not applied on the same cross-section (Figure 4.a); nonetheless, the effect of this eccentricity is not expected to produce any relevant effect on the connection. Finally, two existing small welding points between C1 and C2 profiles at the free beam end are modelled as coupled

nodes, as shown in Figure 6.c; in the other sections, the longitudinal (x) sliding of both profiles is not prevented.

- **Constitutive laws**. As discussed later, both material linear and nonlinear analyses are performed. In the latter, the steel constitutive law is based on a bilinear model with strain hardening; the plastic deformation modulus is one hundredth of the elastic one. On the other hand, given that the hooks are represented by point node-to-node connections, high stresses are expected; thus, to avoid artificial numerical instabilities generated by the arising large plastic strains, the surrounding material is assumed to behave linearly. The same is considered for the free end of the beam, where the point loads, displacements and couplings are also applied to nodes. Finally, the welds between the beam and the L-shaped profile (endplate) are also considered to behave linearly.
- **Contact modeling**. The following interactions are described with contact models: (i) contact between both C-lipped channel profiles that form the beam (Figure 3.a and Figure 3.d), (ii) contact between the beam and the L-shaped endplate, and (iii) contact between the endplate and the upright lateral sides. The first interaction is modeled with surface-to-surface contact using standard frictionless penalty algorithms; this choice is based on the observation of tested specimens, with relevant longitudinal (x) sliding between C1 and C2 profiles. The second interaction is modeled with node-to-surface contact; welds are described by using bonded contact, and ordinary interaction is represented by standard contact. Finally, regarding the third interaction, the aforementioned contact between the endplate and the upright lateral sides is modeled as in the first interaction.
- **Analysis**. The performed simulations are non-linear and static; nonlinearities are solved using an implicit integration algorithm. The geometric nonlinearity (second-order effects) is accounted for by a co-rotational method. Regarding the material nonlinearity, two types of analysis are carried out (for each specimen): Regarding the material nonlinearity, two types of analysis are carried out (for each specimen):
  - Linear elastic analysis to determine the hogging and sagging initial stiffness and stress concentrations at the hot points. The provided results correspond to a moment of ±1 kNm/rad at the connection, for driving forces F = 1.75 and 3.25 kN for hogging and sagging, respectively; this difference is due to the permanent 5 kN force, that produces a hogging moment in the connection.

- Material non-linear analysis to capture the stress redistribution after the first yielding. This analysis is made only for hogging; similar conclusions are expected to be obtained from sagging.

The steel mechanical and geometrical parameters are taken from [13, 14]. The initial (elastic) steel deformation modulus is $E = 210$ GPa and the Poisson ratio is $\nu = 0.3$. In the non-linear analyses, the Newton-Raphson method is utilized.

Numerical results discussion of monotonic tests

The results of the simulations are analyzed in this section in order to achieve the objectives described in section 0. Special attention has been paid to the connection initial stiffness, the stress flows in the material linear elastic range, and their redistribution after the first yield. These three issues are dealt with in the following subsections, respectively.

Initial stiffness

Table 1 displays the calculated initial stiffness (S_0) for each weld geometric configuration for hogging and sagging (Figure 4.b). Values in Table 1 correspond to two assumptions: there is no contact (NC) between the upright lateral side and the endplate along the whole test, and the gap between both elements (Figure 4.b) is zero, i.e. there is initial contact (IC). Noticeably, both contact conditions represent extreme situations that are feasible to occur in actual racks (Figure 3), together with the full range of intermediate situations.

Table 1. Connection initial stiffness

Specimen	Contact condition	S_0 (kNm/rad)	
		Hogging	Sagging
VS	IC	198	184
	NC	154	137
FP	IC	208	193
	NC	166	147
FPIF	IC	216	205
	NC	171	156

Table 1 shows that, for both hogging and sagging, as expected, FPIF performs better than FP, and, in its turn, FP performs better than VS; however, no huge differences are observed. Additionally, also as expected, the stiffness for IC is considerably greater than

that for NC. Finally, the stiffness for hogging is larger than that for sagging; this trend can be explained by the asymmetry of the endplate and hooks configuration (Figure 6.b).

Stress and force distribution in the material linear elastic range

This section presents sectional results for the values of F indicated in section 4 (1.75 kN for hogging and 3.25 kN for sagging).

In order to provide insight on the connection deformation, Figure 7 displays rear views of the hogging and sagging deformed shapes of the FPIF specimen under NC and IC conditions (Table 1). Additionally, Figure 7.a depicts the rotation angle θ, and Figure 7.b illustrates the "reference section"; it is located aside the weld bead (Figure 6.b), and is used along the paper to analyze the sectional stress distribution.

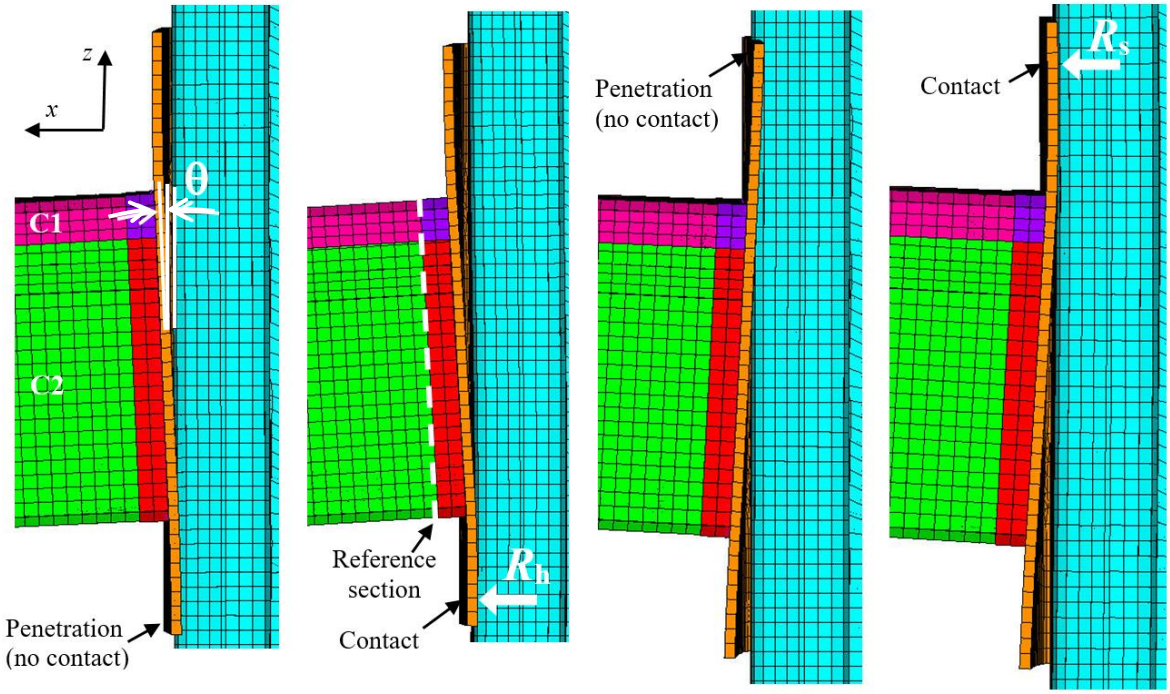

(a) Hogging. NC (b) Hogging. IC (c) Sagging. NC (d) Sagging. IC

Figure 7. Lateral (rear) view of the FPIF deformed shape for hogging and sagging

In Figure 7.a and Figure 7.c, the apparent penetration between the endplate and the upright is highlighted. In Figure 7.b and Figure 7.d, R_h and R_s represent the resultant forces of the contact interaction stress (pressure, Figure 3) for hogging and sagging, respectively. To highlight the influence of such forces, Figure 8 displays R_h, R_s and the horizontal components of the reactions in the hooks for the aforementioned values of F. These forces

are directly obtained from the FE simulation. Other methods for obtaining link forces between the structural components of the beam-to-upright connections have been studied by other researchers; in particular, the component method [28, 29] has proven to successfully assess the force on each joint of pallet rack beam-to-upright connections.

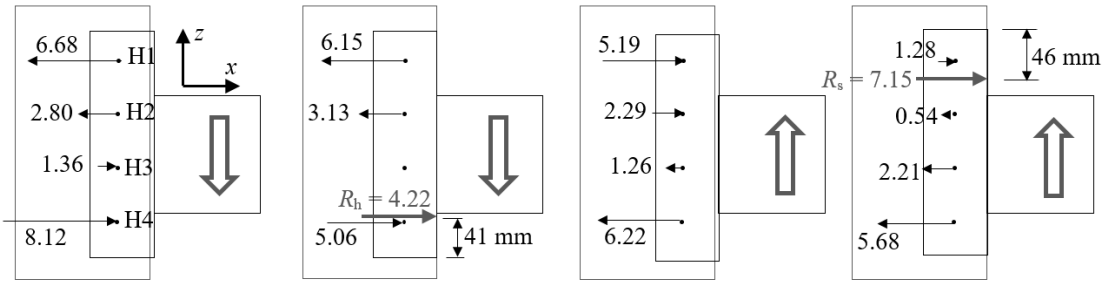

(a) Hogging. NC (b) Hogging. IC (c) Sagging. NC (d) Sagging. IC

Figure 8. Reaction forces (kN) in the hooks and the contact area

As expected, the forces in Figure 8 are rather alike regardless of the weld beads configuration (VS, FP and FPIF). Also as expected, the forces in the extreme hooks (H1 and H4) are smaller for IC than for NC, given the influence of R_h and R_s (Figure 7). Global comparison between hogging and sagging shows that in the latter case, the forces are smaller; this is because the aforementioned 5 kN and F forces generate different sign moments at the hook positions. Additionally, in the IC case, there are relevant dissimilarities between the hook forces for hogging and sagging that are aside R_h (hook H4) and R_s (hook H1), respectively; this can be explained by their different relative position (Figure 6 and Figure 8). Analogously, the change in the sign of the reactions (i.e. the "neutral axis") is produced in between H3 and H4 hooks for hogging and between H1 and H2 for sagging; conversely, for the NC case, this change in sign is produced in between the two intermediate hooks (H2 and H3) for both hogging and sagging. This issue plays a relevant role in the stress distribution (in the section) that is analyzed next.

Figure 9 and Figure 10 display, plots of the distribution of the longitudinal (x) normal stresses along the reference section contour (C1 and C2 profiles, Figure 4.a; the reference section is highlighted in Figure 7.b). Figure 9 and Figure 10 correspond to hogging and sagging, respectively; in both Figures, positive and negative values correspond to tension and compression, respectively.

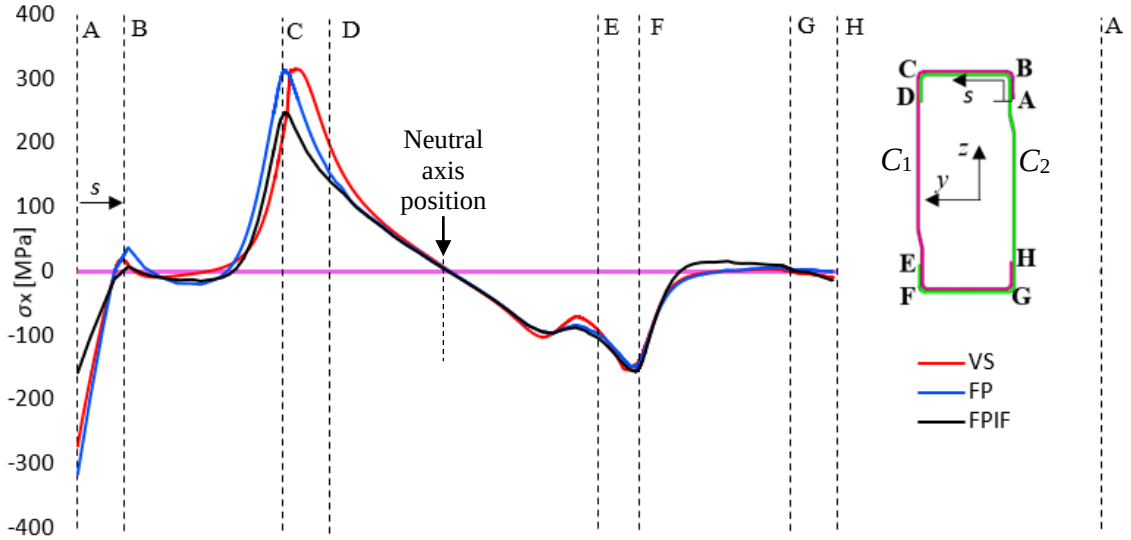

(a) NC case. C1 profile

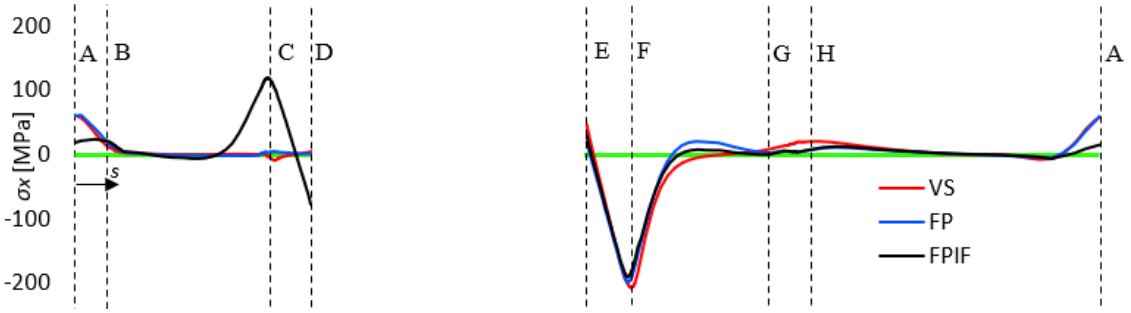

(b) NC case. C2 profile

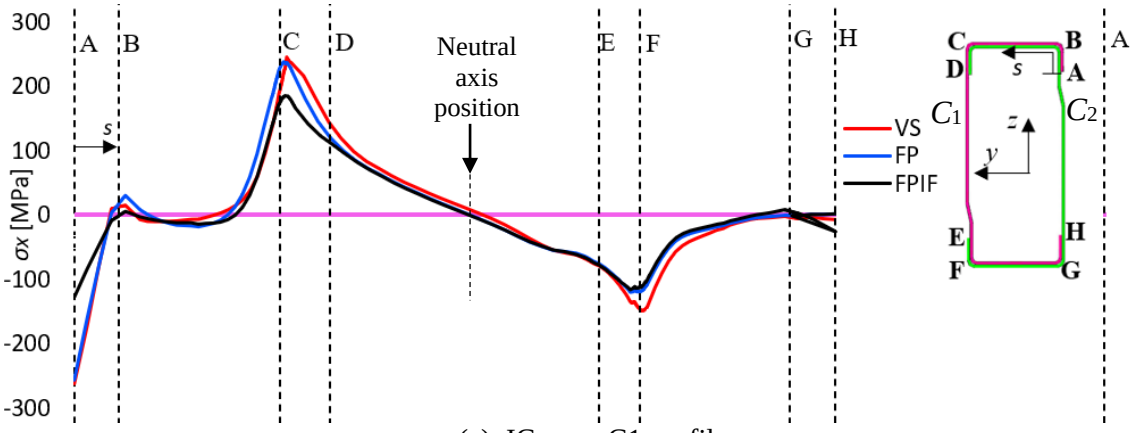

(c) IC case. C1 profile

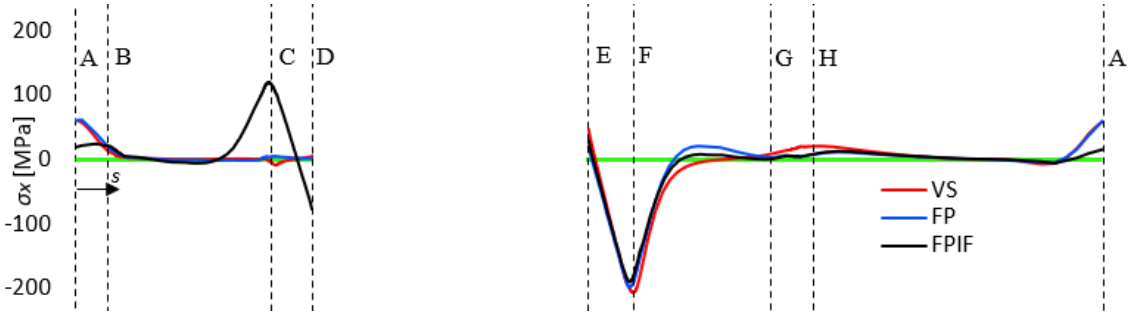

(d) IC case. C2 profile

Figure 9. Longitudinal (*x*) normal stress distribution in the reference section (Figure 7.b) for hogging analyses

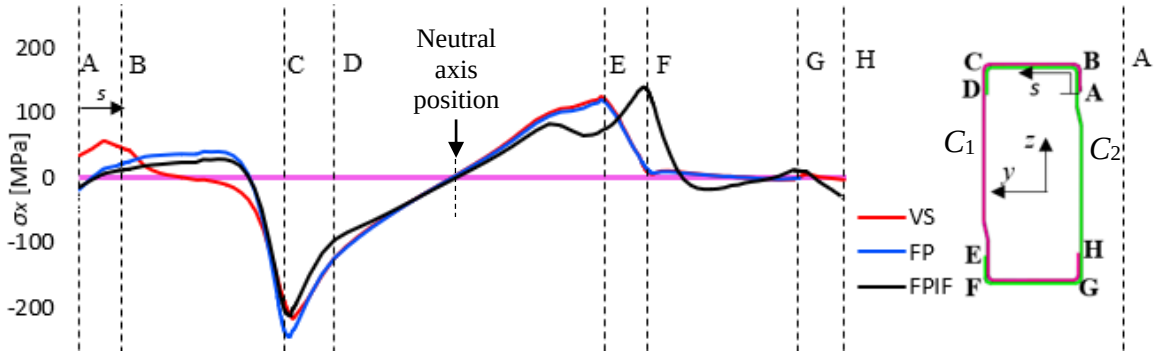

(a) NC case. C1 profile

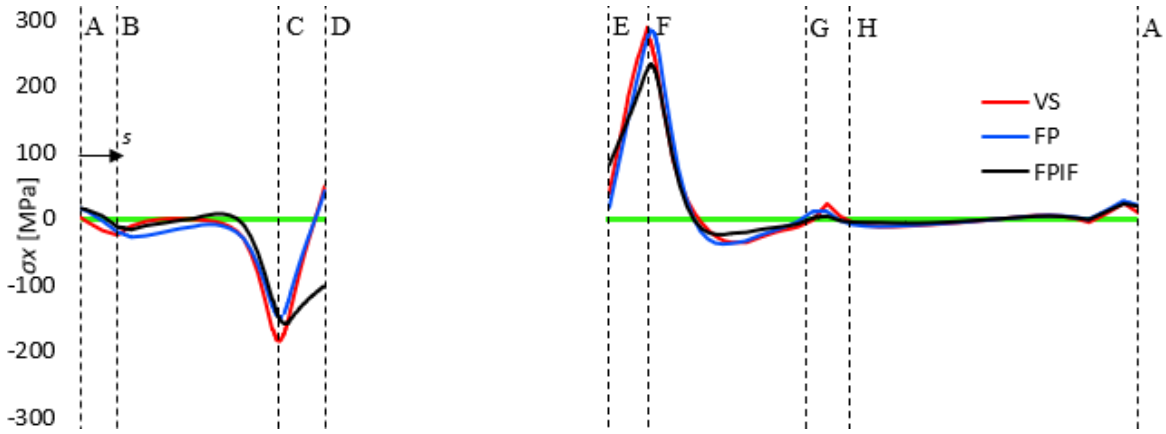

(b) NC case. C2 profile

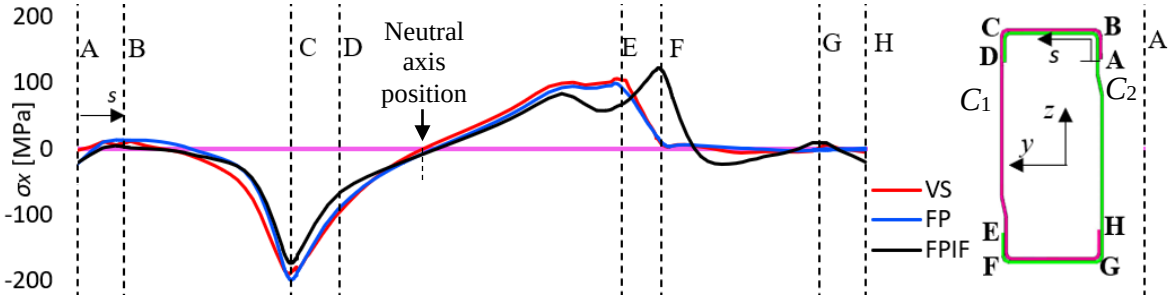

(c) IC case. C1 profile

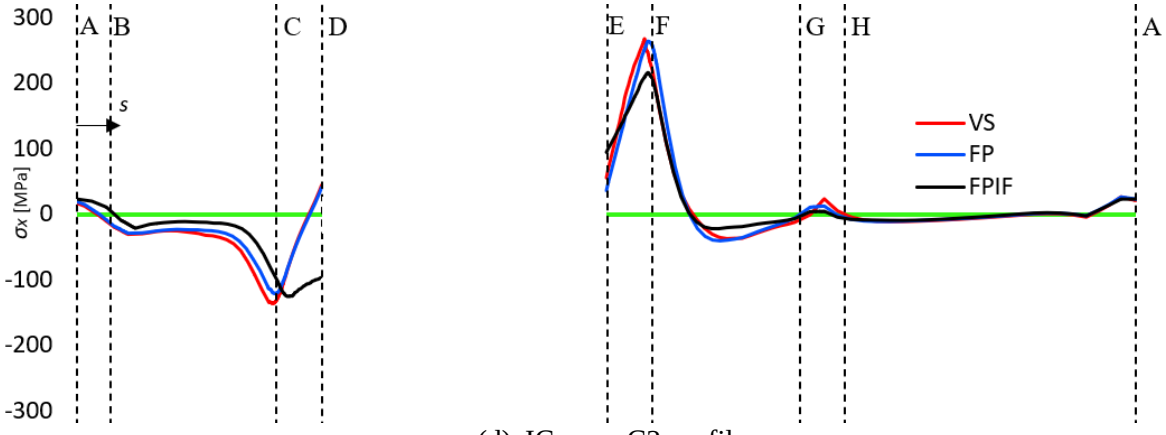

(d) IC case. C2 profile

Figure 10 Longitudinal (*x*) normal stress distribution in the reference section (Figure 7.b) for sagging analyses

The most noticeable overall remark from Figure 9 and Figure 10 is that the maximum tensile stresses for FPIF are smaller than for VS and FP (as expected, are distributed between C1 and C2 profiles). Regarding the comparison between VS and FP, no clear trend is apparent. These circumstances seem to indicate that welding the top and bottom external flanges of profiles C1 and C2 does not provide much benefit, but welding their internal flanges (Figure 3.d) does. Particular considerations are discussed next.

- The stresses are significantly higher in the left sides of both C1 and C2 profiles (segment from C to F). This trend can be explained by the eccentric location of the hooked assembly with respect to the beam axis (Figure 6.a), thus generating significantly higher stiffness in the left side.
- Figure 9 shows that in the left corner of the top unwelded internal flanges (point C of C2 profile for VS and FP), the tensile normal stress is near zero. Obviously, this is not occurring in the FPIF weld, as there are no unwelded flanges. On the contrary, in the bottom internal unwelded flanges (C1 profile, point F), the compressive normal stress is significant, and is rather similar for all the specimens. Also, the stresses exhibit a high gradient (i.e. sharp peak) in the top and bottom left corners (points C and F); this trend can be explicated by the stress flow inside the endplate web that is going to the hooks (to be transferred to the upright), see Figure 8. With respect to this last issue, it is seen that, for VS, this concentration is not located in the corner (point C), but in the left lateral side (between points C and D); this fact is seemingly due to the absence of weld in the top and rounded corners. Corresponding analogous circumstances can be observed in Figure 10.
- Regarding the aforementioned position of the neutral axis, Figure 9 corroborates the observations from Figure 7 and Figure 8: for NC, the axis is roughly located in the middle of the section (Figure 9.a), while for IC, it is situated in a lower position, approaching the contact area (Figure 9.c). This is also apparent in sagging, although inverted (Figure 10.a and Figure 10.c).
- For the hogging VS cases (Figure 9), the tensile stress in point C of profile C1 is not zero, despite there being no weld. Outwardly, this is due to the separation between the reference and end sections (Figure 7.b). This phenomenon is also observed for sagging (Figure 10).
- Figure 9 indicates that the bottom end of the top right lips of profile C1 (point A) is significantly compressed, despite that the top end (point B) is tensioned. This trend

can be explicated as the aforementioned eccentricity of the hooks (Figure 6.b) generates some torsion and, thus, vertical bending (warping moment) of such lips arises. As well, a similar trend appears in Figure 11; conversely, not any similar tendency can be observed in Figure 10, as the bottom right lips of C2 profile undergo vertical bending in the opposite direction.

In order to supplement the information from Figure 9 and Figure 10, Table 2 presents the von Mises stresses in the hottest points (top and bottom left corners of C1 and C2 profiles) of the reference section (Figure 7.b). In Table 2, the von Mises stresses that correspond to the tensioned points are represented with italics.

Table 2. Von Mises stresses (MPa) (C1/C2 profile) at critical points of the reference section (Figure 7.b)

Specimen	**IC**				**NC**			
	Top left corner (C)		**Bottom left corner (F)**		**Top left corner (C)**		**Bottom left corner (F)**	
	Hogging	**Sagging**	**Hogging**	**Sagging**	**Hogging**	**Sagging**	**Hogging**	**Sagging**
VS	*308*/---	223/138	158/126	---/*333*	*347*/---	279/192	166/214	---/*357*
FP	*306*/---	237/145	156/163	---/*326*	*324*/---	305/181	157/244	---/*350*
FPIF	*235/170*	206/151	165/172	*150/265*	*256/176*	261/192	186/232	*172/284*

Table 2 basically extends the observations from Figure 9 and Figure 10 to the von Mises stress. Table 2 also shows that the von Misses stresses in the critical points (top left corner of C1 for hogging, and bottom left corner of C2 for sagging) are higher for sagging than for hogging.

To provide information on the influence of other issues than the weld type, Figure 11 depicts the two in-plane principal stresses in a hogged beam segment that is sufficiently far from the endplate; black and blue arrows correspond to tension and compression, respectively. In Figure 11 the prevalence of bending over shear is less intense than in Figure 9 and Figure 10; hence, the correspondence between the longitudinal (x) normal stresses and the principal ones is less clear.

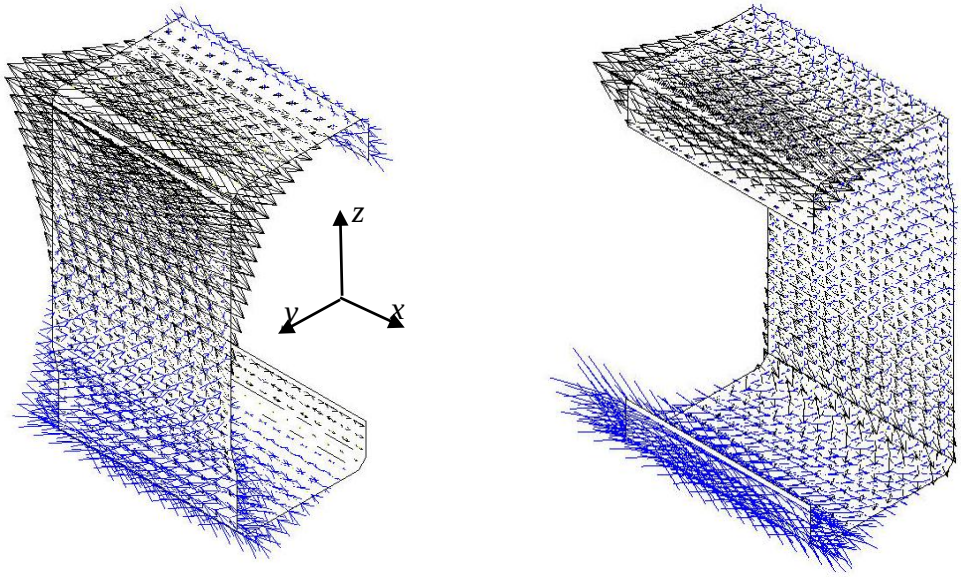

(a) C1 profile (b) C2 profile

Figure 11. Principal stresses in a sufficiently distanced beam segment for hogging

Figure 11 shows that, unsurprisingly, the result does not depend on the weld bead path; for sagging, the stresses revert sign. The stress distribution along the C1 profile web is roughly linear (i.e. approaching the Navier theory); this states that the observed top and bottom stress concentrations in Figure 9 and Figure 10 are apparently due to the proximity of the weld to the highly rigid endplate web.

Stress redistribution in the material nonlinear range

Figure 12.a and Figure 12.b display plots of M vs. θ for NC and IC cases, respectively. Only hogging analyses are performed. In these plots, the failure is considered to occur when the peak value of the moment-rotation curve is reached.

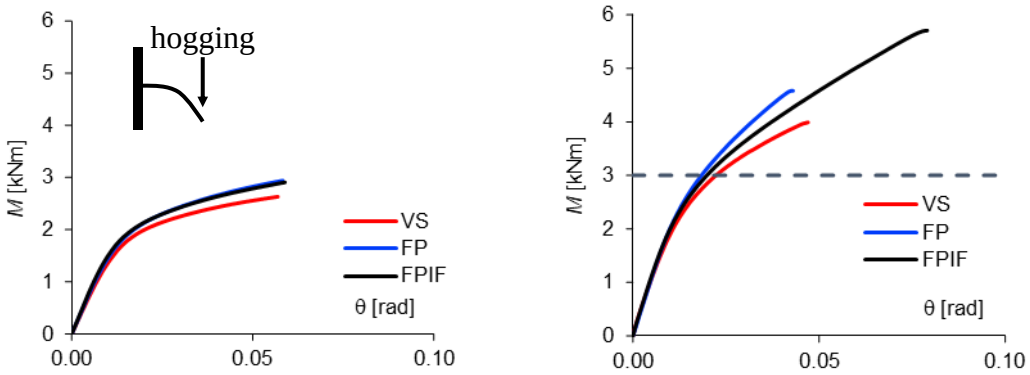

(a) NC (b) IC

Figure 12. Hogging *M*-θ plots

Figure 12.a and Figure 12.b show that, as expected, the VS plot is below those for FP and FPIF. On the other hand, the comparison between Figure 12.a and Figure 12.b shows that contact increases significantly the moment (Figure 7.a and Figure 7.b); therefore, for NC there is no weld failure, while for IC the opposite situation occurs. Noticeably, this weld failure for FP and FPIF should not be understood as an inadequate brittle failure mode, as the hooks have not been modelled; cyclic tests show that for FPIF hooks yield earlier, thus providing a ductile failure mode [14]. Finally, unexpectedly, the FP plot is above the one for FPIF (mainly for IC, Figure 12.b); conversely, Figure 12.b shows that the final moment and rotation capacity of FPIF is significantly higher than those of FP. The latter is expected; the above can be explained by the earlier yield of the endplate due to the intense top flange (inner and outer, Figure 3.c) welding. In this sense, Figure 13 displays von Mises stress maps of the endplate for the FP (Figure 13.a) and FPIF (Figure 13.b) specimens; they correspond to IC and M = 3 kNm (this situation is highlighted in Figure 12.b with a dashed line). Figure 13 shows that the yielded area (grey color) is wider in the FPIF case, extending inside the area encompassed by the beam section.

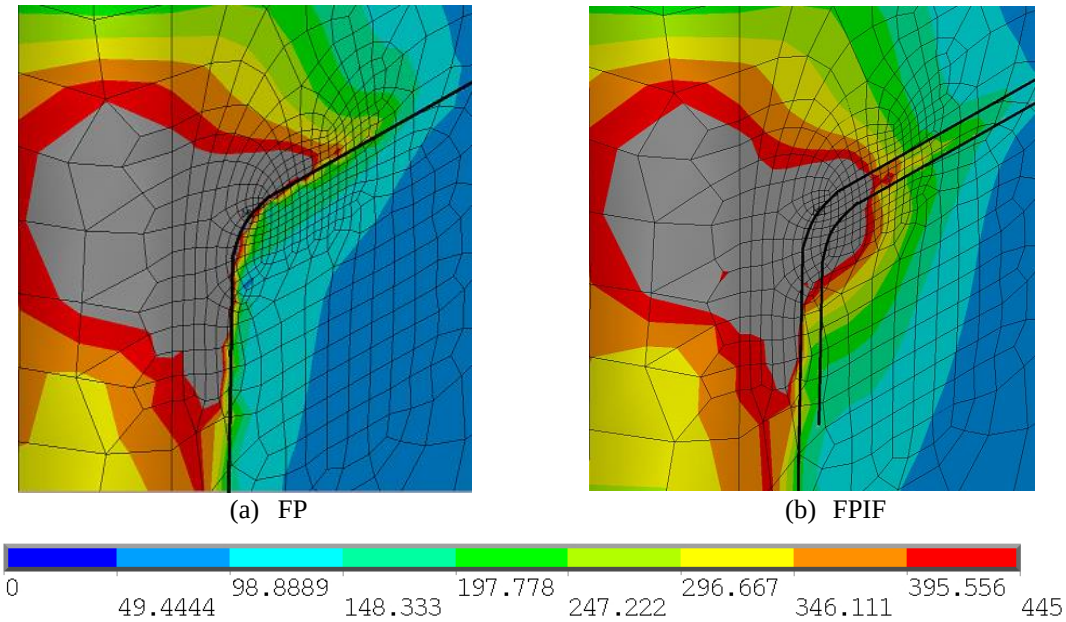

(a) FP (b) FPIF

Figure 13. Von Mises stress maps (MPa) of the endplate for tests in Figure 12.b

Figure 12 shows that the stress redistributions between C1 and C2 profiles are relevant. To provide a deeper insight, the von Misses stresses map near the most tensioned point of the reference section (point C in Figure 9 and Figure 10) is displayed in Figure 14.a; like Figure 13, it corresponds to IC and M = 3 kNm. As in Figure 13, grey refers to yielded regions ($\sigma_{vM} \geq 470$ MPa).

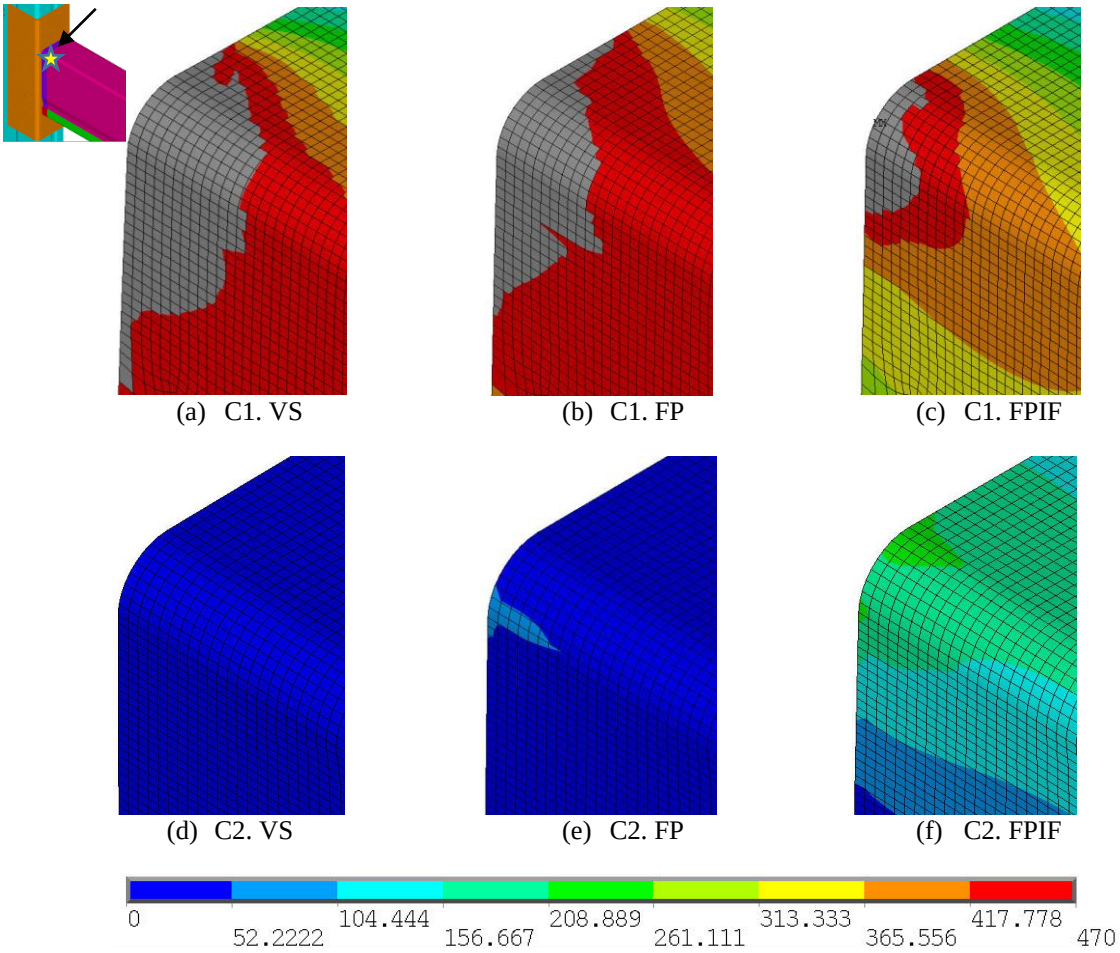

Figure 14. Von Mises stress maps (MPa) of the beam (nearby point ★) for tests in Figure 12.b

Figure 14 shows that the more weld, the more stress is redistributed from the external profile C1 to the internal one C2. This trend is particularly clear for FPIF, as both inner and outer flanges are welded (Figure 3.c).

Comparison between monotonic numerical and experimental results

This section compares the results of the simulations discussed in section 0 with the experiments [14]. In this sense, Figure 15 displays initial segments of numerical (Table 1) and experimental M-θ plots for all the tested specimens; FPIF-A (Figure 15.c) and FPIF-B (Figure 15.d) refer to connections made with steel from different coils.

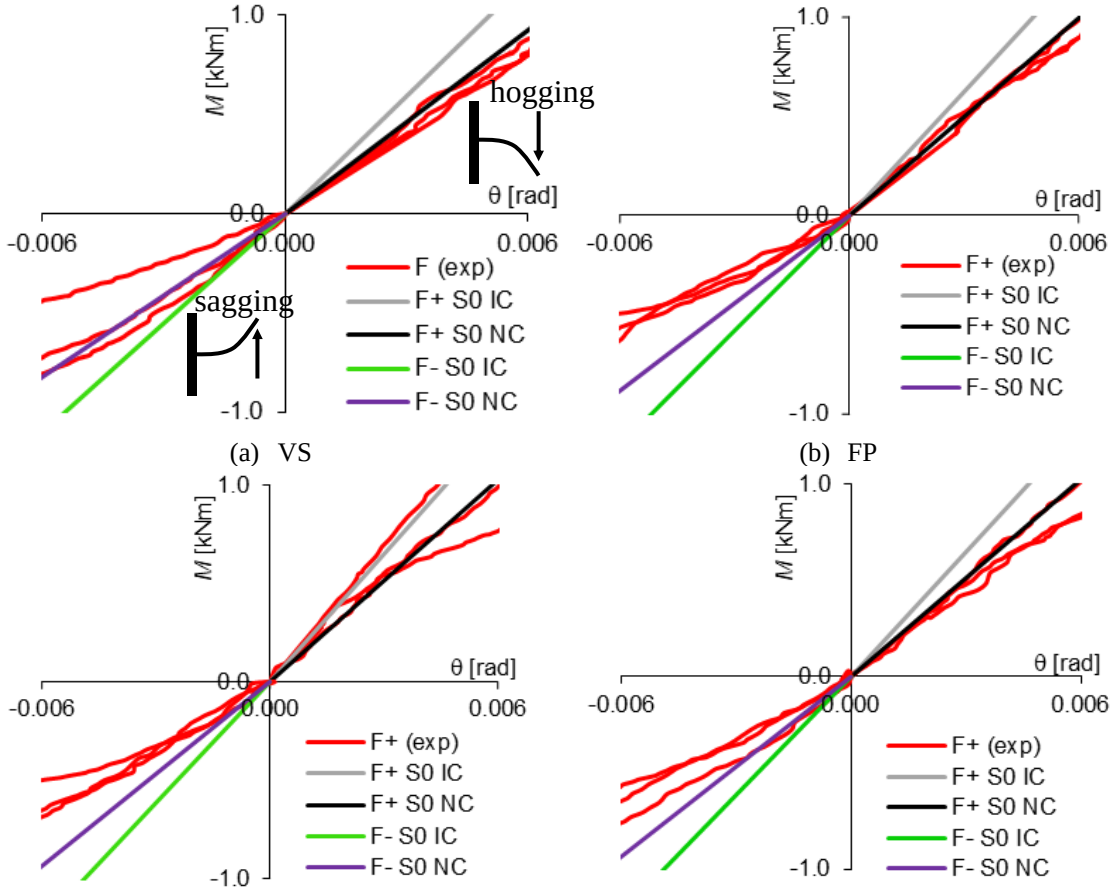

Figure 15. Comparison between experimental and numerical *M*-θ plots in the linear range

Figure 15 shows that in the hogging branches, the numerical slopes obtained without contact between the endplate and the upright (NC, subsection 0) tend to be reasonably close to the initial experimental ones; this coincidence is understood as a proper simulation. Conversely, in the sagging branches, the numerical slopes are higher than the initial experimental ones; this difference can be explained because the hooks flexibility (not incorporated into the numerical model) seems to have a higher influence in the sagging tests than in the hogging ones.

Finally, the hogging monotonic experiments are compared with the numerical simulations; Figure 16 shows the *M*-θ plots in the nonlinear range. Only the experiments with weld failure are included in Figure 16.

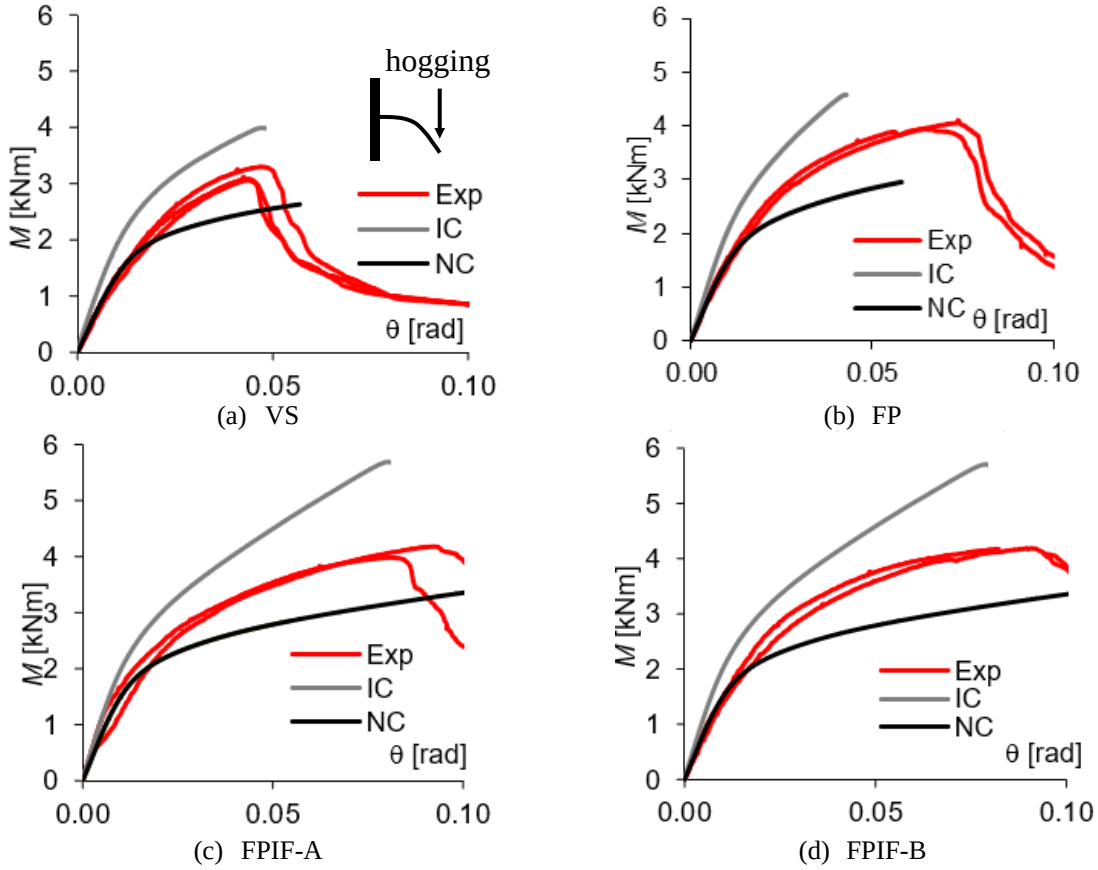

Figure 16. Comparison between experimental and numerical *M*-θ plots in the nonlinear range. Hogging

Figure 16 shows that the initial segments of the curves are well reproduced for the "no contact" case; this circumstance is expected due to the presumable existence of a certain initial gap. For higher angles, the experimental plots are in between the NC and the IC ones. This rather wide margin should not be understood as an inaccurate numerical simulation, as the precise reproduction of the experiments should account (among other issues) for the hooked assembly; this is out of the scope of this study as discussed in section 0.

Conclusions

This paper presents the numerical simulation of a set of seismic monotonic experiments on boltless beam-to-upright connections of adaptive racking systems. The beam is composed of two mutually nested C-lipped channel profiles that are welded to the endplate. The main objective of the analyses is to investigate the performance of three different weld beads geometric configurations: (i) vertical sides (webs) only, (ii) vertical

sides and top and bottom external flanges, and (iii) welding also the top and bottom internal (hidden) flanges. The numerical results are satisfactorily compared to the experimental ones, both in the linear and nonlinear ranges, thus confirming its reliability. More particularly, the initial stiffnesses of the experimental curves coincide with those of the numerical ones; besides, the numerical nonlinear behavior of the two contact conditions (IC and FC) enclose the experimental results. Then, the performed simulations allow a deeper understanding of the behavior of the analyzed connections and provide the following major conclusions:

- The first two welding options do not show much difference in the elastic range, but FP shows to behave better than VS after the yielding onset. The experimental results confirm that the FP option provides significantly better results (in both strength and ductility) than VS.
- The welding of the internal flanges of the C-lipped channel profiles (third option) provides significant benefits as, among other gains, the maximum von Mises stresses are clearly reduced.
- Both the monotonic tests and their numerical simulations demonstrate that the ductility of the FPIF welding solution is better.

References

[1] Hélder D. Craveiro, João Paulo C. Rodrigues, Luís Laím, (2016). Buckling resistance of axially loaded cold-formed steel columns. *Thin-Walled Structures,* **106**: 358-375. DOI: /10.1016/j.tws.2016.05.010

[2] Maurizio Orlando, Giovanni Lavacchini, Barbara Ortolani, Paolo Spinelli, (2017). Experimental capacity of perforated cold-formed steel open sections under compression and bending. *Steel and Composite Structures,* **24**: 201-211. DOI: /10.12989/scs.2017.24.2.201

[3] Bonada J., Casafont, M.; Roure, F.; Pastor, M.M. (2021). Geometrically nonlinear analysis of perforated rack columns under a compression load by means of Generalized Beam Theory. *Thin-walled structures,* **166**: 108102/1-108102/17. DOI: /10.1016/j.tws.2021.108102

[4] Bernuzzi C, Castiglioni CA. (2001). Experimental analysis on the cyclic behaviour of beam-to-column joints in steel storage pallet racks. *Thin-Walled Structures*, **39**(10):841–59. DOI: 10.1016/S0263-8231(01)00034-9

[5] Abdel-Jaber M, Beale RG, Godley MHR. (2006). A theoretical and experimental investigation of pallet rack structures under sway. *Journal on Constructional Steel Research*, **62**(1–2):68–80. DOI: 10.1016/j.jcsr.2005.04.008

[6] Prabha P, Marimuthu V, Saravanan M, Jayachandran SA. (2010). Evaluation of connection flexibility in cold formed steel racks. *Journal on Constructional Steel Research*, **66**(7):863–72. DOI: 10.1016/j.jcsr.2010.01.019

[7] Roure F, Somalo MR, Casafont M, Pastor MM, Bonada J, Peköz T. 2013. Determination of beam-to-column connection characteristics in pallet rack structures: a comparison of the EN and ANSI methods and an analysis of the influence of the moment-to-shear ratios. *Steel Construction*. **6**:132-138. DOI:10.1002/stco.201310018.

[8] Zhao X, Wang T, Chen Y, Sivakumaran KS. (2014). Flexural behavior of steel storage rack beam-to-upright connections. *Journal of Constructional Steel Research*. **99**:161-175. DOI: 10.1016/j.jcsr.2014.04.007

[9] Yin L, Tang G, Zhang M, Wang B, Feng F. (2016). Monotonic and cyclic response of speed-lock connections with bolts in storage racks, *Engineering Structures*, **116**:40–55. DOI: 10.1016/j.engstruct.2016.02.032

[10] Castiglioni CA. 2016. *Seismic Behaviour of Steel Storage Pallet Racking Systems*. Springer. ISBN 978-3-319-28465-1, ISBN 978-3-319-28466-8 (eBook).

[11] Giordano S, Gusella F, Lavacchini G, Orlando M, Spinelli P. (2017). Experimental tests on beam-end connectors of cold-formed steel storage pallet racks. *EUROSTEEL 2017*. Copenhagen, Denmark. DOI: 10.1002/cepa.105

[12] Dai L, Zhao X, Rasmussen KJR. (2018). Flexural behaviour of steel storage rack beam-to-upright bolted connections. *Thin-Walled Structures*, **124**: 202-217. DOI: 10.1016/j.tws.2017.12.010

[13] López Almansa F, Bové O, Ferrer M, Roure F. 2021. Comparison between two types of cyclic tests of racking systems for seismic performance evaluation. *17th World Conference on Earthquake Engineering (17WCEE)*. Sendai, Japan. Art. 0206 (publication in pen-drive).

[14] Bové O, López Almansa F, Ferrer M, Roure F. (2021). Ductility improvement of adjustable pallet rack speed-lock connections: Experimental study. *Journal on Constructional Steel Research.* Accepted. In Press.

[15] Folz, B. and Filiatrault, A. (2001). "SAWS - Version 1.0, A Computer Program for the Seismic Analysis of Woodframe Structures", Structural Systems Research Project Report No. SSRP-2001/09, Dept. of Structural Engineering, UCSD, La Jolla, CA.

[16] Mitra N., Pinching4 model. (OpenSees User Documetation); 2012. http:// opensees.berkeley.edu/wiki/index.php/Pinching4_Material

[17] Gusella, F., Orlando, M. & Spinelli, P. Pinching in Steel Rack Joints (2019): Numerical Modelling and Effects on Structural Response. *Int J Steel Struct* **19**, 131–146 DOI: /10.1007/s13296-018-0095-x

[18] Carlos Aguirre (2004). Seismic behavior of rack structures. *Journal of Constructional Steel Research*. **61,** 607-624 DOI: /10.1016/j.jcsr.2004.10.001

[19] Bajoria KM, Talikoti RS. (2006). Determination of flexibility of beam-to-column connectors used in thin walled cold-formed steel pallet racking systems. *Thin-Walled Structures*, **44**(3):372–380. DOI: /10.1016/j.tws.2006.01.007

[20] Shah SNR, Ramli Sulong NH, Khan R, Jumaat MZ. (2017). Structural performance of boltless beam end connectors. *Advanced Steel Construction*. **13**(2):144-159. DOI: /10.18057/IJASC.2017.13.2.4

[21] Gusella F, Lavacchini G, Orlando M. 2018. Monotonic and cyclic tests on beam-column joints of industrial pallet racks. *Journal of Constructional Steel Research*. **140**:92-107. DOI: 10.1002/cepa.105.

[22] Lyu ZJ, Wu M, Huang YX, Song YM, Cui X (2018). Assessment of the Dynamic Behavior of Beam-to-Column Connections in Steel Pallet Racks under Cyclic Load: Numerical Investigation. *Advances in Civil Engineering.* Article ID 9243216. DOI: /10.1155/2018/9243216

[23] Vujanac R, Miloradović N, Vulović S, Pavlović A. (2020). A Comprehensive Study into the Boltless Connections of Racking Systems. *Metals*. **10**:1-17. DOI: doi.org/10.3390/met10020276

[24] EN 15512. (2009). Steel static storage systems - Adjustable pallet racking systems - Principles for structural design. *European Committee for Standardization*.

[25] EN 16681. (2016). Steel static storage systems - Adjustable pallet racking systems - Principles for seismic design. *European Committee for Standardization*.

[26] Federico Gusella, Sanjay Raja Arwade, Maurizio Orlando, Kara D. Peterman (2019). Influence of mechanical and geometric uncertainty on rack connection structural response, *Journal of Constructional Steel Research*, **153:** 343-355. DOI: /10.1016/j.jcsr.2018.10.021

[27] ANSYS Release 14.0, ANSYS Inc. (2011).

[28] Ślęczka, L. and Kozłowski, A. (2007). Experimental and theoretical investigations of pallet racks connections. *Advanced Steel Construction* **3**: 607-628. DOI: 10.18057/IJASC.2007.3.2.6

[29] Federico Gusella, Maurizio Orlando, Klaus Thiele, (2018). Evaluation of rack connection mechanical properties by means of the Component Method, *Journal of Constructional Steel Research*. **149:** 207-224. DOI: /10.1016/j.jcsr.2018.07.021.

List of acronyms

C1/C2: C-lipped Channel Profiles (Figure 3.a)

DOF: Degree-Of-Freedom

NC/IC: No Contact/Initial Contact (Table 1 and Figure 7)

VS/FP/FPIF: Vertical Sides/ Full Perimeter/Full Perimeter and Internal Flanges (Figure 3)

List of symbols

E: Steel modulus of elasticity

F: Driving force (Figure 4.b)

M: Bending moment (Figure 4.b)

R_h, R_s: Resultant forces of the upright-endplate contact interaction stress for hogging and sagging, respectively (Figure 7)

s: Coordinate along the section plates (Figure 9, Figure 10)

S_0: Initial slope of the moment-rotation curve (Figure 15)

x, y, z: Coordinates (Figure 4, Figure 3, Figure 6, Figure 7, Figure 11, Figure 9, Figure 10)

ν: Poisson ratio

θ: Rotation angle (Figure 3 and Figure 7.a)

σ_{vM}: Equivalent von Mises stress

4 DUCTILITY IMPROVEMENT OF ADJUSTABLE PALLET RACK SPEED-LOCK CONNECTIONS: EXPERIMENTAL STUDY

4.1.1 Article data

Title: Ductility improvement of adjustable pallet rack speed-lock connections: experimental study

Authors: O. Bové, F. López-Almansa ,M. Ferrer, F. Roure

Journal: Journal of Constructional Steel Research (2021)

DOI: https://doi.org/10.1016/j.jcsr.2021.107015

4.1.2 Transcription of the original paper

Ductility improvement of adjustable pallet rack speed-lock connections. Experimental study

Oriol Bové[1], Francisco López-Almansa[2], Miquel Ferrer[3], Francesc Roure[4]

[1] Assistant Professor, Technical University of Catalonia, RMEI, Barcelona, oriolbovetous@upc.edu
[2] Professor, Technical University of Catalonia, Architecture Technology Department, Barcelona, francesc.lopez-almansa@upc.edu
[3] Professor, Technical University of Catalonia, RMEI, Barcelona, miquel.ferrer@upc.edu
[4] Professor, Technical University of Catalonia, RMEI, Barcelona, francesc.roure@upc.edu

ABSTRACT (maximum 250 words)

This paper presents seismic cantilever monotonic and cyclic tests of speed-lock (boltless) beam-to-upright connections of adjustable pallet rack systems; the objective of the monotonic tests is to obtain the bounds that are employed to define the loading protocol of the subsequent cyclic tests. The beam-to-upright connections consist of welding the beam to an intermediate end-plate (L-shaped) that, in its turn, is linked to the upright through a hooked assembly. The performed experiments investigate the connections hysteretic behavior, as it contributes to the rack lateral strength, stiffness, and ductility. More precisely, the main objective of this research is to propose a new strengthened design of the weld beads geometric configuration. This design is oriented for the connection failure not to arise in the weld, but the hooked assembly. This shift is expected to increase the connection ductility; in this sense, specimens with traditional and novel weld geometric designs are tested. In most of the tests performed, the results confirm that the new weld design leads to more ductile failure modes; preliminary evaluations state that the ductility increase might be sufficient to absorb most of the input seismic energy. On the other hand, tests are conducted according to two loading protocols: the traditional one by following European regulations and a new strategy proposed by Prof. Castiglioni accounting for the influence of gravity loads. Comparison between their results shows that the Castiglioni approach is more demanding and seems to reproduce the actual seismic behavior of racks better.

Keywords: *Adjustable pallet racking, Testing, Beam-to-upright connection, Monotonic and Cyclic Behavior, Seismic Performance, Weld Path*

Introduction

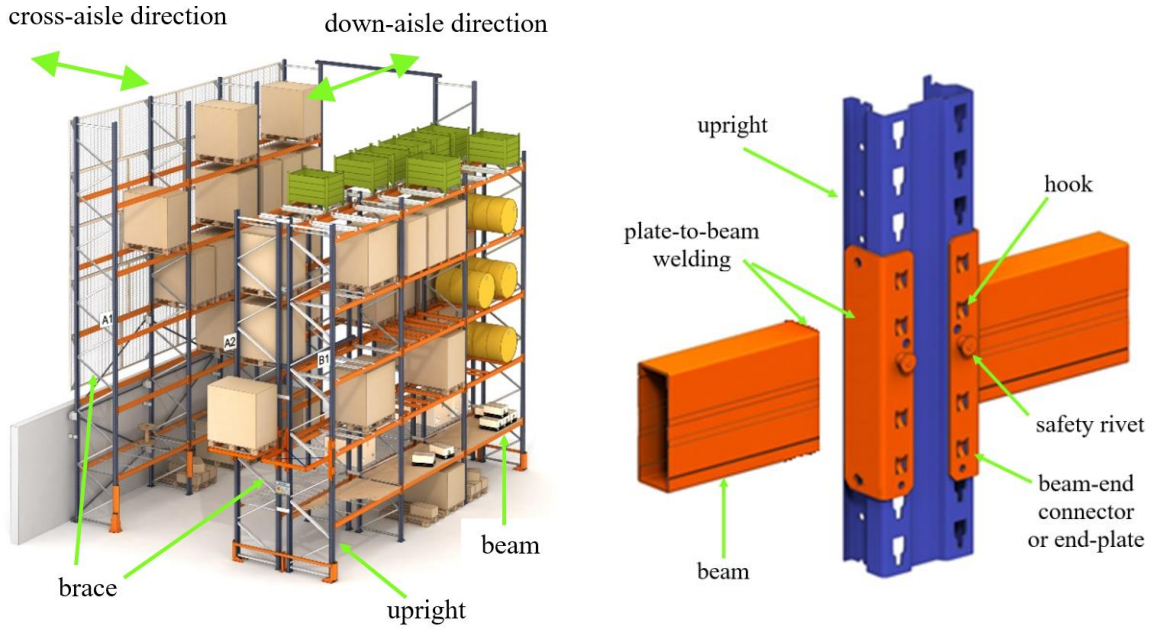

(c) Adjustable pallet-rack (d) Beam-to-upright connection

Figure 1. Analyzed racking systems

Adjustable pallet-rack systems are heavy-duty steel-shelved structures intended to store goods. Figure 1 describes pallet-rack systems. Figure 1.a presents a general view of such a structure; it is composed of vertical (uprights), horizontal (beams), and sloping (braces) bar-like elements. Figure 1.a shows that the longitudinal horizontal direction is termed as *down-aisle* while the transverse one is referred as *cross-aisle*. Commonly, all the structural members are made of thin-gauge cold-formed steel profiles. Speed-lock upright-to-beam connections are employed to facilitate the rack erection, being based on inserting hooks into upright perforations (tabs), as described by Figure 1.b.

The seismic design of pallet racking systems is a relevant issue, given their significant vulnerability and the high seismic hazard of many sites [1-2]. The rack's vulnerability is mainly contributed by their low lateral strength and stiffness and their important live load masses. The live masses are highly variable, randomly distributed, and can slide on the rack; these uncertainties prevent precise estimations of the modal parameters. Regarding the lack of lateral capacity, it can be considered as more critical in the down-aisle direction, given the usual absence of bracing [3-4]; actually, in some cases, only rear bracing is provided (Figure 1.a), thus generating undesired twisting motion. Accordingly, this paper deals with the seismic

performance of adjustable pallet-rack systems in the longitudinal (down-aisle) direction. One of the factors (but not the only one) that contributes to the lateral flexibility is the looseness and low stiffness of the beam-to-upright connections. Figure 1.b shows such a connection, where two beams are framed at both sides of a continuous upright. Each beam is welded to an end-plate; in its turn, such a plate is connected to the upright through several hooks inserted into the upright perforations. Given the unavoidable gap between the hooks and the perforations, it is obvious that these connections exhibit relevant slippage (looseness) and are rather flexible [3], as previously announced. In other words, under down-aisle seismic shaking, the beam-to-upright connections (and the foundation-upright connections) are the weakest and most flexible parts; therefore, their stiffness and energy-absorption capacity are of primary importance to the rack overall seismic resistance. Moreover, the main structural members (mainly the uprights and the braces) are of class 4 [5] (i.e. slender, according to American documents), while the beams can be either of classes 3 or 4 (semi-compact or slender). Hence, energy dissipation cannot rely on the main structural members. This trend makes that the rack behavior factor needs to be established mainly based on the characteristics of the connections.

Given the circumstances discussed in the previous paragraph, important research activity on the seismic design of racks has been undertaken worldwide. Broadly speaking, two major approaches have been proposed for the seismic design of pallet racking systems, namely dissipative and non-dissipative concepts [6]. In the non-dissipative design, little or no damage is accepted; conversely, in the dissipative design, only the overall structural integrity is pursued and, thus, greater damage is accepted. In other words, in the non-dissipative approach, the structure remains in its linear range and, thus, no energy is absorbed; in the dissipative approach, the opposite occurs. The major pros and cons of both design solutions are briefed in the next paragraph.

In the non-dissipative strategy, costly rigid and robust structures are to be designed; on the contrary, in the dissipative case, more economical and less robust racks can be considered. However, such racks need to be sufficiently ductile, and, moreover, relevant damage is to be expected after severe seismic events, thus generating higher repair and replacement costs.

The non-dissipative approach is commonly employed nowadays, perhaps due to the rather low ductility of racks and a certain scarcity of experimental and theoretical studies on their nonlinear behavior. On the contrary, in the seismic design of civil engineering constructions, the

dissipative approach is routinely considered. As discussed later in this section, this research considers the dissipative option.

Regarding more advanced seismic design issues, the work [7] proposes a novel formulation that combines nonlinear dynamic analyses with assessing the cumulative damage in the beam-to-upright connections (thus accounting for fatigue). The later paper [8] utilizes this approach to perform a parametric study of the seismic capacity of a set of representative racks. This latter study shows that the common simplified seismic design approaches are rather inadequate for racks. Also, the research [9] presents nonlinear static (pushover) and Incremental Dynamic Analyses (IDA) for rack structures and compares their results, concluding that pushover is not always on the safe side. Moving to a different approach, the work [10] proposes a methodology for the seismic vulnerability assessment of steel racks in terms of fragility curves. Additionally, [11] deals with a new structural design solution based on seismic (base) isolation of racks. Finally, [12] compares different novel seismic devices for steel storage structures, mainly based on seismic isolation and energy dissipation.

This paragraph deals with the influence of the plate-to-beam weld path in the beam-to-upright connection ductility. Two major types of bending failure of the beam-to-upright connections are possible (Figure 1.b): first, the rupture of the top or bottom ends of the welds between the end-plate and the beam; and second, the sliding of the hooked assembly between the upright and the end-plate; these two failure modes are rather brittle and ductile, respectively. Such failures are illustrated later in Figure 9.a and Figure 9.b, respectively; their occurrence depends on the plate-to-beam weld beads geometric configuration and the hooked assembly strength. Given that this strength commonly degrades during severe seismic excitations, the failure type might depend on the testing protocol. As ductile failures provide relevant advantages, a higher resistance of the welding configuration is preferred. Noticeably, this situation is similar to the classical “strong column - weak beam” recommendation in the seismic design of buildings. In that case, the European regulations [13] state that the column over-strength is 1.3; given the high uncertainty in the resistance estimation (by theoretical or experimental means) of both failure modes, a similar or higher margin may be advisable for beam-to-upright connections. In other words, a relevant welding over-strength is recommended. On the other hand, if a connection completely fails so that the corresponding beam falls, two undesired effects are generated: the subsequent lack of upright buckling restraint usually leads to its immediate

collapse, and the fallen pallets could collide with another part of the rack. In most cases, this leads to the collapse of the rack [14].

Finally, this paragraph describes the scope of this research. As previously announced in this section, this paper deals with the dissipative approach, given the potential advantages of such methodology; in fact, this work is a part of a wider research effort aiming to develop and promote this design strategy. As discussed above in this section, there is a strong need for testing, mainly the components where most of the energy is dissipated; therefore, this research activity includes testing campaigns on the beam-to-upright and the upright-base plate connections [15-16]. The results of these experiments are to be compared with numerical simulations in order to calibrate the employed numerical models. As well, these studies will provide expressions of the *response modification factor R* in the American practice [17-18], being known as ductility *behavior factor q* in the European regulations [19-20]; such expressions might be employed in simplified code-type design strategies [21]. This paper describes the first step of this research, namely the experiments on the beam-to-upright connections. The study focuses on the beam-to-plate welding strength, for reasons discussed earlier in this section.

State-of-the-art of testing of beam-to-upright connections

Several previous test campaigns on this issue have been reported [11,22-33]. The most recent studies related to the presented research are listed and discussed next:

- **[Roure et al. 2013]**. This document [27] compares tests of cantilever boltless (clip-on type) beam-to-column connections performed according to European and American regulations. Significant differences are observed.
- **[Zhao et al. 2014]**. This paper [28] refers to monotonic downward (hogging) experiments of beam-to-upright speed-lock connections. The influence of the beam geometrical sectional parameters is analyzed. The tests are conducted according to the European regulation [5] and the American document [17].
- **[Yin et al. 2016]**. This work [29] describes monotonic and cyclic experiments on speed-lock beam-to-upright connections; both bolted and bolt-less connections are tested. It is concluded that the bolts improve the connection performance, although they certainly impair its speed-lock character. Two weld beads geometric configurations between the

beam and the end-plate are considered: the first, along both lateral sides of the beam, and, the second, along its whole perimeter (all around). The experiments are performed according to European [5] and American regulations [34].

- **[Castiglioni 2016]**. This book [2] discusses the Seismic Behavior of Steel Storage Pallet Racking Systems deeply. Within this context, monotonic and cyclic bending tests on beam-to-upright connections are presented and discussed. The cyclic proofs are carried out according an innovative imposed displacement protocol that differs from the one specified in [35]; both testing procedures are compared.
- **[Giordano et al. 2017]**. This study [30] reports on monotonic and cyclic tests on beam-end connectors of cold-formed steel storage pallet racks. Similar to [29], two weld configurations between the beam and the end-plate are considered: lateral sides and all around.
- **[Dai, Zhao, Rasmussen 2018]**. This article [31] presents cyclic cantilever tests of bolted beam-to-upright connections; the tested specimens differ in the upright thickness, beam height, and number of tabs and bolts. The influence of these parameters is discussed, and comparisons with boltless connections are performed; also, the authors propose using the so-called *Pinching4* model in OpenSees.
- **[Gusella et al. 2018]**. This paper [32] presents monotonic and cyclic tests on both bolted and boltless beam-to-column joints of industrial pallet racks. The tested joints differ in the type of beam-connector (with different welding layouts), the number of tabs, and the relative thickness of the upright and the beam-end connector; the key role of welding in the failure mode is remarked. Significant pinching is identified.
- **[Gusella et al. 2019]**. This paper [33] presents an experimental and numerical study on pinching in the hysteretic behavior of steel rack joints; a numerical model considering the stiffness degradation is proposed. It is concluded that the role of pinching is relevant.

These researches serve as a starting point for the tests presented; the genesis is summarized below. The general testing procedure and mock-up are basically taken from the work of Roure et al. (2013) [27], since those experiments were performed in the same laboratory and using similar specimens. The idea of investigating the performance for different weld bead configurations was inspired by the studies of Gusella et al. (2018) [32], Giordano et al. (2017) [30] and, mainly, Yin et al. (2016) [29]. This last paper describes welds that span the entire perimeter of the beam section; this research takes a step forward by analyzing even more intense weld configurations (with the goal of obtaining ductile failure modes). Additionally, works

Zhao et al. (2014) [29] and Dai, Zhao, Rasmussen (2018) [31] prove the influence on the failure mode of the relative thickness between the upright and the beam-end-connector (end-plate); this paper attempts to demonstrate that a greater equivalent beam thickness (by deeper welding) leads to more ductile failure modes. Finally, regarding the testing protocol, the Castiglioni (2016) book [2] proposes a new protocol that might reproduce more accurately the actual seismic behavior of loaded racks.

Experimental campaign

Objectives of the experiments

The tests mentioned in section 0 refer to the hysteretic bending behavior of beam-to-upright connections. With this aim, seismic monotonic and cyclic proofs are intended. The need for these proofs has been discussed previously in section 0. It should be emphasized here that the hysteretic behavior of the connections cannot be analyzed exclusively by numerical simulation since the connecting elements are highly irregular, thus generating sliding, uneven contact, localized yielding, and other complex phenomena. Therefore, the objectives of the carried-out experiments are: (i) to investigate the behavior (capacity and ductility) of the tested connections, (ii) to propose design alternatives, (iii) to develop incremental and hysteretic constitutive laws (for pushover and dynamic analyses, respectively), and (iv) to compare with both simplified and more complex numerical models (based on Strength of Materials and on Continuum Mechanics theories, respectively). The experiments presented in this paper are designed to achieve such objectives and, as discussed previously, are planned after the studies listed in section 0. Compared to these previous tests, major novelties are: (i) consideration of several alternative weld paths (beads geometric configurations between the beam and the end-plate), (ii) contemplation of different criteria to define (shape) the proofs [2,35], and (iii) comparison between different cyclic testing bounds. Moreover, it should be emphasized that only speed-lock connections (bolt-less) are analyzed. The next subsection discusses these issues more deeply.

Tested specimens

As briefly introduced in section 0, the experiments consist in loading vertically (until failure) beam-to-upright connections, like the one portrayed in Figure 1.b; Figure 2 describes more

specifically the testing specimens. Figure 2.a displays a global image view, showing that each sample is T-shaped, being composed of a segment of an upright and a cantilevered segment of a beam. Figure 2.b displays a closer zoom view of the connection itself. The specimens are full-scale, the upright and beam elements being selected among common commercially available cold-formed products. Their sections are displayed in Figure 2.c and Figure 2.d, respectively. The upright is 500 mm long, and its section is Omega-shaped ("Cee" shape with returns); the plate thickness is 2.5 mm, and the section is 69 mm deep and 122 mm wide. The end-plate (angle beam-end-connector) is 3.5 mm thick, 210 mm long, and their sides are 40 (*xz* plane) and 60 (*yz* plane) mm. The beam is 600 mm long, and its section is formed by assembling two C-lipped channel profiles (highlighted in red and purple in Figure 2.d); their thickness is 1.5 mm, and the section is 110 mm deep and 50 mm wide. As discussed previously, Figure 1.b shows that the beam is welded to the end-plate, which is connected, in turn, to the upright through hooks (studs) inserted into the upright holes.

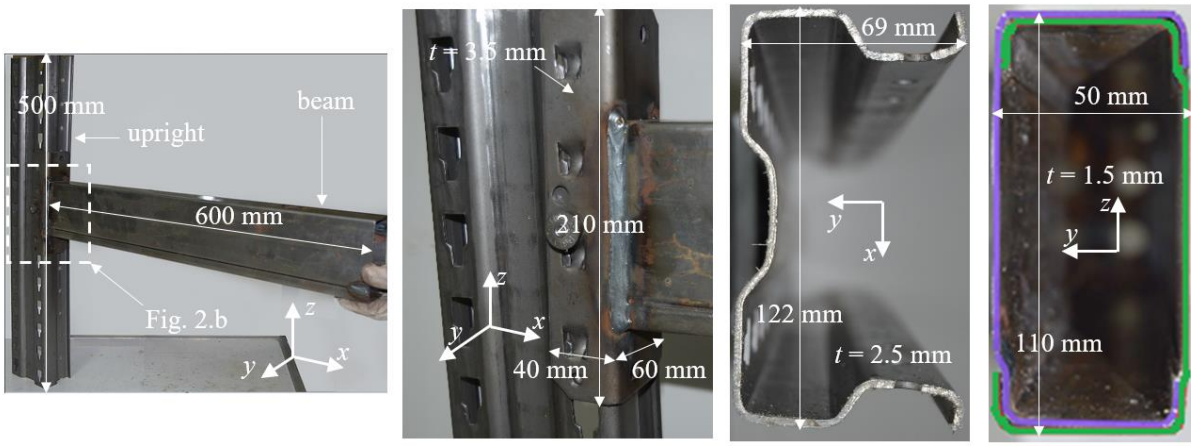

(a) General view (b) Detailed view of a connection (c) Section of an upright (d) Section of a beam

Figure 2. Tested specimens

Four options for the beam-to-upright connection are tested; as suggested by the recent previous researches discussed in section 0, they differ merely on the weld between the beam and the end-plate:

- Welding along the vertical (lateral) sides. This option is named **VS** (Vertical Sides) in this paper.
- Welding along the whole perimeter (vertical and horizontal sides). This solution is denoted as **FP** (Full Perimeter). This welding affects only the external flanges of the beam, while the internal ones are not directly connected to the end-plate (red in the top and purple in the

bottom, Figure 2.d); in other words, the weld chord gets only the external parts of the assembled shape.

- Welding along the vertical (lateral) and the top sides (like FP although without welding the bottom side). This solution is named **IU**, as the geometric configuration resembles an inverted U.
- Welding along the whole perimeter and, unlike the FP and IU options, also connecting the internal flanges of the beam to the plate (double-sided welding); that welding is performed from the outside. This case is denoted as **FPIF** (Full Perimeter and Internal Flanges).

Figure 3.a, Figure 3.b, Figure 3.c and Figure 3.d display, respectively, images and sketches of these four connection options; the sketch in Figure 3.d describes how the C-lipped channel profiles are cut in order to allow the weld to connect the inner and outer flanges (even the folded ends) to the end-plate.

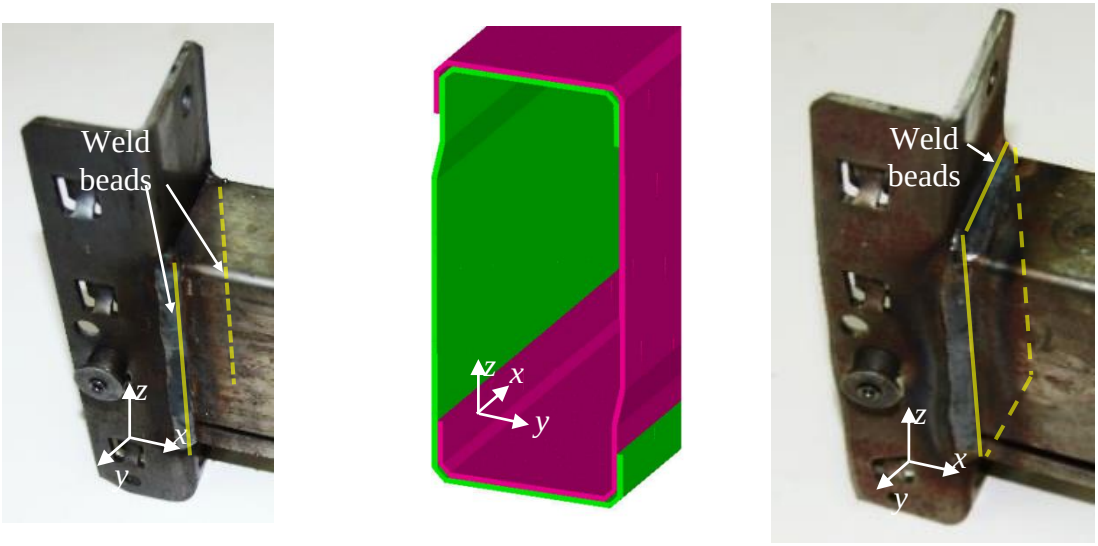

(d) Vertical Sides (VS) (e) Full Perimeter (FP)

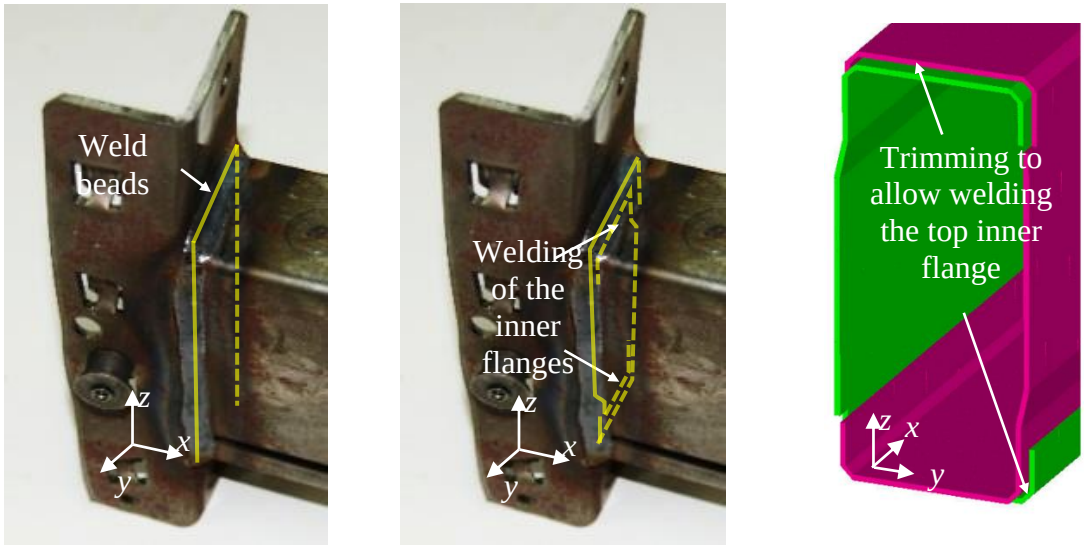

(f) Inverted U (IU) (g) Full Perimeter and Internal (hidden) Flanges (FPIF)

Figure 3. Beam to end-plate weld beads configurations

The first welding option (Figure 3.a) refers to the unmodified commercially available product, while the other (Figure 3.b, Figure 3.c and Figure 3.d) incorporate alterations aiming to strengthen the plate-to-beam welding. Noticeably, all these variations maintain the speed-lock character of the connection.

The steel grade for the uprights and the end-plates is S355 MC [36] and S275 [37]; apart from these nominal values, the actual mechanical parameters of the steel are determined after coupon tests. Also, the plate thickness is experimentally measured. In the performed tests, steel from 5 different coils has been utilized; Table 3 displays the experimental mechanical and geometrical parameters for each of them.

Table 3. Steel properties

Coil No.	Element	Thickness (mm)			Yield stress f_y (MPa)			Ultimate stress f_u (MPa)			Young Modulus E (GPa)
		Nominal	Mean	Charact.	Nominal	Mean	Charact.	Nominal	Mean	Charact.	Mean
1	Beam	1.5	1.483	1.46	275*	485.46	472.97	430–580	498.75	483.56	207.1
2	Beam	1.5	1.513	1.49	275*	470.72	463.80	430–580	486.47	478.50	214.8
3	Upright	2.5	2.55	2.55	355	406.94	401.35	430–550	487.31	485.22	202.5
4	End-plate	3.5	3.50	3.50	355	445.82	414.08	430–550	497.92	445.82	224.1
5	End-plate	3.5	3.543	3.39	355	428.69	407.03	430–550	476.93	449.24	211.4

*The values of f_y and f_u were increased by cold re-rolling

The important differences shown in Table 3 between the nominal (coil) and measured (element) yield stresses can be explained by the alleged excess of strength in the coil itself; conversely, the yield stress increase due to the folding process is not relevant, as the coupon specimens are taken from the flat parts of the section. Moreover, coils 1 and 2 were re-rolled to obtain the desired thickness; hence, in such a case, the yield stress increase is higher. Another consequence is the important brittleness attained: f_y and f_u are very close for beams; this low margin is not in accordance with the seismic design standards. Nonetheless, yielding occurs in the end-plate and the upright tabs, not in the beam profile. In fact, the objective of this research (strengthening the weld) is to avoid the brittle failure of the beam. Finally, a notable Young Modulus scattering between coils is observed; this issue is expected to influence the initial stiffness of the connection.

Testing set-up

Figure 4 describes the testing mock-up; Figure 4.a displays a global image view, and Figure 4.b presents a side sketch.

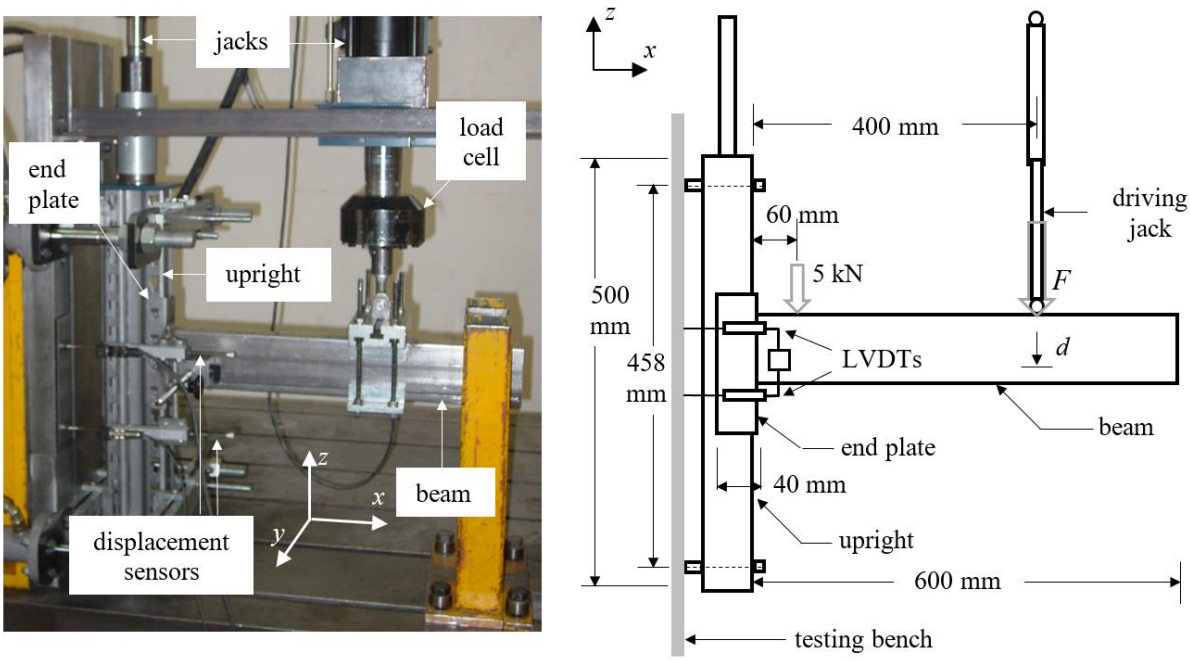

(c) General view (d) Lateral sketched view

Figure 4. Testing mock-up

Figure 4 shows that the upright and the beam segments are positioned (like in actual racks) in vertical and horizontal directions, respectively; their support conditions are described next. The upright segment is pinned at its top and bottom ends; all displacements are restrained at both ends. The beam segment's right end is free to rotate about *z* and *y* axes (bending), while the *x*-axis rotation (torsion) is prevented.

As discussed more deeply in subsection 0, the experiments consist basically in imposing, by using the right jack (Figure 4.a), vertical displacements to the right end of the beam segment; both downward and upward displacements are applied. The left jack slightly compresses the upright segment permanently to avoid uplift when the beam is pushed up (Figure 4.a).

Two major sets of sensors are employed: an assembly of two horizontal displacement transducers to measure the end-plate rotation about *y* axis (θ), and a load cell to measure the jack force.

Conducted experiments

As said above, two types of experiments are carried out: monotonic tests and cyclic tests. For both, regarding the particular regulations for adjustable pallet racking systems, standard [5] is

contemplated for general testing set-up issues. As well, the directions of the Eurocode 3 for constructional steel are also broadly accounted for; more precisely, [38] contains general rules and [39] deals with joints. The monotonic and cyclic tests are broadly discussed next.

- **Monotonic tests**. Both downward (beam hogging bending) and upward (beam sagging bending) monotonic proofs are carried out; their main objective is to define the limits of the imposed displacement laws of the cyclic experiments. Such cyclic bounds can be selected either using the racking code [20] or the generic regulation for connections [35]; the latter document is considered in this research. On the other hand, as indicated by the regulations [20], a minimum of three tests are performed in downward and reverse directions. Finally, Figure 4.b shows that an initial constant descendent vertical force of 5 kN is applied to the beam near its connection with the upright; this force is exerted through a lever mechanism, as displayed by Figure 5. Such 5 kN load has several objectives: (i) to represent somehow the shear force on the connection due to the gravity effect of the stored goods, (ii) to reproduce approximately the proportion between shear force and bending moment in actual connections, (iii) to avoid the undesired influence of gap, and (iv) to prevent hook slippage in upward tests. The value of this load is taken from [20]. In brief, all the considerations about pallet racks to define the monotonic tests are based on [20], while the cycling bounds (limits) for the subsequent cyclic tests have been taken according to [35].
- **Cyclic tests**. Two versions of cyclic tests are carried out: some are based on [35], while others consider the alternative testing method described in [2]. In both cases, the cycling bounds are selected according to the monotonic proofs shaped as [35], while the test arrangement follows [20]. As a consequence of this last issue, the 5 kN load mentioned above is also applied. Such load is not considered either in [35] or in [2]; this absence can be explained as [35] is intended to general steel connections (the issues discussed in the previous paragraph do not apply), and [2] does not deal with full speed-lock connections (since a locking bolt is placed, thus avoiding the gap between hooks and perforations, and hook slippage).

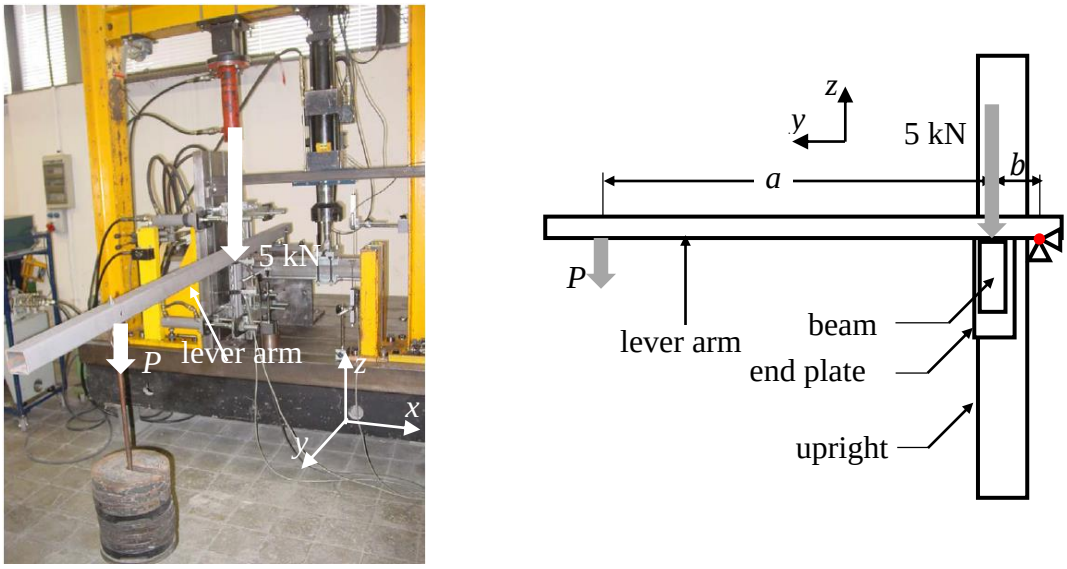

(a) General view (b) Front sketched view

Figure 5. 5 kN vertical force lever mechanism

Table 4 describes the main characteristics of the carried-out experiments. The tests' names, VS, FP, IU, and FPIF, stand for Vertical Sides (Figure 3.a), Full Perimeter (Figure 3.b), Inverted U (Figure 3.c), and Full Perimeter and Internal Flanges, respectively (Figure 3.d). M and C refer to Monotonic and Cyclic, respectively. In the monotonic tests, – and + correspond to upward and downward directions, respectively; tests FPIF-A and FPIF-B merely differ in the employed steel coil. In the cyclic tests, ECCS and CAS indicate the norm or document used to state the imposed displacement law ([35] and [2], respectively). The IU weld configuration is employed in the CAS tests, as the bottom horizontal side is not expected to work under tension; therefore, the IU specimens should be expected to perform like the FP ones. The test FPIF-C-0 was developed according to [2] without using the 5 kN force (Figure 5) and performing only the four initial loading cycles. Finally, the replica tests are distinguished by adding (1), (2), (3) to their name.

Table 4. Carried out experiments

Type	Name	Dates (No. of tests)	Coil No.
Monotonic	VS-M^+	30/06/2017, 04/07/2017(2)	1-3-4
	VS-M^-	30/06/2017, 03/07/2017(2)	1-3-4
	FP-M^+	03/07/2017, 05/07/2017, 08/01/2018	1-3-4
	FP-M^-	03/07/2017, 08/01/2018, 09/01/2018	1-3-4
	FPIF-A-M^+	24/10/2017, 26/10/2017(2)	1-3-4
	FPIF-A-M^-	05/07/2017, 31/10/2017(2)	1-3-4
	FPIF-B-M^+	24/07/2018(2),25/07/2018	2-3-5
	FPIF-B-M^-	25/07/2018,26/07/2018(2)	2-3-5
Cyclic	VS-C-ECCS	28/11/2017, 04/05/2018, 07/05/2018	1-3-4
	FP-C-ECCS	10/01/2018, 11/01/2018, 25/04/2018	1-3-4
	IU-C-CAS	22/05/2019 (4)	2-3-5
	FPIF-C-0	26/07/2018	2-3-5
	FPIF-C-ECCS	08/05/2018, 05/06/2018	1-3-4
	FPIF-C-ECCS-I	03/05/2018*	1-3-4
	FPIF-C-ECCS-II	21/11/2017*	1-3-4
	FPIF-C-CAS	27/07/2018(2), 15/06/2020,16/06/2020	2-3-5

*Cycles limits not according the corresponding monotonic tests (Figure 3.b)

In Table 4, the FPIF-C-ECCS tests performed on 03/05/2018 (I) and 21/11/2017 (II) were conducted by using different cycle bounds than in the other similar proofs; specifically, the further used the bounds of FP tests, and the latter used a different positive limit ($\theta_y^+ = 15$ mrad instead of $\theta_y^+ = 11.7$ mrad, Table 5); as stated in Table 4, such tests are referred next as FPIF-C-ECCS-I and FPIF-C-ECCS-II, respectively. This action aims is to analyze the influence of the cyclic bounds on the results; this issue is discussed in subsection 0.

Table 4 shows that not any VS-C-CAS experiment was carried out; the reason is that, for such type of test, early failure was detected in all the cases.

The main outputs of the monotonic experiments are the moment-rotation laws of the tested beam-to-upright connections; as discussed previously, such information is employed to establish the bounds of the cyclic experiments displacement laws. In this sense, Figure 6 displays the calculation of the initial and equivalent slopes (S_0 and S_{EN}), the yielding and ultimate moments (M_y and M_u), and rotation limits (θ_y and θ_u). These operations are performed according to [20,35]. M_{Rd} is the resisting moment obtained according to [5].

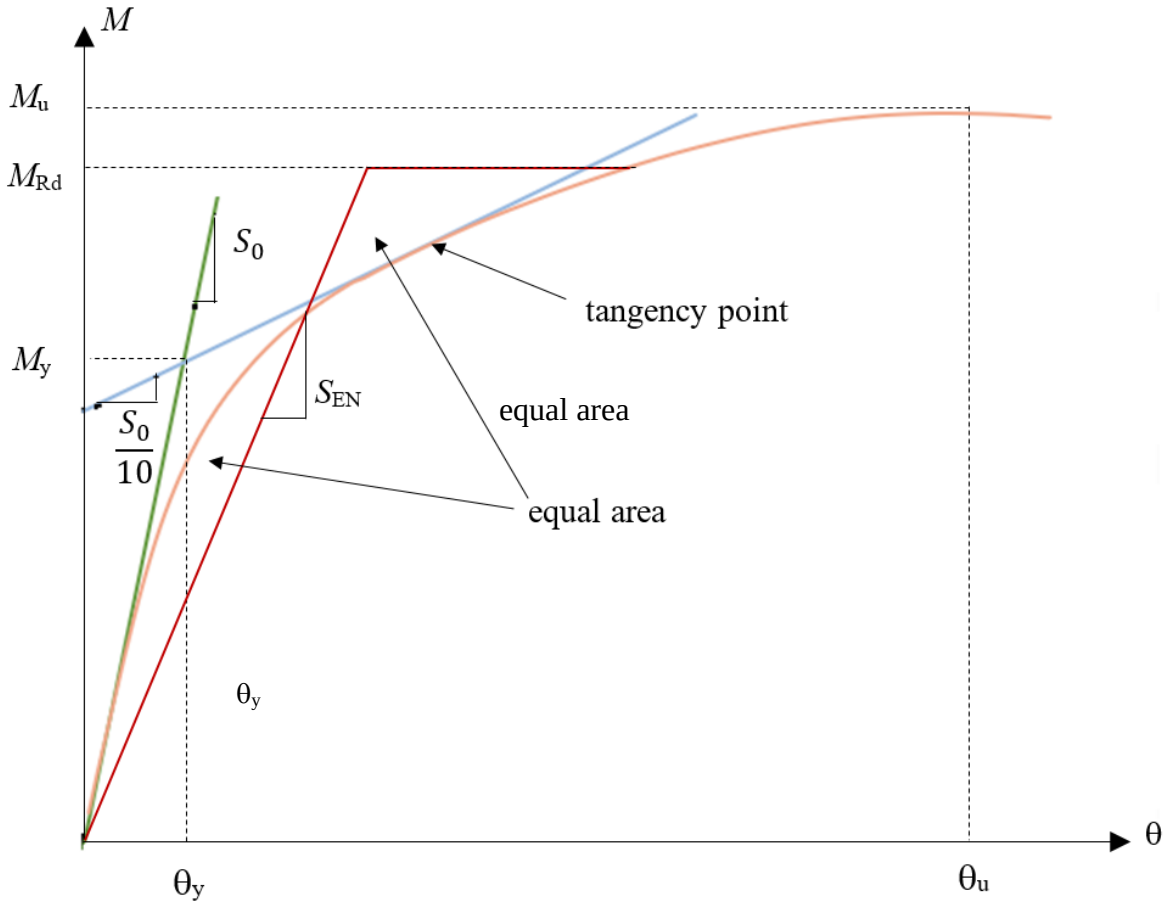

Figure 6. Determination of the initial and equivalent slopes and the yield and ultimate points after a monotonic moment-rotation curve

Figure 6 shows that the yield point (M_y, θ_y) is defined as the intersection between the tangent at the origin (slope S_0) and the tangent to the curve with slope $S_0 / 10$; the ultimate values (M_u, θ_u) correspond to the zero-slope (peak) point of the curve. The equivalent slope (S_{EN}) is generated through the equal-energy criterion; the area under the curve is equal to the one under the bilinear approximation formed by the horizontal line for M_{Rd} and the straight line with slope S_{EN}.

Table 4 shows that two displacement protocols are imposed in the cyclic tests, namely according to [2,35]. Both documents consider four increasing cycles and several sets of three constant inelastic cycles, whose amplitude is increased until failure. Precise descriptions are included next.

- **[ECCS 45 1986]**. This regulation states that the protocol consists of one cycle for each of the intervals $[\theta_y^+/4, \theta_y^-/4]$, $[2\,\theta_y^+/4, 2\,\theta_y^-/4]$, $[3\,\theta_y^+/4, 3\,\theta_y^-/4]$ and $[\theta_y^+, \theta_y^-]$, then three

cycles at the interval $[2\,\theta_y^+, 2\,\theta_y^-]$, and finally three cycles at each of the intervals $[2\,(n+1)\,\theta_y^+, 2\,(n+1)\,\theta_y^-]$ (n = 1, 2, ...).

- **[Castiglioni 2016]**. The recommendations of [20,35] do not account for the actual asymmetric rotation histories (i.e. not centered at zero rotation) when seismic shaking is combined with gravity loads; thus, a modification is proposed herein. The imposed displacement law is established in terms of the vertical displacement of the pushing point (d, Figure 4); it consists of one cycle for each of the intervals $[d_y^+/4, d_y^-/4]$, $[2\,d_y^+/4, 2\,d_y^-/4]$, $[3\,d_y^+/4, 3\,d_y^-/4]$ and $[d_y^+, d_y^-]$, and two or three cycles at the intervals $[(2+n)\,d_y^+ + \Delta d_n^+, (2+n)\,d_y^- + \Delta d_n^-]$ (n = 0, 1, ...). In these expressions, d_y^+ and d_y^- are the yield displacements (corresponding to rotations θ_y^+ and θ_y^-, respectively), and Δd_n^+ and Δd_n^- are the displacement amplitudes until the force-controlled part of the cycle reaches the force correspondent to gravitational load. For further clarity, Figure 7 displays the proposed plastic cycles; positive forces induce hogging bending (downward force), F_y is the yielding force (corresponding to moment M_y), and F_g is the gravity force corresponding to the considered loading level.

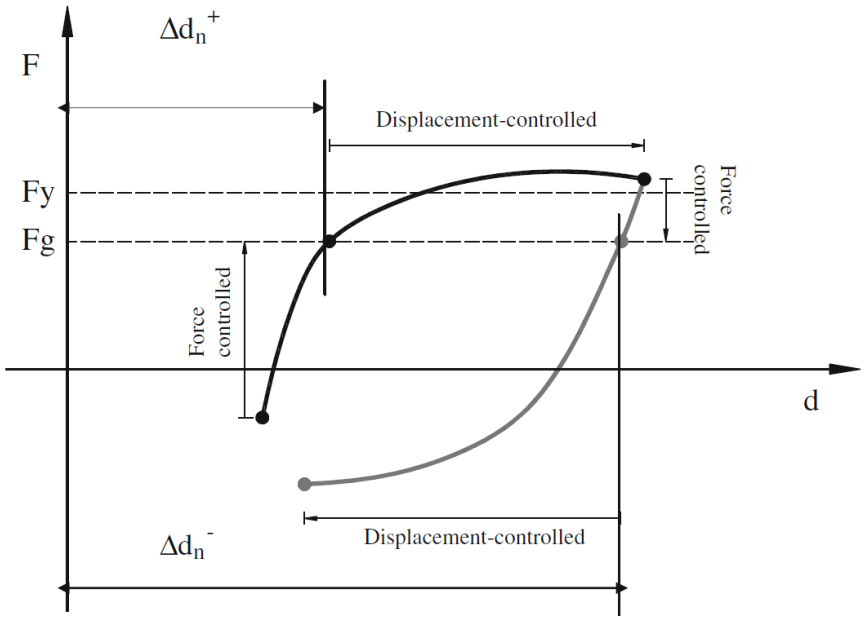

Figure 7. Upward and downward plastic loading-unloading cycles [2]

Figure 7 shows that both the positive (increasing downward displacement) and negative (decreasing downward displacement) branches consist of force-controlled and displacement-controlled segments; thus, the gravity force (F_g) is the border between them. The test end is defined with respect to F_g; ordinarily, it arises in the positive branch: either in its force-

controlled part (the specimen fails to develop F_g) or, in its displacement-controlled part (the restoring force decreases below F_g). Obviously, the end can also occur when beam sectional collapse arises. The test should be performed for different values of F_g (in terms of percentage of F_y); [2] suggests the following percentages: 25, 50, 66 and 75%.

Results of the experiments

Monotonic experiments

This subsection describes and discusses the results of the monotonic tests (M^+ and M^-) that are listed in Table 4. Figure 8 displays the measured moment-rotation curves. The plotted moments include the effect of the constant 5 kN load (Figure 4 and Figure 5).

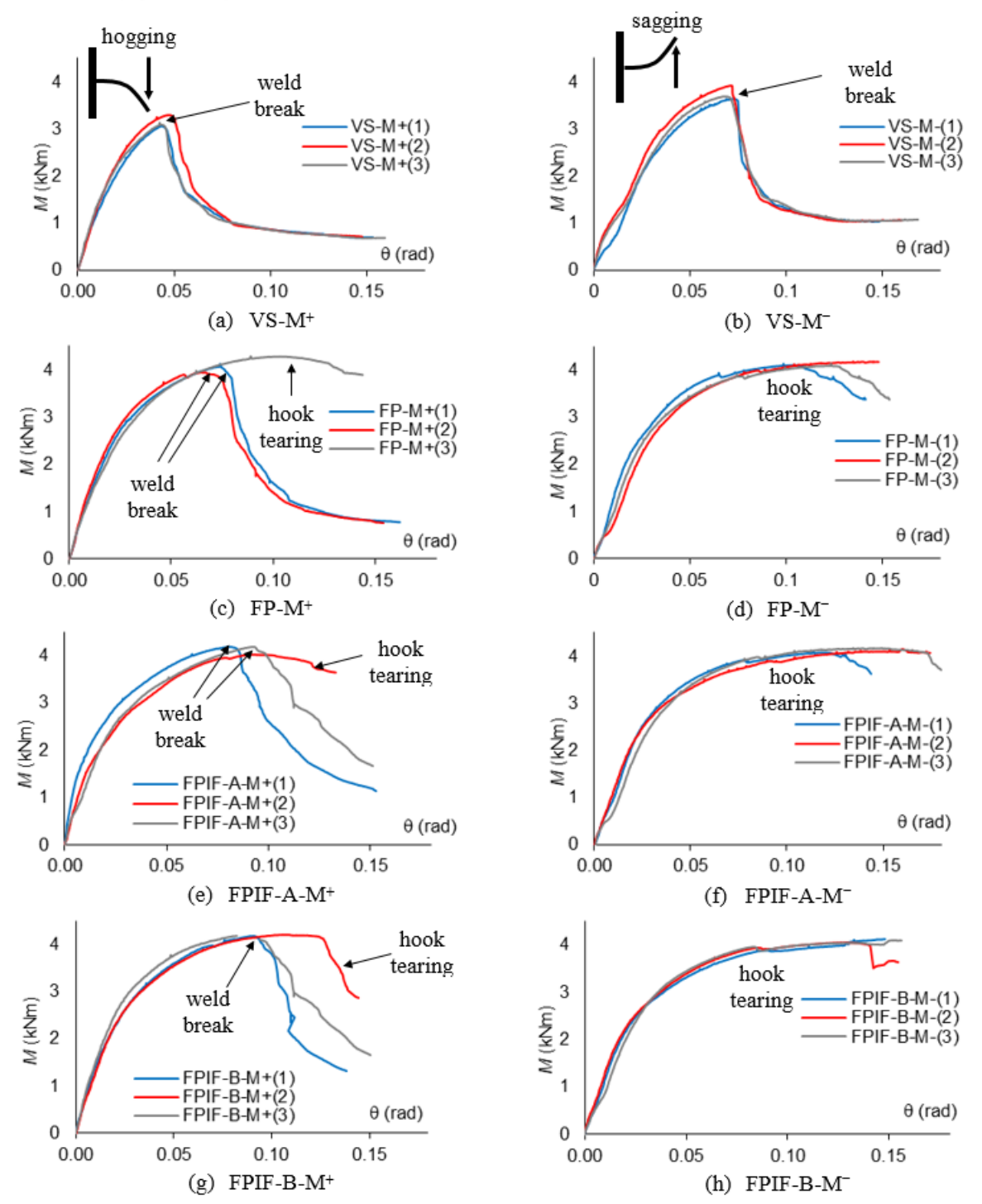

Figure 8. Moment-rotation plots for the monotonic tests (Table 4)

The sudden drops in Figure 8.a, Figure 8.b, Figure 8.c (tests No. 1 and 2), Figure 8.e (tests No. 1 and 3) and Figure 8.g (tests No. 1 and 3) correspond to the brittle failure of the welding between the end-plate and the beam. In the other cases the tearing in the hooks and perforations

(tabs) is observed. An example of each failure type is displayed in Figure 9.a and Figure 9.b, respectively.

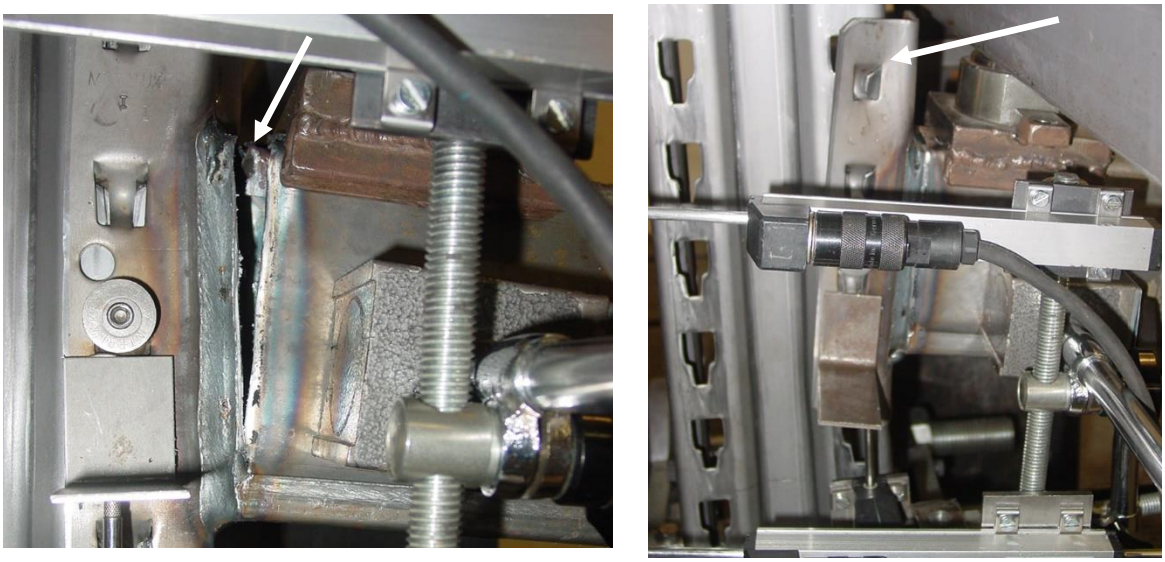

(a) Weld break (test FP-M^+(1))

(b) Hooks and perforations tearing (test FP-M^+(3))

Figure 9. Major failure types in the monotonic tests (Table 4)

The curves for each weld geometry that exhibit the same failure type have been averaged to facilitate a global comparison between the different results of Figure 8. The resulting curves are displayed in Figure 10.a (hogging) and Figure 10.b (sagging); light lines correspond to weld break and heavy lines to hook tearing.

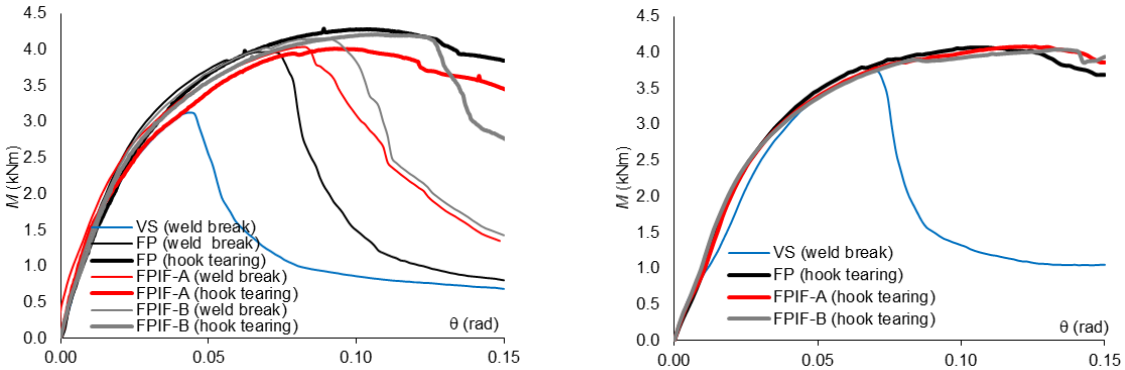

(a) Hogging (b) Sagging

Figure 10. Averaged moment-rotation plots for the monotonic tests

Figure 10 shows that the specimens with hooked assembly failure behave similarly, regardless of the weld bead geometry. Analogously, Figure 10.a indicates that the monotonic curves with weld break show relevant coincidence before the weld crack; regarding the post-failure, as expected, the more weld is applied, the later the weld failure occurs (i.e. at higher values of rotation of the connection).

Table 5 displays the parameters described in Figure 6 obtained from the monotonic tests (Figure 8). The last two columns in Table 5 describe the failure mode; "Weld" refers to the rupture of the welding (*break*, Figure 9.a), and "Hook" means large deformation and slide of the hooks inside the upright perforations (*tearing*, Figure 9.b). The monotonic IU tests had not been carried out; the positive (downward) and negative (upward) values are taken from the FP-M^+ and VS-M^- tests, respectively. Such correspondences have been established based on their behavior similarity. In both cases, slight corrections [5] are introduced, given that the material, yet being formally the same, corresponds to a different coil (Table 3 and Table 4).

Table 5. Parameters derived after the monotonic experiments (Table 4)

Weld beads configuration	Test	Test No.	S_0 (kNm/rad)		S_{EN} (kNm/rad)		M_y (kNm)		θ_y (mrad)		M_u (kNm)		M_{Rd}* (kNm)		θ_u (mrad)		Failing component	
			M^+	M^-	M^+	M^-	M^+	M^-	M^+	M^-	M^+	M^-	M^+	M^-	M^+	M^-	M^+	M^-
VS (Figure 3.a)	VS-M^+, VS-M^-	1	137	81	111	77	2.75	3.39	20.5	41.8	3.06	3.64			43.8	75.2	Weld	Weld
		2	134	160	125	97	2.97	3.10	22.1	19.4	3.29	3.90			47.0	72.2	Weld	Weld
		3	147	138	124	97	2.72	3.08	18.5	18.5	3.12	3.69			43.7	69.1	Weld	Weld
		Mean	**139**	**126**	**120**	**90**	**2.81**	**3.19**	**20.4**	**26.6**	**3.16**	**3.74**	**2.25**	**2.68**	**44.8**	**72.2**	-	-
IU** (Figure 3.c)	FP-M^+, VS-M^-	1	158	69	104	76	2.94	3.17	18.6	45.9	3.74	3.31			70.1	71.0	-	-
		2	182	97	116	89	2.89	3.23	15.9	33.5	3.59	3.54			63.7	68.9	-	-
		3	178	154	98	89	2.82	2.70	15.9	17.6	3.91	3.34			101	66.0	-	-
		Mean	**173**	**107**	**106**	**85**	**2.88**	**3.03**	**16.8**	**32.3**	**3.75**	**3.40**	**2.93**	**2.44**	**78.3**	**68.6**	-	-
FP (Figure 3.b)	FP-M^+, FP-M^-	1	149	100	105	95	3.33	3.62	22.3	36.2	4.07	4.10			74.0	102	Weld	Hook
		2	167	99	115	80	3.29	3.52	19.7	35.4	3.94	4.17			64.6	148	Weld	Hook
		3	165	117	99	83	3.28	3.49	19.6	28.2	4.25	4.08			111	125	Hook	Hook
		Mean	**160**	**105**	**106**	**86**	**3.30**	**3.54**	**20.5**	**33.3**	**4.09**	**4.12**	**3.21**	**3.33**	**83.2**	**125**	-	-
FPIF-A (Figure 3.d)	FPIF-A-M^+, FPIF-A-M^-	1	266	128	148	89	2.67	3.27	10.0	25.6	4.17	4.08			82.0	114	Weld	Hook
		2	181	110	115	96	2.89	3.23	15.9	29.4	4.01	4.07			94.0	173	Hook	Hook
		3	263	106	111	101	2.42	3.44	9.20	32.5	4.17	4.15			93.0	154	Weld	Hook
		Mean	**237**	**115**	**125**	**95**	**2.66**	**3.31**	**11.7**	**29.2**	**4.12**	**4.10**	**2.46**	**2.48**	**90**	**147**	-	-
FPIF-B (Figure 3.d)	FPIF-B-M^+, FPIF-B-M^-	1	146	112	105	91	3.31	3.22	22.6	28.7	4.17	4.09			92.0	160	Weld	Hook
		2	151	125	105	96	3.22	3.23	21.3	26.0	4.19	4.15			109	127	Hook	Hook
		3	171	104	125	94	3.24	3.44	18.9	33.1	4.18	4.07			83.0	155	Weld	Hook
		Mean	**156**	**114**	**112**	**94**	**3.26**	**3.30**	**20.9**	**29.3**	**4.18**	**4.10**	**3.00**	**2.93**	**94.7**	**147**	-	-

*Modified characteristic value obtained from M_u according to [5]

**These experiments were not performed. The indicated values come from FP-M^+ and VS-M^-

Figure 8 and Table 5 show that the welding configuration significantly influences the connection monotonic performance, both in moment capacity and rotation ductility: as expected, the longer welding bead (FPIF), the better performance. More precisely, in all the VS tests, failure arises in the welding, while both FP and FPIF sagging tests always show a hook failure mode (tearing). Additionally, FP and FPIF hogging tests show both weld and hook failures. However, the influence of the welding path in both the initial and equivalent stiffness is not relevant, as the observed variations are rather erratic and are frequently uncorrelated with the alleged weld stiffness (this trend can also be seen in Figure 10). Going to more particular issues, a moderate pinching-like phenomenon occurs in some tests for small pulling forces (No. 1 in Figure 8.b, No. 2 in Figure 8.d, No. 3 in Figure 8.f and No. 3 in Figure 8.h); it is apparently due to lateral slippage of the end-table hooks inside perforations of the upright. Finally, the difference between the positive and negative values of θ_u can be explained by the early failure of the welding displayed in Figure 8.c.

Cyclic experiments

Analogously to subsection 0, this subsection presents the results of the cyclic tests (C-0, C-ECCS, and C-CAS) listed in Table 4. Apart from the particular case of the FPIF-C-0 test, the limits of the cyclic experiments C-ECCS and C-CAS are selected from the positive and negative average values of the yield rotation in Table 5. Regarding this issue, the precise correspondences are as follows: the bounds of VS-C-ECCS, FP-C-ECCS, and FPIF C-ECCS are taken from VS, FP, and FPIF-A monotonic test, respectively; the bounds of IU-C-CAS and FPIF-C-CAS are taken from IU, and FPIF-B monotonic test, respectively. In this sense, Table 4 shows the right correspondence between the material coils and the matching monotonic and cyclic tests.

As discussed in subsection 0, test FPIF-C-0 (Table 4) did not include the 5 kN load (Figure 4 and Figure 5); then, in order to investigate the influence of such force, Figure 11 displays a comparison between the M-θ plots of test FPIF-C-0 and the first four cycles of test FPIF-C-CAS (for 50%). Figure 11 shows that both proofs exhibit significant pinching, with important near-horizontal branches in the vicinity of the origin point. In the FPIF-C-CAS test, the bounds of the four plotted loops have been established as

described in the previous paragraph. Conversely, in the FPIF-C-0 test, the bounds for negative rotation angle (sagging) have been extended by basically ignoring most of the aforementioned horizontal branches (pinching); otherwise, almost no energy dissipation would be observed in the left part of the hysteresis loop. This circumstance (the abnormal extension of the pinching branches in the sagging part of the FPIF-C-0 test) can be explained by the partial pullout of the hooks in the upright perforations (the safety rivet prevents the total pullout, Figure 1.b). These considerations endorse the use of the aforementioned 5 kN force in order to avoid these undesirable effects. However, it should be kept in mind that the hook sliding might feasibly occur in real unloaded rack segments undergoing seismic excitation.

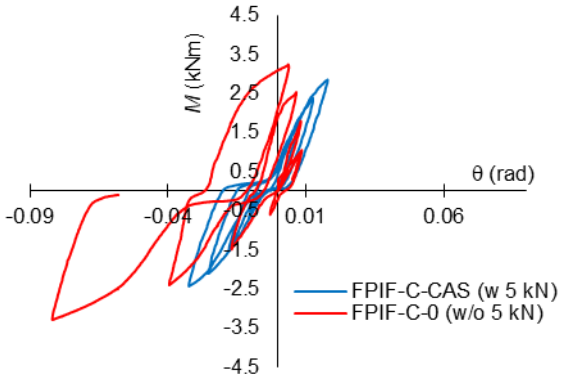

Figure 11. M-θ plots of test FPIF-C-0 and the first four cycles of test FPIF-C-CAS (for 50%)

Figure 12 displays the moment-rotation loops of C-ECCS and C-CAS tests. Like in the monotonic experiments (Figure 8), in Figure 12 the positive and negative moments and rotations correspond to downward and upward driving forces, respectively.

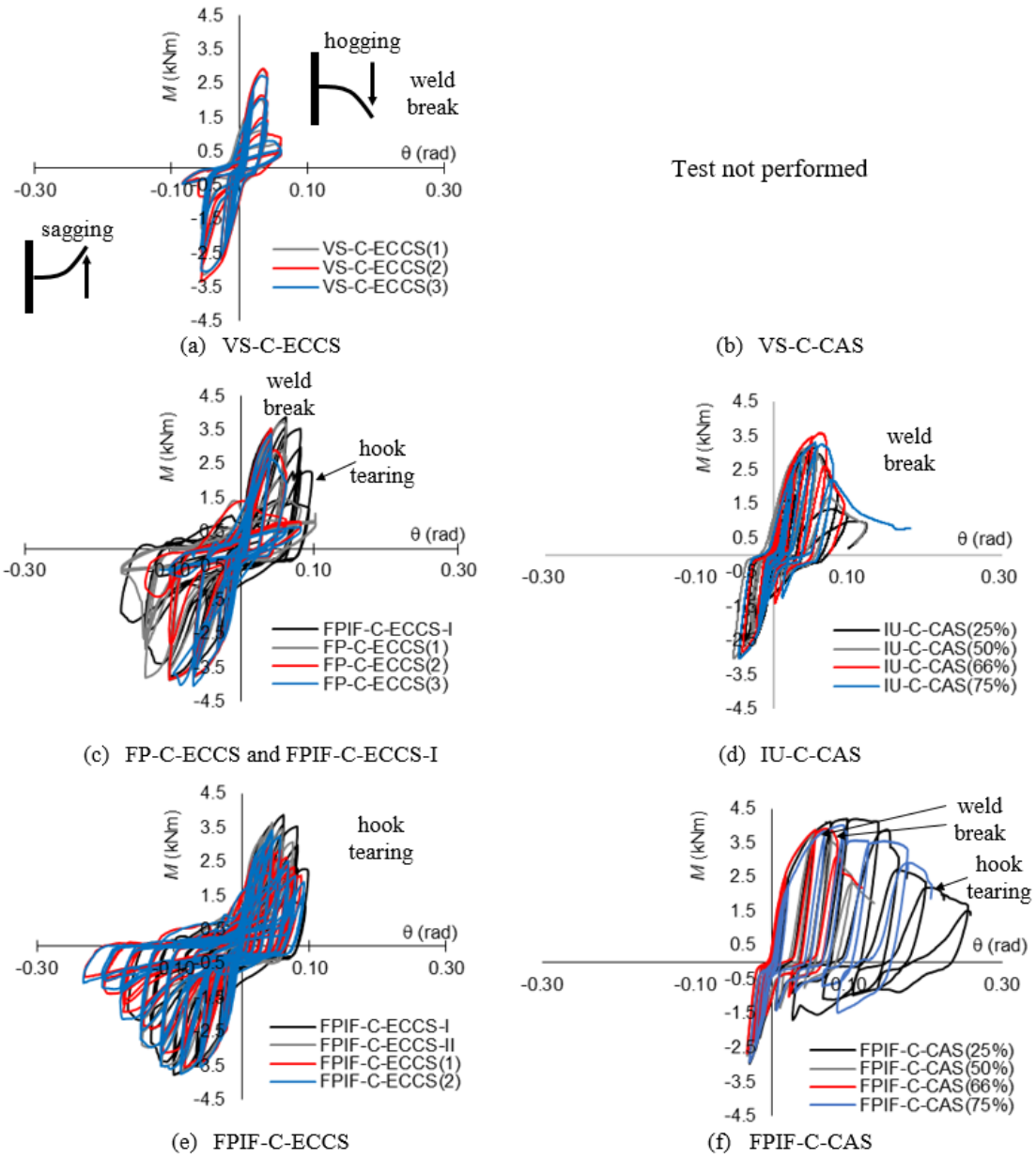

Figure 12. Moment-rotation plots for the cyclic tests (Table 4)

Analogously to Figure 9, Figure 13 displays representative examples of the failure modes. As in the monotonic experiments, the failure can be produced either due to weld break, or excessive hook/end-plate/upright deformation. Noticeably, the weld rupture always starts at the top front corner, as shown in Figure 13.a.

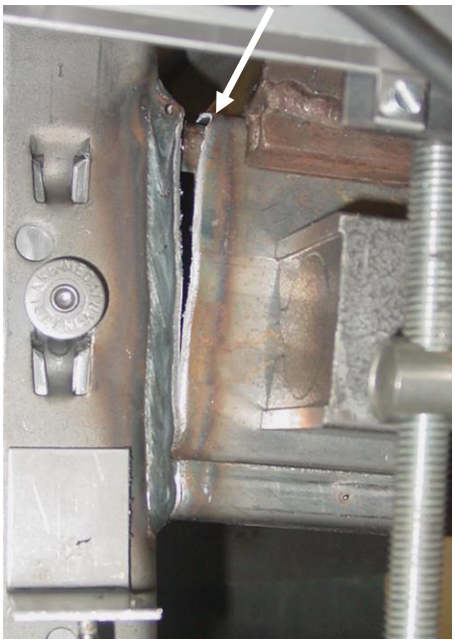

(a) Weld break (front view of test IU-C-CAS for 50%)

(b) Hooks and perforations tearing (rear view of test FPIF-C-ECCS-I)

Figure 13. Failure modes in the cyclic tests (Table 4)

Analogously to Table 5, Table 6 displays the most meaningful output parameters of the cyclic tests (Table 4). In the column labeled “Date”, each test is identified by the date it was performed; “Mean” refers to the average of the experiments belonging to the same category. The column labeled “Gravity load percentage” contains the percentages of F_y in the Castiglioni tests. In the subsequent columns, the maximum rotation (θ_{max}) corresponds to the peak positive and negative values, the displacement ductility (μ) refers to the considered average yield rotation (after the monotonic tests, Table 5), the number of cycles includes even the initial ones (although their encompassed area is rather small), the absorbed energy is the area encompassed by the hysteresis loops, the failing component is indicated as in Table 5 (for the monotonic tests), and, finally, the last column (labeled “Test end”) only refers to the Castiglioni experiments and describes whether the end is produced in the displacement or force-controlled branch.

Table 6. Parameters derived after the cyclic experiments

Name	Date	Gravity load percentage	θ_{max} (mrad)		μ (θ_{max} / θ_y)		Number of cycles	Absorbed energy (kJ)	Failing component	Test end
			+	–	+	–				
VS-C-ECCS	28/11/2017	-	61	83	2.99	3.12	9	0.61	Weld	-
	04/05/2018	-	61	83	2.99	3.12	9	0.57	Weld	-
	07/05/2018	-	61	83	2.99	3.12	10	0.66	Weld	-
	Mean		**61**	**83**	**2.99**	**3.12**	**9⅓**	**0.61**	-	-
FP-C-ECCS	10/01/2018	-	103	166	5.02	4.98	15	2.57	Weld	-
	11/01/2018	-	82	133	4.00	3.99	11	1.37	Weld	-
	25/04/2018	-	82	112	4.00	3.36	11	1.17	Weld	-
	Mean		**89**	**137**	**4.34**	**4.11**	**12⅓**	**1.70**	-	-
IU-C-CAS	22/05/2019	75%	180	46	10.71	1.42	6½	0.51	Weld	Force branch
	22/05/2019	66%	92.2	41	5.49	1.27	7	0.46	Weld	Displacement branch
	22/05/2019	50%	121	53	7.20	1.64	8	0.56	Weld	Displacement branch
	22/05/2019	25%	114	54	6.79	1.67	10	0.76	-	Displacement branch
FPIF-C-ECCS	08/05/2018	-	87	227	7.44	7.77	22	3.85	Hook	-
	05/06/2018	-	91	232	7.78	7.95	24	3.99	Hook	-
	Mean		**89**	**230**	**7.61**	**7.86**	**23**	**3.92**	-	-
FPIF-C-ECCS-I*	03/05/2018	-	97	166	8.29	5.68	15	3.05	Hook	-
FPIF-C-ECCS-II*	21/11/2017	-	75	146	6.41	5.00	16	2.87	Hook	-
FPIF-C-CAS	15/06/2020	75%	200	28.9	9.57	0.99	8½	1.46	Hook	Displacement branch
	27/07/2018	66%	120	32	5.74	1.09	6½	0.51	Weld	Displacement branch
	27/07/2018	50%	133	32	6.36	1.09	7½	0.61	Weld	Displacement branch
	16/06/2020	25%	256	29.3	12.25	1.00	11½	1.46	Hook	Displacement branch

*The ductility is determined from the actual yield angle (θ_y)

Figure 12 and Table 6 provide relevant information about the carried out cyclic experiments. For further clarity, Figure 14 presents some of the results in Figure 12, although organized differently.

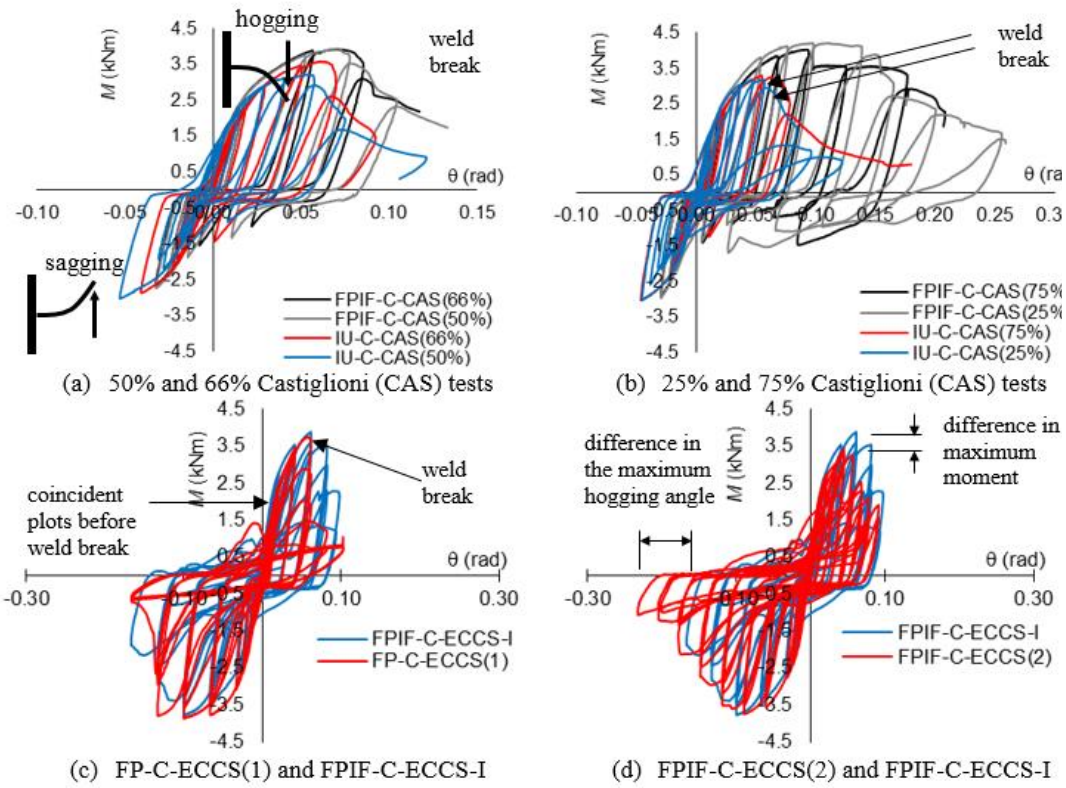

Figure 14. Comparison between some moment-rotation plots in Figure 12

The observations arising from Figure 12, Table 6, and Figure 14 are discussed next.

- **Common remarks**. All the tests exhibit a rather relevant ductility, both in terms of displacement and absorbed energy; even the first cycles encompass a significant area. Also regarding ductility, failure arises after substantial stiffness and strength degradation. The most negative circumstance is the pinching effect due to the gap between the end-plate hooks and the upright perforations (Figure 13.b).
- **Comparison between ECCS and CAS**. As expected, in the C-ECCS tests, the cycles are asymmetric in terms of rotation; this can be explained by the difference in the positive and negative values of θ_y (Table 5). Conversely, the loops are more clearly asymmetric in the C-CAS tests; moreover, such asymmetry increases as the test progresses (subsection 0). Global comparison between the ECCS and Castiglioni tests shows that, as expected, the C-CAS tests are more demanding than the C-ECCS ones, in the sense that the obtained performance of the tested connection (in terms of the number of cycles and dissipated energy) is smaller. This dissimilarity seems to indicate that the testing protocol in [2] should be generally preferred as being closer to reality (the actual behavior depends on the weight of the stored goods).
- **Comparison between CAS for 75%, 66%, 50% and 25% of F_y**. The results of C-CAS and C-ECCS tests tend to converge as the percentage of the gravity force decreases; this trend is predictable, as the assumed gravity force is the main difference between both testing protocols. Nonetheless, this tendency is interrupted when experiments of the same type

present arbitrarily distinct failure modes; for example, for the FPIF test series (Figure 12.d), two of the specimens (50% and 60%, Figure 14.a) present a weld break while the other specimens (25% and 75%, Figure 14.b) do not.

- **Comparison between VS, FP, IU and FPIF**. As anticipated by the results of the monotonic experiments (subsection 0), FPIF performs better than FP and, in turn, FP performs better than VS. This trend is clearly shown by the column "Failure mode" in Table 6: in all the VS and FP tests failure arises in the welding, while in the FPIF experiments such brittle failure mode occurs in two cases only. The Castiglioni tests require particular discussion as they are the only ones including IU (Inverted U) welding; in this sense, as expected, the behavior of FPIF is better than that of IU even for weld break (CAS 50% and 66%, Figure 14.a). In the FPIF cases where weld failure is avoided, the behavior of such connection type is significantly better than IU (CAS 25% and 75%, Figure 14.b).
- **Particular comparison between FP-C-ECCS and FPIF-C-ECCS-I**. This contrast follows the general trends pointed out in the previous paragraph; more specifically, FPIF specimens do not present a weld failure, while FP ones do. On the other hand, as expected, the weld path does not considerably affect the cyclic behavior before such failure is produced. For higher clarity, plots FP-C-ECCS(1) and FPIF-C-ECCS-I are contrasted in Figure 14.c. FP-C-ECCS(1) has been chosen (instead of 2 or 3 tests) as it presents a later weld break and, consequently, clearly shows the aforementioned pre-failure plot coincidence.
- **Particular comparison between FPIF-C-ECCS and FPIF-C-ECCS-I**. This contrast is displayed in Figure 14.d. The difference between the negative angles of both tests can be easily explained by the definition of the cycle bounds. More significantly, larger sagging angles lead to smaller maximum hogging moments. This behavior is rather similar to the well-known Bauschinger effect (of materials behavior). It can be attributed to the higher deterioration (tearing) of the hook-perforation assemblies as it affects the connection moment capacity both for positive and negative moments. Comparison with FPIF-C-ECCS-II provides similar remarks.

As a supplementary remark, it is observed that the ECCS cyclic plots (Figure 12.a, Figure 12.c, Figure 12.e, Figure 14.c and Figure 14.d) show notable differences between the three specimens in terms of strength and stiffness degradation. These two issues are of paramount interest for understanding the seismic behavior of pallet racks' beam-to-upright connections. Figure 15.a displays the averaged backbone curves for each weld configuration. The backbone curve can describe strength degradation; this graph is drawn by joining the maximum moment points (M_i) of each loading grade (group of three cycles with the same amplitude θ_i) of the cyclic test curves. Stiffness degradation is represented by the evolution of each loading grade's secant stiffness (S_i)

throughout the rotation angle ($S_i = M_i / \theta_i$). Figure 15.b displays, also for each weld configuration, plots of S_i vs. θ_i. Noticeably, in Figure 15, FPIF-C-ECCS-I and FPIF-C-ECCS-II are not averaged with the rest of FPIF-A specimens for presenting different cyclic bounds.

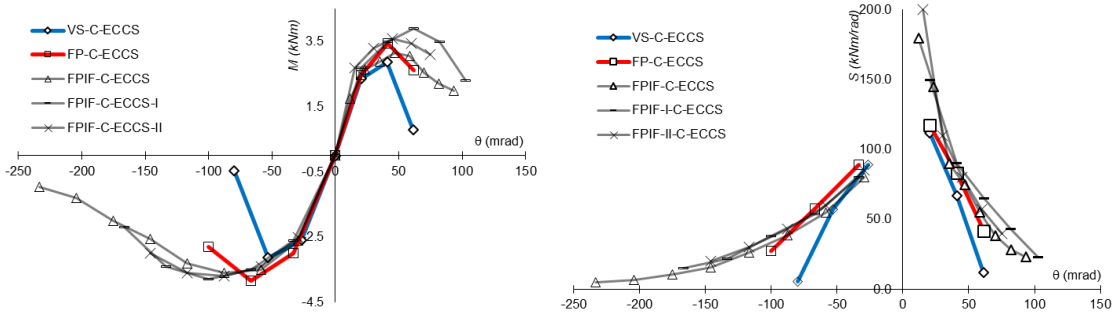

a) Backbone curves b) Secant stiffness vs. rotation angle

Figure 15. Stress and stiffness degradation. ECCS tests.

Figure 15 shows that strength and stiffness degradations occur more progressively for FPIF than for the rest of the specimens due to the hook ductile failure mode; the failure of FPIF specimens (Table 4) is smoother than the sudden weld break of the rest of the weld configurations. Furthermore, both strength and stiffness degradations prove to be more severe in the hogging branch, especially for FPIF. Finally, Figure 15.b shows that FPIF exhibits a significantly higher value of initial stiffness, as already observed in the monotonic tests (Table 3); nonetheless, as the test progresses, this difference vanishes.

Table 6 displays the dissipated energy in the cyclic experiments; as discussed, the values for FPIF are significantly higher than those for the other welding paths (VS, FP, and IU). However, in order to highlight the seismic capacity of the proposed welding solution, these values need to be compared with common input and hysteretic energy levels in medium-to-high seismicity regions; the following paragraph contains a preliminary appraisal.

Nowadays, Japan is the only country that includes input energy spectra in its regulations; the Japanese design code [40] states that the maximum input energy (i.e. corresponding to the spectrum plateau and to the most seismic prone zones of Japan) in terms of equivalent velocity ranges between V_E = 234 cm/s for rock and V_E = 312 cm/s for soft soil. These values can be converted into actual input energy as $E_I = ½\ m\ (V_E)^2$; in that expression, m is the mass of the structure under consideration. On the other hand, studies carried out from Colombian and Turkish records [41,42] provide rather similar results. All this information is compared next with the energy dissipation capacity of racks. A typical value of the beam span length for racks is 2 m, and the maximum load can be assumed as 3 kN/m. As the rack lateral motion during severe seismic shaking is basically rigid-body (i.e. rigid uprights and beams connected by rotational springs), it can be reasonably assumed that the seismic input energy is distributed rather uniformly between

all the beam-to-column connections. Therefore, it can be concluded that a mass of 300 kg corresponds to each connection; in that situation, the input energy per connection (in soft soil) is $E_I = ½\ m\ (V_E)^2 = ½\ 300 \times 3.12^2 = 1460$ J = 1.46 kJ. Table 6 shows that this value is clearly below the energy absorption capacity of the tested FPIF connections (ranging between 2.87 kJ and 3.99 kJ, except for CAS loading protocols, which are more demanding); conversely, it exceeds the capacities for VS, IU, and FP. Moreover, the seismic hysteretic energy (i.e. the energy contributable to damage) will be smaller than the input one. These considerations seem to indicate the seismic ability of the proposed welding solution.

Comparison between monotonic and cyclic experiments

This subsection contrasts the cyclic and monotonic proofs. In this sense, Figure 16 displays comparisons between the cyclic tests (Figure 12) and the corresponding monotonic experiments (Figure 8). The cyclic and monotonic plots are drawn in grey and black, respectively; this criterion is also considered for the additional information on the failure type (hook or weld). Figure 16.a and Figure 16.b refer to VS and FP specimens, respectively; given that the Castiglioni tests for such weld configurations were not performed (Figure 12.b and Figure 12.d), all the plotted curves correspond to the ECCS protocol (this is indicated in the captions). Figure 16.c and Figure 16.d relate to FPIF specimens for ECCS and CAS testing protocols, respectively. In order to emphasize the suitability of the comparisons in Figure 16, it should be kept in mind that tests FPIF-A-M^+, FPIF-A-M^- and FPIF-C-ECCS (Figure 16.c) use the same steel coils (1-3-4, Table 4); also tests FPIF-B-M^+, FPIF-B-M^- and FPIF-C-CAS (Figure 16.d) utilize the same identical coils (2-3-5, Table 4).

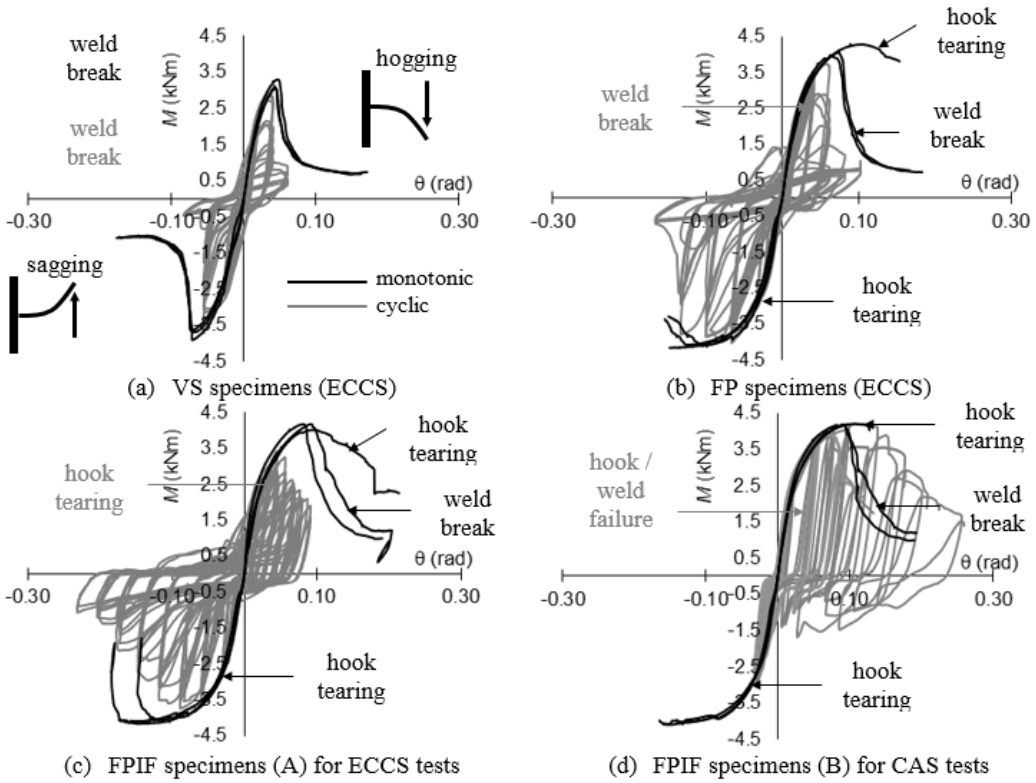

Figure 16. Comparison between monotonic and cyclic tests

Figure 16 shows that, as expected, the monotonic plots are basically the backbone curves of the cyclic loops. More precisely, the closest coincidence emerges in the initial cycles vs. the growing segments of the monotonic curves; conversely, the differences between both types of plots become more significant as damage progresses. Deeper considerations are discussed next, separately for the ECCS and CAS experiments.

- **ECCS tests**. Figure 16.a, Figure 16.b and Figure 16.c show that the force (moment) strength is higher in the monotonic tests (for both hogging and sagging); this circumstance can be explained by the cumulated damage in the hook-perforation assembly and the low-cycle (plastic) fatigue in the weld.
- **CAS tests**. Figure 16.d shows a meaningful coincidence between the hogging monotonic and cyclic branches corresponding to the same failure type. This proximity might be explained by the smaller absorbed energy, thus leading to less cumulated damage (Table 6). Further research is necessary to confirm this trend.

In brief, Figure 16 shows that, except perhaps for the CAS tests, the monotonic laws cannot be considered, in their present form, for numerical dynamic analysis because they differ significantly from the cyclic laws.

- **Conclusions**

This paper aims to investigate the seismic performance of racking systems; in order to do this, vertical cantilever monotonic and cyclic tests of speed-lock upright-to-beam connections are presented and discussed. Such connections consist in welding the beam to an intermediate L-shaped end-plate; in its turn, this element is connected to the upright through a hooked assembly. Noticeably, the beam section is made of two nested C-lipped profiles. The tested specimens differ in the weld path between the end-plate and the upright. Four beads geometries have been utilized; in crescent order of weld bead length, they are: VS (Vertical Sides only), IU (Inverted U, i.e. vertical sides and top flange), FP (Full Perimeter, i.e. vertical sides and top and bottom flanges) and FPIF (Full Perimeter and Internal Flanges, i.e. FP but welding not only the external flanges of both nested C-lipped profiles, but also the internal ones). This last weld configuration constitutes the main contribution of this work and aims to guarantee that the failure arises in the hooked assembly (connection between the end-plate and the upright) instead of in the weld; this shift is expected to generate a rather ductile failure mode. The cyclic tests have been conducted according to both the European document [35] and a recently proposed modification (CAS, [2]); its main novelty is a modification of the imposed displacement protocol accounting for the gravity loads influence. In both testing protocols, the test arrangement of [20] (even the 5kN load) has been used as it is more suitable for pallet racks.

The carried-out experiments provide the following major conclusions:

- The four tested weld paths provide different results; in global terms, as expected, the longer the weld beads, the better the performance. This trend is observed in terms of strength, stiffness, and absorbed energy; regarding this last issue, shorter beads generally lead to early weld break, while this undesired brittle failure mode is totally avoided in the FPIF weld configuration tested under the ECCS protocol. Preliminarily, this indicates a satisfactory behavior of the proposed weld bead geometric configuration.
- The CAS testing protocol is more demanding than the ECCS one and fits better the actual conditions of racks under the combined effect of seismic excitations and gravity loads.
- The cyclic test results are very sensitive to the testing protocols (ECCS vs. CAS) and also little sensitive to the cyclic bounds. Further research might be necessary to define the protocol and the limits better.
- Although the monotonic plots are basically the backbone curves of the cyclic loops, their comparison shows significant differences in their final segments, while the pre-failure ones are rather similar. This trend can be explained by the influence of the cumulated damage in the cyclic tests.

Further research, currently in progress, involves numerical simulations of these experiments, and also additional experimental & numerical studies, aiming to furtherly understand the influence of the proposed FPIF weld solution and to obtain behavior factors of full racks.

Acknowledgments

This work has received financial support from the Spanish Government (MINECO, project BIA2017-88814-R) and the European Commission (FEDER). These supports are gratefully acknowledged.

References

[1] Castiglioni CA et al. 2014. Seismic behaviour of steel storage pallet racking systems. EU research project SEISRACKS2. Final Report EUR 27583 EN. *European Commission, Research Fund for Coal and Steel*. DOI:10.2777/931597.

[2] Castiglioni CA. 2016. *Seismic Behaviour of Steel Storage Pallet Racking Systems*. Springer. ISBN 978-3-319-28465-1, ISBN 978-3-319-28466-8 (eBook).

[3] Bajoria KM, Sangle KK, Talicotti RS. 2010. Modal analysis of cold-formed pallet rack structures with semi-rigid connections. *Journal of Constructional Steel Research*. **66**:428-441. DOI:10.1016/j.jcsr.2009.10.005.

[4] Adamakos K, Vayas I. 2014. Tragverhalten von Palettenregalsystemen unter Erdbebenbeanspruchung (in German). *Stahlbau*. **83**:35-46. DOI:10.1002/stab.201410126.

[5] EN 15512. 2009. Steel static storage systems - Adjustable pallet racking systems - Principles for structural design. *European Committee for Standardization*.

[6] Ballio G, Bernuzzi C, Castiglioni CA. 1999. An approach for the seismic design of steel storage pallet racks (in German). *Stahlbau*. **68**:919-928.

[7] Bernuzzi C, Simoncelli M. 2016. An advanced design procedure for the safe use of steel storage pallet racks in seismic zones. *Thin-Walled Structures*. **109**:73–87. DOI:10.1016/J.TWS.2016.09.010.

[8] Bernuzzi C, Simoncelli M. 2017. Steel storage pallet racks in seismic zones: Advanced vs. standard design strategies. *Thin-Walled Structures*. **116**:291–306. DOI: 10.1016/j.tws.2017.03.002.

[9] Mei A, Orlando M, Salvatori L, Spinelli P. 2021. Nonlinear Static And Incremental Dynamic Analyses For Seismic Down-Aisle Behavior Of Rack Structures. *Ingegneria Sismica*, **38**(2):21-45.

[10] Gabbianelli G, Cavalieri F, Nascimbene R. 2020. Seismic vulnerability assessment of steel storage pallet racks. *Ingegneria Sismica*, **37**(2):18-40.

[11] Tagliafierro B, Montuori R, Castellano MG. 2021. Shake table testing and numerical modelling of a steel pallet racking structure with a seismic isolation system. *Thin-Walled Structures*, **164**:107924. DOI: 10.1016/j.tws.2017.05.024.

[12] Simoncelli M, Tagliafierro B, Montuori R. 2020. Recent development on the seismic devices for steel storage structures. *Thin-Walled Structures*, **155**:106827. DOI:10.1016/j.tws.2020.106827.

[13] EN 1998. 2004. Design of structures for earthquake resistance. *European Committee for Standardization*.

[14] Sangle KK, Bajoria KM, Talicotti RS. 2012. Elastic stability analysis of cold-formed pallet rack structures with semi-rigid connections. *Journal of Constructional Steel Research*. **71**:245-262. DOI:10.1016/j.jcsr.2011.11.002.

[15] López Almansa F, Bové O, Ferrer M, Roure F. 2021. Comparison between two types of cyclic tests of racking systems for seismic performance evaluation. *17th World Conference on Earthquake Engineering (17WCEE)*. Sendai, Japan. Art. 0206 (publication in pen-drive).

[16] Ferrer M, Bové O, López Almansa F, Roure F. 2021. Comparison between two types of seismic tests of racking systems. 9th European Conference on Steel and Composite Structures (Eurosteel 2020). Sheffield, UK. DOI: 10.1002/cepa.1513.

[17] ANSI-RMI MH16.1 2008. Specification for the Design, Testing and Utilization of Industrial Steel Storage Racks. *Rack Manufacturers Institute.* Charlotte (USA).

[18] FEMA 460. 2005. Seismic Considerations for Steel Storage Racks Located in Areas Accessible to the Public. *Federal Emergency Management Agency*.

[19] FEM 10.2.08. 2010. Recommendations for the design of static steel pallet racks in seismic conditions. FEM racking and shelving product group (European Racking Federation).

[20] EN 16681. 2016. Steel static storage systems - Adjustable pallet racking systems - Principles for seismic design. *European Committee for Standardization*.

[21] Adamakos K, Avgerinou S, Vayas I. 2013. Estimation of the behavior factor of steel storage pallet racks. *COMPDYN 2013*. Kos Island, Greece. DOI:10.7712/120113.4673.C1118.

[22] Krawinkler H, Cofie NG, Astiz MA, Kircher CA. 1979. Experimental study on the seismic behavior of industrial storage racks. Report No. 41. *John A. Blume Earthquake Engineering Center, Stanford University*.

[23] Markazi FD, Beale RG, Godley MHR. 1997. Experimental analysis of semi-rigid boltless connectors. *Thin-Walled Structures*, **28**(1):57–87. DOI:10.1016/S0045-7949(01)00058-X.

[24] Bernuzzi C, Castiglioni CA. 2001. Experimental analysis on the cyclic behaviour of beam-to-column joints in steel storage pallet racks. *Thin-Walled Structures*. **39**(10):841–59. DOI:10.1016/S0263-8231(01)00034-9.

[25] Abdel-Jaber M, Beale RG, Godley MHR. 2006. A theoretical and experimental investigation of pallet rack structures under sway. *Journal on Constructional Steel Research*, **62**(1–2):68–80. DOI:10.1016/j.jcsr.2005.04.008.

[26] Prabha P, Marimuthu V, Saravanan M, Jayachandran SA. 2010. Evaluation of connection flexibility in cold formed steel racks. *Journal on Constructional Steel Research*, **66**(7):863–72. DOI:10.1016/j.jcsr.2010.01.019.

[27] Roure F, Somalo MR, Casafont M, Pastor MM, Bonada J, Peköz T. 2013. Determination of beam-to-column connection characteristics in pallet rack structures: a comparison of the EN and ANSI methods and an analysis of the influence of the moment-to-shear ratios. *Steel Construction*. **6**:132-138. DOI:10.1002/stco.201310018.

[28] Zhao X, Wang T, Chen Y, Sivakumaran KS. 2014. Flexural behavior of steel storage rack beam-to-upright connections. *Journal of Constructional Steel Research*. **99**:161-175. DOI:10.1016/j.jcsr.2014.04.007.

[29] Yin L, Tang G, Zhang M, Wang B, Feng F. 2016. Monotonic and cyclic response of speed-lock connections with bolts in storage racks. *Engineering Structures*, **116**:40–55. DOI: 10.1016/j.engstruct.2016.02.032.

[30] Giordano S, Gusella F, Lavacchini G, Orlando M, Spinelli P. 2017. Experimental tests on beam-end connectors of cold-formed steel storage pallet racks. *EUROSTEEL 2017*. Copenhagen, Denmark.

[31] Dai L, Zhao X, Rasmussen KJR. 2018. Cyclic performance of steel storage rack beam-to-upright bolted connections. *Journal of Constructional Steel Research*. **148**:28-48. DOI:10.1016/j.jcsr.2018.04.012.

[32] Gusella F, Lavacchini G, Orlando M. 2018. Monotonic and cyclic tests on beam-column joints of industrial pallet racks. *Journal of Constructional Steel Research*. **140**:92-107. DOI: 10.1002/cepa.105.

[33] Gusella F, Orlando M, Spinelli P. 2019. Pinching in Steel Rack Joints: Numerical Modelling and Effects on Structural Response. *International Journal of Steel Structures*. **19**(1):131-146. DOI:10.1007/s13296-018-0095-x.

[34] ANSI/AISC 341-05 2005. Seismic provisions for structural steel buildings. *American Institute of Steel Construction*.

[35] ECCS 45 1986. Recommended Testing Procedure for Assessing the Behaviour of Structural Steel Elements under Cyclic Loads. *European Convention for Constructional Steelwork*.

[36] EN 10149. 2013. Hot rolled flat products made of high yield strength steels for cold forming. *European Committee for Standardization.*

[37] EN 10025. 2004. Hot rolled products of structural steels. *European Committee for Standardization.*

[38] EN 1993 1-1. 2005. Design of steel structures - Part 1-1: General rules and rules for buildings. *European Committee for Standardization*.

[39] EN 1993 1-8. 2004. Design of steel structures - Part 1-8: Design of joints. *European Committee for Standardization*.

[40] BSL. The Building Standard Law of Japan. 2009. *The Building Center of Japan, Tokyo*. English version available at https://www.bcj.or.jp/en/services/reference/, last accessed July 2021.

[41] Benavent Climent A, López Almansa F, Bravo González DA. 2010. Design energy input spectra for moderate-to-high seismicity regions based on Colombian earthquakes. *Soil Dynamics & Earthquake Engineering*. **30**(1):1129-1148. DOI:10.1016/j.soildyn.2010.04.022.

[42] López Almansa F, Yazgan U, Benavent Climent A. 2013. Design energy input spectra for high seismicity regions based on Turkish registers. *Bulletin of Earthquake Engineering*. **11**(4):885–912. DOI: 10.1007/s10518-012-9415-2.

List of acronyms

C: Cyclic.

CAS: **[**Castiglioni et al. 2016].

ECCS: **[**ECCS 45 1986]. I and II refer to the cycles limits (Table 4), 0 means that the 5 kN force (Figure 5) was not used. The alike tests are distinguished by adding (1), (2), (3).

EN: **[**EN 16681 2016].

FP: Full Perimeter.

FPIF: Full Perimeter and Internal Flanges.

IU: Inverted U.

VS: Vertical Sides.

M: Monotonic (+/–: downward/upward). A and B refer to the employed steel (Coil No., Table 4).

List of symbols

Main symbols

a, *b*: Distance values (Figure 5)

d: Vertical displacement (Figure 4, Figure 7)

E: Modulus of elasticity (steel)

f: Resistance (stress)

F: Pushing force (Figure 4, Figure 7)

M: Bending moment (Figure 6)

n: Number of cycles (Figure 7)

P: Lever force (Figure 5)

q: Behavior factor in the European regulations

R: Response modification factor in the American practice

W: Mechanical work done by the driving jack

x, *y*, *z*: Coordinates

S: Slope of the moment-rotation curve (Figure 6)

Δ: Increment

ν: Poisson ratio

θ: Rotation angle (Figure 4.b, Figure 6)

Indexes

d: Design

EN: Refers to the employed EN (Euro Norm) (Figure 6)

g: Gravity (Figure 7)

i: Index.

max: Maximum value

R: Resisting

s: Steel

u: Ultimate (Figure 6)

y: Yielding (Figure 6)

0: Initial (Figure 6)

+, –: Downward, upward displacement (hogging, sagging, respectively)

5 CONCLUSIONS AND FUTURE INVESTIGATIONS

This chapter summarizes all the work done in the Thesis, pointing out its main contributions and novelties. Future and parallel lines of research can be found in the last paragraph.

The main goals of this Thesis are to provide tools to (i) facilitate the inexpensive design of unbraced non-uniform pallet racks and to (ii) improve the stiffness, ductility, and energy dissipation capacity of individual connections. Additionally, an important side objective was to gain understanding of the parameters that mostly contribute to the global behavior of racks. In this way, beam-to-upright connections have been found to be of paramount importance. Moreover, another side-objective was to acquire knowledge on the parameters that mostly impact the cyclic performance of beam-to-upright connections, while also pointing out the possible influence of testing protocols. All these objectives and side objectives have been successfully achieved.

The main scientific contribution of this work is directly related to the objectives. On the one hand, an approach for the predesign of non-regular pallet racks has been developed; as part of this methodology, an efficient single-column approach to model the behavior of a full pallet rack is developed. On the other hand, a methodology for improving the stiffness, ductility, and energy dissipation capacity of beam-to-upright connections is provided.

Finally, the current and future lines of research derived from the results of this Thesis are listed below:

- A novel GBT single-column model for pallet racks, similar to the one presented in ***Section 2*** is under development. This GBT model will consider distortional and local effects on columns and beams. Additionally, the effect of the upright perforations will also be considered. The GBT formulations will be based on work [6].
- An experimental campaign on floor connections will be performed, including cyclic testing.
- Global pushover analyses of racks are under development; the aim is to demonstrate the benefits of the presented novel connection to the global behavior of racks.

6 BIBLIOGRAPHY

[1] Castiglioni CA. (2016). Seismic Behaviour of Steel Storage Pallet Racking Systems. Springer. ISBN 978-3-319-28465-1, ISBN 978-3-319-28466-8 (eBook).

[2] Storage Racks in Seismic Areas (SEISRACKS), Research Programme of the Research Fund for Coal and Steel RTD, Final Report, May 2007 http//www.csiberkeley.com.

[3] Castiglioni CA et al. (2014). Seismic behaviour of steel storage pallet racking systems. EU research project SEISRACKS2. Final Report EUR 27583 EN. European Commission, Research Fund for Coal and Steel. DOI:10.2777/931597.

[4] Hélder D. Craveiro, João Paulo C. Rodrigues, Luís Laím, (2016). Buckling resistance of axially loaded cold-formed steel columns. *Thin-Walled Structures,* **106**: 358-375. DOI: /10.1016/j.tws.2016.05.010

[5] Maurizio Orlando, Giovanni Lavacchini, Barbara Ortolani, Paolo Spinelli, (2017). Experimental capacity of perforated cold-formed steel open sections under compression and bending. *Steel and Composite Structures,* **24**: 201-211. DOI: /10.12989/scs.2017.24.2.201

[6] Bonada J., Casafont, M.; Roure, F.; Pastor, M.M. (2021). Geometrically nonlinear analysis of perforated rack columns under a compression load by means of Generalized Beam Theory. *Thin-walled structures*, **166**: 108102/1-108102/17. DOI: /10.1016/j.tws.2021.108102

[7] Xianzhong Zhao, Chong Ren, Ru Qin (2017). An experimental investigation into perforated and non-perforated steel storage rack uprights. *Thin-Walled Structures.* **112** (159-172) DOI: /10.1016/j.tws.2016.11.016

[8] Adamakos K, Vayas I. (2014). Tragverhalten von Palettenregalsystemen unter Erdbebenbeanspruchung (in German). *Stahlbau*. **83**:35-46. DOI:10.1002/stab.201410126.

[9] EN 15512. (2009). Steel static storage systems - Adjustable pallet racking systems - Principles for structural design. *European Committee for Standardization*.

[10] Farkas J., Jarmai K. (2013). "Optimum Design of Steel Structures" Springer, Hungary.

[11] EN 1990. Eurocode 3. 2002. *Basis of structural design. European Committee for Standardization*.

[12] EN 1993 1-1. 2005. Design of steel structures - Part 1-1: General rules and rules for buildings. *European Committee for Standardization*.

[13] EN 1993-1-3, Eurocode 3: Design of steel structures – Part 1. 3: General rules – Supplementary rules for coldformed members and sheeting.

[14] EN 1993 1-8. 2004. Design of steel structures - Part 1-8: Design of joints. *European Committee for Standardization*.

[15] EN 1998. 2004. Design of structures for earthquake resistance. *European Committee for Standardization*.

[16] EN 15620. 2009. Steel static storage systems - Adjustable pallet racking systems – Tolerances, deformations and clearances. *European Committee for Standardization.*

[17] EN 16681. 2016. Steel static storage systems - Adjustable pallet racking systems - Principles for seismic design. *European Committee for Standardization*.

[18] Rack Manufacturers Institute. (2000). *Specification for the design, testing, and utilization of industrial steel storage racks*. Rack Manufacturers Institute.

[19] Nocedal J. Wright S. J. 2006. "Numerical Optimization", 2nd Ed., Springer New York.

[20] Liu M. 2015. "Fast Procedure for Practical Member Sizing Optimization of Steel Moment Frames". Pract.. Per. on Struct. Design and Const. 20(4). https://doi.org/10.1061/(ASCE)SC.1943-5576.0000240

[21] Mueller M., Liu M., Burns S. 2002. "Fully Stressed Design of Frame Structures and Multiple Load Paths" J. Struct. Eng. 128(6). https://doi.org/10.1061/(ASCE)0733-9445(2002)128:6(806)

[22] Manickarajah D., Xie M., Steven G. 2000. “Optimisation of columns and frames against buckling” Computers and Structures 75, 45–54. https://doi.org/10.1016/S0045-7949(99)00082-6

[23] Szalai J. (2010). “Use of eigenvalue analysis for different levels of stability design” SDSS‘Rio 2010 Stability and Ductility of Steel Structures, Rio de Janeiro, Brazil.

[24] Perelmuter A., Slivker V. (2001). “The Problem of Interpretations of the Stability Analysis Results” European Conf. on Comp. Mech., Cracow, Poland.

[25] Sangle KK, Bajoria KM, Talicotti RS. (2012). Elastic stability analysis of cold-formed pallet rack structures with semi-rigid connections. *Journal of Constructional Steel Research*. **71**:245-262. DOI:10.1016/j.jcsr.2011.11.002.

[26] Lewis, G. M. (1991). Stability of rack structures. Thin-Walled Structures, 12(2), 163-174.ç

[27] Godley, M. H. R. (2002). *The Behaviour of Drive-in Storage Structures*. International Specialty Conference on Cold-Formed Steel Structures, Orlando, Florida, USA.

[28] Hua V., Rasmussen K. (2006). “The behaviour of drive-in racks under horizontal impact load”. Research report no R871. School of Civil Engineering Sydney, The University of Sydney, Sydney.

[29] Cheng B., Wu Z.Y. (2015). “Simplified Method for Calculating the Lateral Stiffness of Drive-In Storage Racks” Pract.. Per. on Struct. Design and Const. 21(1). https://doi.org/10.1061/(ASCE)SC.1943-5576.0000266

[30] Bernuzzi C., Gobetti A.,Gabbianelli G.,Simoncelli M. (2014). “Warping influence on the resistance of uprights in steel storage pallet racks” J. Const. Steel Research 101, 224–241. https://doi.org/10.1016/j.jcsr.2014.05.014

[31] Bernuzzi C., Gobetti A.,Gabbianelli G.,Simoncelli M. (2015). “Simplified Approaches to Design Medium-Rise Unbraced Steel Storage Pallet Racks. I: Elastic Buckling Analysis” J. Struct. Eng. 141(11). https://doi.org/10.1061/(ASCE)ST.1943-541X.0001271

[32] Bernuzzi C., Gobetti A.,Gabbianelli G.,Rosti A. (2016). “Beam design for steel storage racks” J. Const. Steel Research 116, 156-172. https://doi.org/10.1016/j.jcsr.2015.09.007

[33] Bonada J., Casafont M., Roure F., Pastor M.M. (2018). “Introduction of sectional constraints in a first-order GBT formulation for open-cross sections.” Eight International Conference on Thin-Walled Structures, Lisboa, Portugal.

[34] Casafont M., Bonada J., Pastor M.M., Roure F., Susin A. (2017). “Linear buckling analysis of perforated cold-formed steel storage rack columns by means of the Generalised Beam Theory.” International Journal of Structural Stability and Dynamics, 18(1), 1-32. https://doi.org/10.1142/S0219455418500049

[35] Crosbie M.W.J. (1998). “The design and analysis of static pallet racking systems.” Master Thesis, Sheffield Hallam University, Sheffield, U.K.

[36] Sena F., Rasmussen K. (2016). “Finite element (FE) modelling of storage rack frames” J. Const. Steel Research 126, 1–14. https://doi.org/10.1016/j.jcsr.2016.06.015

[37] Tilburgs K. (2013). “Those peculiar structures in cold-formed steel:“racking & shelving”” Steel Const. Design and Research 6 (2), 95-106. https://doi.org/10.1002/stco.201310016

[38] Trouncer A, Rasmussen,K (2016). “Ultra-light gauge steel storage rack frames. Part 2 – Analysis and design considerations of second order effects” J. Const. Steel Research 124 37-46. https://doi.org/10.1016/j.jcsr.2016.05.015

[39] Kanyilmaz, A., Castiglioni, C. A., Brambilla, G., & Chiarelli, G. P. (2016). Experimental assessment of the seismic behavior of unbraced steel storage pallet racks. *Thin-Walled Structures*, *108*, 391-405.

[40] Shah, S. N. R., Sulong, N. R., Jumaat, M. Z., & Shariati, M. (2016). State-of-the-art review on the design and performance of steel pallet rack connections. *Engineering Failure Analysis*, *66*, 240-258.

[41] ANSYS Release 14.0, ANSYS Inc. (2011).

[42] Bernuzzi C, Castiglioni CA. (2001). Experimental analysis on the cyclic behaviour of beam-to-column joints in steel storage pallet racks. *Thin-Walled Structures*, **39**(10):841–59. DOI: 10.1016/S0263-8231(01)00034-9

[43] Abdel-Jaber M, Beale RG, Godley MHR. (2006). A theoretical and experimental investigation of pallet rack structures under sway. *Journal on Constructional Steel Research*, **62**(1–2):68–80. DOI: 10.1016/j.jcsr.2005.04.008

[44] Prabha P, Marimuthu V, Saravanan M, Jayachandran SA. (2010). Evaluation of connection flexibility in cold formed steel racks. *Journal on Constructional Steel Research*, **66**(7):863–72. DOI: 10.1016/j.jcsr.2010.01.019

[45] Roure F, Somalo MR, Casafont M, Pastor MM, Bonada J, Peköz T. (2013). Determination of beam-to-column connection characteristics in pallet rack structures: a comparison of the EN and ANSI methods and an analysis of the influence of the moment-to-shear ratios. *Steel Construction*. **6**:132-138. DOI:10.1002/stco.201310018.

[46] Zhao X, Wang T, Chen Y, Sivakumaran KS. (2014). Flexural behavior of steel storage rack beam-to-upright connections. *Journal of Constructional Steel Research*. **99**:161-175. DOI: 10.1016/j.jcsr.2014.04.007

[47] Yin L, Tang G, Zhang M, Wang B, Feng F. (2016). Monotonic and cyclic response of speed-lock connections with bolts in storage racks, *Engineering Structures*, **116**:40–55. DOI: 10.1016/j.engstruct.2016.02.032

[48] Giordano S, Gusella F, Lavacchini G, Orlando M, Spinelli P. (2017). Experimental tests on beam-end connectors of cold-formed steel storage pallet racks. *EUROSTEEL 2017*. Copenhagen, Denmark. DOI: 10.1002/cepa.105

[49] Dai L, Zhao X, Rasmussen KJR. (2018). Flexural behaviour of steel storage rack beam-to-upright bolted connections. *Thin-Walled Structures*, **124**: 202-217. DOI: 10.1016/j.tws.2017.12.010

[50] López Almansa F, Bové O, Ferrer M, Roure F. (2021). Comparison between two types of cyclic tests of racking systems for seismic performance evaluation. *17th World Conference on Earthquake Engineering (17WCEE)*. Sendai, Japan. Art. 0206 (publication in pen-drive).

[51] Bové O, López Almansa F, Ferrer M, Roure F. (2021). Ductility improvement of adjustable pallet rack speed-lock connections: Experimental study. *Journal on Constructional Steel Research.* Accepted. In Press.

[52] Folz, B. and Filiatrault, A. (2001). "SAWS - Version 1.0, A Computer Program for the Seismic Analysis of Woodframe Structures", Structural Systems Research Project Report No. SSRP-2001/09, Dept. of Structural Engineering, UCSD, La Jolla, CA.

[53] Mitra N., Pinching4 model. (OpenSees User Documetation); (2012). http:// opensees.berkeley.edu/wiki/index.php/Pinching4_Material

[54] Gusella, F., Orlando, M. & Spinelli, P. Pinching in Steel Rack Joints (2019): Numerical Modelling and Effects on Structural Response. *Int J Steel Struct* **19**, 131–146 DOI: /10.1007/s13296-018-0095-x

[55] Yin, L., Tang, G., Li, Z., Zhang, M., & Feng, B. (2018). Responses of cold-formed steel storage racks with spine bracings using speed-lock connections with bolts I: Static elastic-plastic pushover analysis. *Thin-Walled Structures*, *125*, 51-62.

[56] Yin, L., Tang, G., Li, Z., & Zhang, M. (2018). Responses of cold-formed steel storage racks with spine bracings using speed-lock connections with bolts II: Nonlinear dynamic response history analysis. *Thin-Walled Structures*, *125*, 89-99.

[57] Nuñez, E., Aguayo, C., & Herrera, R. (2020). Assessment of the seismic behavior of selective storage racks subjected to Chilean earthquakes. *Metals*, *10*(7), 855.

[58] Castiglioni, C. A., Kanyilmaz, A., Brambilla, G., & Chiarelli, G. P. (2015). Steel Storage Pallet Racking Systems in Seismic Areas: Full Scale Push-over Tests and Numerical Simulations. In *The Sixth Symposium on Steel Structures, 2015 Eskisehir* (pp. 1-15).

[59] Adamakos, K., Vayas, I., & Avgerinou, S. (2013, June). Estimation of the behavior factor of steel storage pallet racks. In *Proceedings of the 4th ECCOMAS Thematic Conference on Computational Methods in Structural Dynamics and Earthquake Engineering, Kos Island, Greece* (pp. 12-14).

[60] Carlos Aguirre (2004). Seismic behavior of rack structures. *Journal of Constructional Steel Research*. **61,** 607-624 DOI: /10.1016/j.jcsr.2004.10.001

[61] Bajoria KM, Talikoti RS. (2006). Determination of flexibility of beam-to-column connectors used in thin walled cold-formed steel pallet racking systems. *Thin-Walled Structures*, **44**(3):372–380. DOI: /10.1016/j.tws.2006.01.007

[62] Shah SNR, Ramli Sulong NH, Khan R, Jumaat MZ. (2017). Structural performance of boltless beam end connectors. *Advanced Steel Construction*. **13**(2):144-159. DOI: /10.18057/IJASC.2017.13.2.4

[63] Gusella F, Lavacchini G, Orlando M. (2018). Monotonic and cyclic tests on beam-column joints of industrial pallet racks. *Journal of Constructional Steel Research*. **140**:92-107. DOI: 10.1002/cepa.105.

[64] Lyu ZJ, Wu M, Huang YX, Song YM, Cui X (2018). Assessment of the Dynamic Behavior of Beam-to-Column Connections in Steel Pallet Racks under Cyclic Load: Numerical Investigation. *Advances in Civil Engineering.* Article ID 9243216. DOI: /10.1155/2018/9243216

[65] Vujanac R, Miloradović N, Vulović S, Pavlović A. (2020). A Comprehensive Study into the Boltless Connections of Racking Systems. *Metals*. **10**:1-17. DOI: doi.org/10.3390/met10020276

[66] Federico Gusella, Sanjay Raja Arwade, Maurizio Orlando, Kara D. Peterman (2019). Influence of mechanical and geometric uncertainty on rack connection structural response, *Journal of Constructional Steel Research*, **153:** 343-355. DOI: /10.1016/j.jcsr.2018.10.021

[67] Ślęczka, L. and Kozłowski, A. (2007). Experimental and theoretical investigations of pallet racks connections. *Advanced Steel Construction* **3**: 607-628. DOI: 10.18057/IJASC.2007.3.2.6

[68] Federico Gusella, Maurizio Orlando, Klaus Thiele, (2018). Evaluation of rack connection mechanical properties by means of the Component Method, *Journal of Constructional Steel Research*. **149:** 207-224. DOI: /10.1016/j.jcsr.2018.07.021.

[69] Gusella F, Orlando M, Spinelli P. (2019). Pinching in Steel Rack Joints: Numerical Modelling and Effects on Structural Response. *International Journal of Steel Structures*. **19**(1):131-146. DOI:10.1007/s13296-018-0095-x.

[70] ECCS 45 1986. Recommended Testing Procedure for Assessing the Behaviour of Structural Steel Elements under Cyclic Loads. *European Convention for Constructional Steelwork*.

[71] Bajoria KM, Sangle KK, Talicotti RS. (2010). Modal analysis of cold-formed pallet rack structures with semi-rigid connections. *Journal of Constructional Steel Research*. **66**:428-441. DOI:10.1016/j.jcsr.2009.10.005.

[72] Ballio G, Bernuzzi C, Castiglioni CA. (1999). An approach for the seismic design of steel storage pallet racks (in German). *Stahlbau*. **68**:919-928.

[73] Bernuzzi C, Simoncelli M. (2016). An advanced design procedure for the safe use of steel storage pallet racks in seismic zones. *Thin-Walled Structures*. **109**:73–87. DOI:10.1016/J.TWS.2016.09.010.

[74] Bernuzzi C, Simoncelli M. (2017). Steel storage pallet racks in seismic zones: Advanced vs. standard design strategies. *Thin-Walled Structures*. **116**:291–306. DOI: 10.1016/j.tws.2017.03.002.

[75] Mei A, Orlando M, Salvatori L, Spinelli P. (2021). Nonlinear Static And Incremental Dynamic Analyses For Seismic Down-Aisle Behavior Of Rack Structures. *Ingegneria Sismica*, **38**(2):21-45.

[76] Gabbianelli G, Cavalieri F, Nascimbene R. (2020). Seismic vulnerability assessment of steel storage pallet racks. *Ingegneria Sismica*, **37**(2):18-40.

[77] Tagliafierro B, Montuori R, Castellano MG. (2021). Shake table testing and numerical modelling of a steel pallet racking structure with a seismic isolation system. *Thin-Walled Structures*, **164**:107924. DOI: 10.1016/j.tws.2017.05.024.

[78] Jacobsen, E., & Tremblay, R. (2017). Shake-table testing and numerical modelling of inelastic seismic response of semi-rigid cold-formed rack moment frames. *Thin-Walled Structures*, *119*, 190-210.

[79] Sideris, P., Filiatrault, A., Leclerc, M., & Tremblay, R. (2010). Experimental investigation on the seismic behavior of palletized merchandise in steel storage racks. *Earthquake spectra*, *26*(1), 209-233.

[80] Simoncelli M, Tagliafierro B, Montuori R. (2020). Recent development on the seismic devices for steel storage structures. *Thin-Walled Structures*, **155**:106827. DOI:10.1016/j.tws.2020.106827.

[81] Bové O ,Ferrer M, López Almansa F, Roure F. (2021). Comparison between two types of seismic tests of racking systems. 9th European Conference on Steel and Composite Structures (Eurosteel 2020). Sheffield, UK. DOI: 10.1002/cepa.1513.

[82] ANSI-RMI MH16.1 (2008). Specification for the Design, Testing and Utilization of Industrial Steel Storage Racks. *Rack Manufacturers Institute.* Charlotte (USA).

[83] FEMA 460. (2005). Seismic Considerations for Steel Storage Racks Located in Areas Accessible to the Public. *Federal Emergency Management Agency*.

[84] FEM 10.2.08. (2010). Recommendations for the design of static steel pallet racks in seismic conditions. FEM racking and shelving product group (European Racking Federation).

[85] Adamakos K, Avgerinou S, Vayas I. (2013). Estimation of the behavior factor of steel storage pallet racks. *COMPDYN 2013*. Kos Island, Greece. DOI:10.7712/120113.4673.C1118.

[86] Krawinkler H, Cofie NG, Astiz MA, Kircher CA. (1979). Experimental study on the seismic behavior of industrial storage racks. Report No. 41. *John A. Blume Earthquake Engineering Center, Stanford University*.

[87] Markazi FD, Beale RG, Godley MHR. (1997). Experimental analysis of semi-rigid boltless connectors. *Thin-Walled Structures*, **28**(1):57–87. DOI:10.1016/S0045-7949(01)00058-X.

[88] Prabha P, Marimuthu V, Saravanan M, Jayachandran SA. (2010). Evaluation of connection flexibility in cold formed steel racks. *Journal on Constructional Steel Research,* **66**(7):863–72. DOI:10.1016/j.jcsr.2010.01.019.

[89] Dai L, Zhao X, Rasmussen KJR. (2018). Cyclic performance of steel storage rack beam-to-upright bolted connections. *Journal of Constructional Steel Research*. **148**:28-48. DOI:10.1016/j.jcsr.2018.04.012.

[90] ANSI/AISC 341-05 (2005). Seismic provisions for structural steel buildings. *American Institute of Steel Construction*.

[91] EN 10149. (2013). Hot rolled flat products made of high yield strength steels for cold forming. *European Committee for Standardization.*

[92] EN 10025. (2004). Hot rolled products of structural steels. *European Committee for Standardization.*

[93] BSL. The Building Standard Law of Japan. (2009). *The Building Center of Japan, Tokyo*. English version available at https://www.bcj.or.jp/en/services/reference/

[94] Benavent Climent A, López Almansa F, Bravo González DA. (2010). Design energy input spectra for moderate-to-high seismicity regions based on Colombian earthquakes. *Soil Dynamics & Earthquake Engineering*. **30**(1):1129-1148. DOI:10.1016/j.soildyn.2010.04.022.

[95] López Almansa F, Yazgan U, Benavent Climent A. (2013). Design energy input spectra for high seismicity regions based on Turkish registers. *Bulletin of Earthquake Engineering*. **11**(4):885–912. DOI: 10.1007/s10518-012-9415-2.

[96] Bové, O., Casafont, M., Ferrer, M., López-Almansa, F., & Roure, F. (2021). Analytical design method for the improvement of steel structures stability. *ce/papers*, *4*(2-4), 2221-2224.

[97] Bové, O., Ferrer, M., Almansa, F. L., & Roure, F. (2021). Comparison Between Two Types of Seismic Tests of Racking Systems. *ce/papers*, *4*(2-4), 1992-1998.

[98] Bové, O., Casafont, M., Ferrer, M., López-Almansa, F., & Roure, F. (2020). Systemized Structural Predesign Method for Selective Racks. *Journal of Structural Engineering*, *146*(12), 04020276.

Appendix A A CONFERENCE PAPER RELATED WITH THIS THESIS

The conference paper displayed in this Annex was presented in Eurosteel 2021. It describes a systemized predesign method intended for general structures; this study can help the understanding of the methodology (specific for pallet racks) presented in ***Section 2.***

ce/papers
The online collection for conference papers in civil engineering
Ernst & Sohn A Wiley Brand

ORIGINAL ARTICLE

eurosteel SHEFFIELD 2021
Ernst & Sohn A Wiley Company

Analytical design method for the improvement of steel structures stability

Oriol Bové, Miquel Casafont[1], Miquel Ferrer[1], Francesc López-Almansa[1], Francesc Roure[1]

Correspondence

Ass. Prof. Oriol Bové
Technical University of Catalonia
RMEEI-ETSEIB
Avda. Diagonal 647
08028 Barcelona
Email: oriol.bove@upc.edu

Abstract

This article presents a design method for the improvement of steel structures stability by modifying their structural elements parameters. The available parameters can be selected from a predefined list of stiffness and ultimate capacities for joints and steel members. The proposed procedure is based on determining the critical load factor (ratio between the critical and the demanding loads: $\alpha_{cr} = P_{cr} / P_{Ed}$) and analyzing its sensitivity with respect to the design parameters, by using its gradient vector and Hessian matrix. The methodology is well suited for structures where the second order effects are relevant. A simple two parameter example is presented, and the general procedure for finite element analysis is outlined.

Keywords

Steel Structures Stability, Buckling Analysis

1 Introduction

The optimal design of lightweight structures subjected to instabilities is a relevant issue, given that, in this type of structures, the second order effects can be relevant. On the other hand, the geometrically non-linear analyses are computationally costly. Therefore, simplified and computationally efficient formulations are strongly required. It is remarked that this work is part of a wider research on optimization of pallet racks.

This paper presents special techniques for the improvement of stability on structures subjected to relevant second order effects. The research starts from similar work having been performed at [1]. In this paper, an iterative procedure is set up for gradually shifting the material from the "strongest" part (less impact on structural stability) of the structure to its "weakest" part (highest impact on structural stability), while keeping the structural weight roughly constant. Regarding this sensitivity of stability with respect to the design parameters, the works by Perelmuter [2] and Szalai [3] have also been studied. Such methodologies might be useful to find innovative solutions and to determine the cost sensitivity with respect to the design parameters [4].

In the present work, analytical indicators are used to quantify the effect on the structural stability of the modification of a given structural parameter (i.e. sectional stiffness); these indicators are aimed to assess the design. Additionally, a simple mathematical expression is determined as an approximation of the linear critical load factor (in terms of the design parameters). .

Previous to the FEM-oriented formulation, a simple example is worked analytically, using the closed form of the governing ODE (Ordinary Differential Equation) and illustrative cost-minimizing-based criteria. It is remarked that, in this research, the external loads are considered to be not dependent on the stiffness. This is because the study is focused on structures that present a low self-weight if compared to the external gravity loads. Critical load gradient for stability improvement

The structural stability is quantified in terms of the dimensionless critical load factor, being defined as the ratio between the critical and the demanding loads: $\alpha_{cr} = P_{cr} / P_{Ed}$.

The critical load of a given structure never decreases when a single stiffness parameter grows. As a result, such structure has no relative maximums in terms of linear stability. Nonetheless, when the critical load factor is greater than 10, the Eurocode 3 [5] permits the designer to perform a linear analysis. This is because it is considered that, under these circumstances, the second order effects are not relevant. Thus, it is concluded that a design strategy based on the improvement of the linear stability makes sense when the critical load factor is less than 10. On the other hand, when that factor is smaller or equal than 1, the structure is unstable, and such factor needs to be improved (increased) until finding a design minimum value of $\alpha_{cr} = \alpha_{cr}^{(0)}$.

As consequence of the above considerations, if the critical load factor is low and it is improved by modifying the structural parameters, the lateral displacement of the structure will be decreased, and the structural moments will be less affected by the second order effects (i.e. will be lower too). This justifies that a good prediction of the increment of the critical load factor between two solutions can be useful for design purposes. The objective is to find an expression that helps the engineer to choose what structural element is better to change (modify) when a global analysis fails

(non-convergence, structural or displacement check fails, etc.). The gradient of α_{cr} with respect to the design parameters (stiffness) is the maximum slope of the function α_{cr}. The gradient vector $\nabla\alpha_{cr}$ can be used to predict the critical load value of nearby solutions, where few structural variations are made. This can be used as a guide for the structural design when these conditions are found: (i) $\alpha_{cr} < 10$, so second order effects are relevant, (ii) the nodal lateral displacements are excessive, and (iii) the bending moments of the columns are too high.

2 Illustrative example

A simple example is analytically worked out next to facilitate the understanding of the proposed concept. It is assumed that the cost of the structural elements increases linearly with respect to the design parameters.

The example consists on a single freestanding column that has a linear rotational spring connected to its bottom section (Figure 1). The column length (*L*) and the material Young modulus (*E*) are known. The design parameters (unknowns) are the stiffness of the linear rotational spring (*k*) and the column moment of inertia (*I*). The column is submitted to a constant axial force (*P*) only; in other words, as to perform a buckling analysis, no transverse loads are considered. On the other hand, the column is assumed to be straight and vertical, i.e., no geometrical imperfections are considered.

The non-dimensionless slenderness coefficient is defined by $\lambda = \sqrt{P/E\,I}$. The lateral displacement function depending on the vertical coordinate (*x*) is *w*(*x*). The general governing stability differential equation of such free standing column submitted to a constant axial force is: $w^{\mathrm{iv}} + \lambda^2 w^{\mathrm{ii}} = 0$. The equation is solved under the appropriate boundary conditions; once resolved, it is concluded that the critical load must satisfy the following condition

$$\frac{E\,I\,\lambda^3 \sin(L\,\lambda)}{k} - \lambda^2 \cos(L\,\lambda) = 0 \qquad (1)$$

The solution of this equation shows that the corresponding deformed shape is $w(x) = A\left[\cos(\lambda\,x) - 1 - \frac{E\,I\,\lambda}{k}\sin(\lambda\,x)\right]$. Note that the clamped-free column situation corresponds to $k/I \to \infty$, and it is found that $P_{cr} = \frac{\pi^2 E\,I}{4\,L^2}$ and $w(x) = A[\cos(\lambda\,x) - 1]$ as expected (Figure 1.a). The pinned free beam case is found by imposing $k/I \to 0$ and it is shown that $P_{cr} \to 0$ and $w(x) = A\frac{x}{L}$, which also makes sense, as this system have zero lateral stiffness without the need of any vertical load; and the mode corresponds to the rotation of the beam along the pin (Figure 1.b). For any other value of $k/I \in (0,\infty)$ the critical loads $P_{cr}(k,I)$ must verify the condition (1) and $w(x) = A\left[\cos(\lambda\,x) - 1 - \frac{E\,I\,\lambda}{k}\sin(\lambda\,x)\right]$ (Figure 1.c). In other words, Figure 1 displays three cases: (a) the rotational spring is much stiffer than the column, (b) the opposite situation, and (c) an intermediate situation (both stiffness are comparable).

$P_{cr} = \frac{\pi^2 E\,I}{4\,L^2}$	$P_{cr} \to 0$	$\frac{E\,I\,\lambda^3 \sin(L\,\lambda)}{k} + \lambda^2 \cos(L\,\lambda) = 0$
		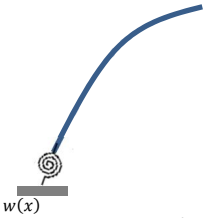
$w(x) = A[\cos(\lambda\,x) - 1]$	$w(x) = A\frac{x}{L}$	$w(x) = A\left[\cos(\lambda\,x) - 1 - \frac{E\,I\,\lambda}{k}\sin(\lambda\,x)\right]$
(a) $k/I \to \infty$	(b) $k/I \to 0$	(c) $k/I \in (0,+\infty)$

Figure 1 Example of a freestanding column

As the condition $\frac{E\,I\,\lambda^3\,sin(L\,\lambda)}{k} + \lambda^2\,cos(L\,\lambda) = 0$ is nonlinear, the explicit expression of $\lambda(k,I)$ is, in general, not possible to find. Nonetheless, it is possible to derivate the expression with respect to *I* and *k* ($\frac{\partial P_{cr}}{\partial I}$ and $\frac{\partial P_{cr}}{\partial k}$) and to isolate such results, thus providing:

$$\frac{\partial P_{cr}}{\partial I} = \frac{(EIP^2 + kLP^2)\,sin(L\lambda) + (EIL - 2EIk)\,cos(L\lambda)P^2\lambda}{(3EI^2P + IkLP)\,sin(L\lambda) + (EI^2L - 2EI^2k)\,cos(L\lambda)P\lambda}$$

$$\frac{\partial P_{cr}}{\partial k} = \frac{2EIP^2 sin(L\lambda)}{(k^2LP + 3EIkP)sin(L\lambda) + (EIkLP - 2EIk^2)cos(L\lambda)\lambda} \qquad (2)$$

The following values of the known parameters are assumed: $I = 1{\cdot}10^6$ mm^4, $k = 6{\cdot}10^8$ N/mm, $E = 210000$ N/mm^2, $L = 1000$ mm, $P = 2.946{\cdot}10^5$ N. For such values, the partial derivatives result in $\frac{\partial P_{cr}}{\partial I} = 0.16$ and $\frac{\partial P_{cr}}{\partial k} = 2.244 \cdot 10^{-4}$. The cost for an increment of one unit of moment of inertia and joint stiffness are respectively: $C_I = 1.25$ m. u./mm^4 and $C_k = 1200$ m. u./$(\frac{\mathrm{N}}{\mathrm{mm}})$. It is concluded that $\frac{\partial P_{cr}}{\partial I}/C_I < \frac{\partial P_{cr}}{\partial k}/C_k$. Thus, it is deduced that, under these circumstances, improving the bottom spring stiffness is a better decision than increasing the moment of inertia of the profile, since it provides cheaper benefits.

3 Derivation of the stability factor gradient in FEA

In the previous paragraph an analytic example of the linear stability gradient determination and use has been shown. In this chapter, a formulation for a finite element analysis is developed. For this paragraph, the design parameters are: member moments of inertia I_{m_i} and joint rotational stiffness k_{r_i}. For simplicity, these parameters are referred as $\boldsymbol{\psi} = (\psi_1, \ldots, \psi_n)$, the global stiffness matrix of the single column model can be written in as:

$$\mathbf{K} = \mathbf{K^{(0)}} + \sum_{i=1,\cdots,n} \psi_i\,\mathbf{K^{(i)}} \qquad (3)$$

where $\mathbf{K^{(0)}}$ includes the assembled terms of the linear stiffness matrix that do not depend on the design parameters, namely the cross-section area of the members (which are not considered to contribute to the lateral stiffness); and $\mathbf{K^{(i)}}$ can be easily derived for each finite element (upright, beam or rotational stiffness). On the other hand, the internal forces of the structure are directly obtained from the external loads. Thus, the geometric stiffness matrix $\mathbf{K_G}$ can be assumed to be constant.

The gradient of the stability factor can be obtained from the derivative with respect the design parameters ψ_i of the following expression obtained from [3]:

$$(\mathbf{K} + \alpha_{cr}\mathbf{K}_G)\,\boldsymbol{\phi}_{cr}=\mathbf{0}$$

$$\boldsymbol{\phi}_{cr}^{T}\,(\mathbf{K} + \alpha_{cr}\mathbf{K}_G)\,\boldsymbol{\phi}_{cr} = \boldsymbol{\phi}_{cr}^{T}\,\mathbf{0} = \mathbf{0} \quad (4)$$

Due to the linear nature of the relationship between the design parameters and the terms in equation (4), its derivation becomes straightforward and results in:

$$\nabla\alpha_{cr} = \left(\frac{\partial\alpha_{cr}}{\partial\psi_1}\dots\frac{\partial\alpha_{cr}}{\partial\psi_n}\right)^{T} \quad (5)$$

where:

$$\frac{\partial\alpha_{cr}}{\partial\psi_i} = \frac{\boldsymbol{\phi}_b^{T}\,\mathbf{K}^{(i)}\,\boldsymbol{\phi}_b}{\boldsymbol{\phi}_b^{T}\,\mathbf{K}_G\,\boldsymbol{\phi}_b} \quad (6)$$

In equation (6), $\boldsymbol{\phi}_b$ is the buckling mode (vectors whose components describe the shape of the structure when buckling).

As discussed in the previous Section, these partial derivatives with respect to the different parameters can be used to know which member is the best to replace to improve the critical load of the structure. The following parameter is defined to quantify the influence of changing a specific member [4] (modifying their parameters, in fact):

$$SIm_i = 100\frac{\frac{\partial\alpha_{cr}}{\partial I_i}}{\sum_j\frac{\partial\alpha_{cr}}{\partial I_j}} = 100\frac{\boldsymbol{\phi}_b^{T}\,\mathbf{K}^{(i)}\,\boldsymbol{\phi}_b}{\sum_j\boldsymbol{\phi}_b^{T}\,\mathbf{K}^{(j)}\,\boldsymbol{\phi}_b} \quad (7)$$

where SIm_i is the Parameter Sensitivity Indicator corresponding to a given member i expressed in percentage (the summation in the denominator includes all the members, but not the joints). A similar parameter can be defined for the rotational springs:

$$SIr_i = 100\frac{\frac{\partial\alpha_{cr}}{\partial kr_i}}{\sum_j\frac{\partial\alpha_{cr}}{\partial kr_j}} = 100\frac{\boldsymbol{\phi}_b^{T}\,\mathbf{K}^{(i)}\,\boldsymbol{\phi}_b}{\sum_j\boldsymbol{\phi}_b^{T}\,\mathbf{K}^{(j)}\,\boldsymbol{\phi}_b} \quad (8)$$

In equation 8, k_r are the rotational spring coefficients, SIr_i is the Parameter Influence Indicator corresponding to rotational stiffness i (the summation in the denominator includes all the joints, but no the members). The members and joints are treated separately because the moments of inertia and the rotational springs have different dimensional units. In the design, the SIm_i and SIr_i parameters can be very useful to the designer to understand the global behavior of a structure and the evolution of its design towards the best solution.

4 Critical load factor approximation using FEM

The second-order Taylor approximation of $\alpha_{cr}(\boldsymbol{\psi})$ is used to determine the critical load factor:

$$\alpha_{cr} \approx Q_\alpha = \alpha_{cr}(\boldsymbol{\psi}_0) + \nabla\alpha_{cr}(\boldsymbol{\psi}-\boldsymbol{\psi}_0) + \frac{1}{2}(\boldsymbol{\psi}-\boldsymbol{\psi}_0)^{T}\,\mathbf{H}\,(\boldsymbol{\psi}-\boldsymbol{\psi}_0) \quad (9)$$

where: $\boldsymbol{\psi}_0$ is the vector of design parameters corresponding to a solution with a known stability factor, $\boldsymbol{\psi}$ is the vector of design parameters corresponding to another solution, and $\mathbf{H}$ is the Hessian matrix, its components being:

$$H_{ij} = \frac{\partial^2\alpha_{cr}}{\partial\psi_i\,\partial\psi_j} = 2\frac{\boldsymbol{\phi}_b^{T}\left(\mathbf{K}^{(i)}+\frac{\partial\alpha_{cr}}{\partial\psi_i}\mathbf{K}_G\right)\frac{\partial\boldsymbol{\phi}_b}{\partial\psi_j}}{\boldsymbol{\phi}_b^{T}\,\mathbf{K}_G\,\boldsymbol{\phi}_b} \quad (10)$$

The derivate of the buckling mode with respect to the considered design parameter is given by

$$\frac{\partial\boldsymbol{\phi}_b}{\partial\psi_j} = (\mathbf{K}-\alpha_{cr}\mathbf{K}_G)^{-1}\left(-\mathbf{K}^{(j)} - \frac{\partial\alpha_{cr}}{\partial\psi_j}\mathbf{K}_G\right)\boldsymbol{\phi}_b \quad (11)$$

From the computation point of view, the calculation of the stability factor trough equation (9) for all the possible solutions (or for a given selected group of possible solutions) is much less time-consuming than solving equation (1). It is noted that this prediction of the critical load factor for any structure is possible without generating and assembling the stiffness matrix at each iteration, since the value of $Q_\alpha(\boldsymbol{\psi})$ is calculated with a simple formula.

5 Use of the sensitivity parameters

The techniques described in sections **3** and **4** might be used for the following purposes: i) to determine the design parameter whose change best improves the stability (highest value of SIm_i for member moments of inertia and SIr_i for rotational spring stiffness) ii) to find a quadratic expression that approximates the value of the critical load with respect to the design parameters (Q_α) iii) to obtain the most economically efficient structural change in terms of stability (highest value of $\frac{\Delta\alpha_{cr}}{\Delta C}\approx\frac{\partial\alpha_{cr}}{\partial\psi_i}\frac{\Delta\psi_i}{\Delta C}$). The latter parameter is possibly the most interesting in a design algorithm, since it maximizes the increment of stability while minimizes the cost increment. It is seen that this parameter ($\frac{\Delta\alpha_{cr}}{\Delta C}$) has been used in section **2** in an analytic (rather than FEA) context.

The proposed design algorithm starts from the less expensive (and thus, less stable) possible solution. The stability is improved by upsizing the structural element (member or connection) whose change maximizes $\frac{\Delta\alpha_{cr}}{\Delta C}$. The process is repeated until the structural requirements are fulfilled.

6 Conclusions

A simplified stability-based method design technique is presented. The proposed strategy is significantly faster than the conventional design approaches since the member and joint indicators help the designer to detect the elements that best contribute to the global stability. As well, an approximate expression of the critical load is provided. The proposed approach might be useful for sensitivity analyses.

Further research includes applications to stability design of racking systems, given their high sensitivity to such issue.

Symbols and acronyms

0: Initial value (first iteration), as super index
A: Amplitude (transverse displacement)
C: Cost
cr: Critical
E: Steel modulus of deformation (Young), demand
d: Design
FEA, FEM: Finite Element Analysis, Finite Element Method
H, H_{ij}: Hessian matrix containing the derivatives of the Critical Load Factor with respect to the design parameters, coefficient of the Hessian matrix
i, *j*: Subindexes, number of iteration (as superindexes)
I, *L*: Moment of inertia and length of a member (bar)
k: Rotational spring stiffness
K, $\mathbf{K}_G$: Stiffness matrix, Geometric Stiffness matrix
m, *r*: Member, rotational spring
n: Number of elements
P: Axial compressive force
Q: Quadratic approximation
SIm: Parameter Influence Indicator corresponding to member stiffness

SIr: Parameter Influence Indicator corresponding to rotational stiffness
w, *x*: Transverse displacement, coordinate along the length of a bar
α_{cr}: Critical Load Factor (ratio between the critical and the demanding loads, N_{cr} / N_{Ed})
$\boldsymbol{\phi}_b$: Buckling mode (shape)
λ: Slenderness coefficient ($\boldsymbol{\lambda} = \sqrt{\boldsymbol{P/EI}}$)
$\boldsymbol{\psi}$, ψ_i: Vector of Design Parameters, Design Parameter

References

[1] Manickarajah, D.; Xie, M.; Steven, G. (2000). *Optimisation of columns and frames against buckling*. Computers and Structures **75**, 45–54.

[2] Perelmuter A., Slivker V. (2001). "*The Problem of Interpretations of the Stability Analysis Results*" European Conf. on Comp. Mech., Cracow, Poland.

[3] Szalai J. (2010). "*Use of eigenvalue analysis for different levels of stability design*" SDSS'Rio 2010 Stability and Ductility of Steel Structures, Rio de Janeiro, Brazil.

[4] Farkas J., Jámrai K. (2013). "*Optimum Design of Steel Structures*" Springer, Hungary.

[5] EN1993-1-1. (2005). *Eurocode 3: Design of steel structures – Part 1-1: General rules and rules for buildings*. European Committee for Standardization.